National Library of Canada
Bibliothèque nationale du Canada

Acquisitions and Bibliographic Services Branch
Direction des acquisitions et des services bibliographiques

395 Wellington Street
Ottawa, Ontario
K1A 0N4

395, rue Wellington
Ottawa (Ontario)
K1A 0N4

Your file Votre référence

Our file Notre référence

NOTICE

The quality of this microform is heavily dependent upon the quality of the original thesis submitted for microfilming. Every effort has been made to ensure the highest quality of reproduction possible.

If pages are missing, contact the university which granted the degree.

Some pages may have indistinct print especially if the original pages were typed with a poor typewriter ribbon or if the university sent us an inferior photocopy.

Reproduction in full or in part of this microform is governed by the Canadian Copyright Act, R.S.C. 1970, c. C-30, and subsequent amendments.

AVIS

La qualité de cette microforme dépend grandement de la qualité de la thèse soumise au microfilmage. Nous avons tout fait pour assurer une qualité supérieure de reproduction.

S'il manque des pages, veuillez communiquer avec l'université qui a conféré le grade.

La qualité d'impression de certaines pages peut laisser à désirer, surtout si les pages originales ont été dactylographiées à l'aide d'un ruban usé ou si l'université nous a fait parvenir une photocopie de qualité inférieure.

La reproduction, même partielle, de cette microforme est soumise à la Loi canadienne sur le droit d'auteur, SRC 1970, c. C-30, et ses amendements subséquents.

Canada

UNIVERSITY OF ALBERTA

THE MINERAL CHEMISTRY AND MAGMA EVOLUTION OF THE BIG SPRUCE LAKE ALKALINE COMPLEX, N.W.T., CANADA

by

LULU DAI ©

A thesis submitted to the Faculty of Graduate Studies and Research in partial fulfillment of the requirement for the degree of **MASTER OF SCIENCE.**

DEPARTMENT OF GEOLOGY

Edmonton, Alberta
FALL, 1994

National Library
of Canada

Acquisitions and
Bibliographic Services Branch

395 Wellington Street
Ottawa, Ontario
K1A 0N4

Bibliothèque nationale
du Canada

Direction des acquisitions et
des services bibliographiques

395, rue Wellington
Ottawa (Ontario)
K1A 0N4

Your file   Votre référence

Our file   Notre référence

The author has granted an irrevocable non-exclusive licence allowing the National Library of Canada to reproduce, loan, distribute or sell copies of his/her thesis by any means and in any form or format, making this thesis available to interested persons.

L'auteur a accordé une licence irrévocable et non exclusive permettant à la Bibliothèque nationale du Canada de reproduire, prêter, distribuer ou vendre des copies de sa thèse de quelque manière et sous quelque forme que ce soit pour mettre des exemplaires de cette thèse à la disposition des personnes intéressées.

The author retains ownership of the copyright in his/her thesis. Neither the thesis nor substantial extracts from it may be printed or otherwise reproduced without his/her permission.

L'auteur conserve la propriété du droit d'auteur qui protège sa thèse. Ni la thèse ni des extraits substantiels de celle-ci ne doivent être imprimés ou autrement reproduits sans son autorisation.

ISBN 0-315-95024-2

Canadä

UNIVERSITY OF ALBERTA

RELEASE FORM

NAME OF AUTHOR: **Lulu Dai**

TITLE OF THESIS: **The Mineral chemistry and magma evolution of the Big Spruce Lake alkaline complex, N.W.T., Canada**

DEGREE: **Master of Science**

YEAR THIS DEGREE GRANTED: **1994**

Permission is hereby granted to the University of Alberta Library to reproduce single copies of this thesis and to lend or sell such copies for private, scholarly or scientific research purposes only.

The author reserves all other publication and other rights in association with the copyright in the thesis, and except as hereinbefore provided neither the thesis nor substantial portion thereof may be printed or otherwise reproduced in any material form whatever without the author's prior written permission.

Lulu Dai

Lulu Dai
#203 10808, 84Av
Edmonton, Alberta
T6E 2J2

June 16 , 1994

UNIVERSITY OF ALBERTA

FACULTY OF GRADUATE STUDIES AND RESEARCH

The undersigned certify that they have read, and recommend to the Faculty of Graduate Studies and Research for acceptance, a thesis entitled **THE MINERAL CHEMISTRY AND MAGMA EVOLUTION OF THE BIG SPRUCE LAKE ALKALINE COMPLEX, N.W.T., CANADA** submitted by **LULU DAI** in partial fulfillment of the requirement for the degree of **MASTER OF SCIENCE**.

D.G.W. Smith

T. Chacko

R.W. Luth

M. Dudas

M. Dudas

June 16, 1994

Date

Dedications

to my parents

and

yuanpeng

Abstract

The chemical mineralogy of rock-forming and accessory minerals has been studied in the Big Spruce Lake alkaline complex for a group of four intrusive centres containing silica-saturated to oversaturated and silica-undersaturated rocks and a spatially- and temporally-associated satellite intrusive centre.

The major mineral groups include clinopyroxene, clinoamphibole, trioctahedral mica, feldspar, feldspathoid and olivine. The compositions of the clinopyroxenes define a trend from Mg- and Fe-rich augite to aegirine augite and aegirine as the host rocks vary from silica-saturated and oversaturated types to silica-undersaturated types. Similarly, the amphiboles range from calcic species (kaersutite, hastingsite, edenitic hornblende, edenite, *etc.*) through sodic-calcic species (winchite and katophorite) to subsolidus sodic species (riebeckite). Primary magmatic amphiboles are abundant in the saturated series, but are lacking in all the undersaturated rocks. The feldspars range from Ca-rich to Na-rich plagioclase (An_{45} to An_{16}) and alkali feldspar ($Ab_{98}Or_2$ to Ab_9Or_{91}). Micas range from Mg-rich to Fe-rich biotite. The compositions of nepheline is $Ne_{75}Ks_{19}Qz_6$.

Apatite, zircon, titanite, ilmenite and Ti-magnetite are present throughout the complex. Other accessory minerals include pyrochlore, perovskite, allanite, carbocernaite and fluorite; they are present only in the nepheline-bearing and carbonatitic rocks.

Field evidence, petrography and mineral chemistry are consistent with the silica-saturated to oversaturated rock series and silica-undersaturated rock series being linked by fractional crystallization coupled with amphibole dissolution from a common magma source, and with the nepheline syenite and carbonatite corresponding the silicate-carbonate conjugate immiscible fractions from a silica-undersaturated liquid.

Fractionation of various mineral assemblages has controlled the trend of magma evolution. Three stages of magma evolution are suggested to be responsible for the formation of the complex. The early stage, which included the formation of saturated to

oversaturated rock series, was dominated by fractional crystallization of calcic clinopyroxene, calcic amphibole and calcic plagioclase. This fractionation led to Mg and Ca depletion and Si, Fe and alkali enrichment in the evolving magma. The second stage was dominated by resorption of amphiboles and fractionation of alkali feldspar that created a silica-undersaturated liquid. Crystallization from this melt during a third stage produced the peralkaline silica-undersaturated rocks. Carbonatite was formed at the same time by silicate-carbonate liquid immiscibility.

Mass balance calculations are consistent with the above suggestions and indicate three stages of magma evolution: (1): a. fractionation from alkali basalt to gabbroic magma by crystallization of olivine-magnetite pyroxenite; b. fractionation from gabbroic melt to alkali syenitic melt by subtraction of a mineral assemblage similar to that in diorite, (2) evolution from alkali syenitic melt to foyaitic melt by fractionation of alkali feldspar and actinolite coupled with resorption of about 11% hastingsite, (3) continuous crystallization from foyaitic magma gives rise to foyaite-melteigite cumulates and presumably a felsic silica-undersaturated melt as well.

It is inferred that a critically undersaturated alkali olivine basalt best represents the possible parent magma of the Big Spruce Lake alkaline complex. The lamprophyre from the satellite centre is another candidate for the original parental magma of the complex, if it is genetically related to the main intrusion.

Acknowledgment

I sincerely thank Prof. Dorian G.W. Smith for providing the opportunity for me to study the Big Spruce Lake alkaline complex at the Department of Geology. I am also grateful to Prof. Smith for the invaluable academic guidance, assistance and encouragement from which I have benefited a lot throughout my graduate studies.

I gratefully acknowledge Dr. P.A. Cavell who provided original rock sample, thin sections, field maps & notes and some other related materials. Also, the late Prof. R.St.J. Lambert provided a large number of thin sections, field photographs and notes for the research. I obtained a lot of knowledge about the project from them. Paul Wagner is gratefully acknowledged for the operation of microprobe for the mineral analyses in the department microprobe laboratory. Dr. T. Chacko and Dr. R.W. Luth are thanked for giving help and guidance regarding this research.

I especially wish to thank graduate student, Andrew Locock. Andrew has provided lots of constructive suggestions to the research and, many times when he had found an exciting paper, he would bring a copy to me. Andrew also assisted me greatly by reading part of my earliest thesis draft. It has always been my pleasure to have discussions with many friendly graduate student colleagues, such as James, Chris, Donggao and others in the department.

Special thanks to Yuanpeng for constant help and encouragement to me. I want to thank my parents and my sisters; their understanding has always been strong support to me wherever I am.

Financial support during this study was provided by teaching and research assistantship from the Department of Geology and Dr. Dorian G.W. Smith. The experimental work was supported by NSERC (Canada) operating grant #A4254 to Dr. Dorian G.W. Smith.

Table of Contents

page

Chapter

1. Introduction....1
2. General geology....4
3. Petrography....7
  3.1 Centre 1....7
    3.1.1. The gabbros....7
      3.1.1.1 The Big Feldspar Gabbro....7
      3.1.1.2 The Leucocratic Laminated Gabbro....8
      3.1.1.3 The Rhythmic Banded Gabbro....9
    3.1.2 The olivine magnetite pyroxenite....10
    3.1.3 The diorite....10
  3.2 Centre 2....12
    3.2.1 The alkaline syenites....12
      3.2.1.1 Quartz-free syenite....12
      3.2.1.2 Quartz syenite....13
    3.2.2 The porphyry dykes....13
      3.2.2.1 Porphyritic quartz syenite dyke....13
      3.2.2.2 Comendite....13
      3.2.2.3 Porphyritic nepheline-sanidine phonolite dyke....14
  3.3 Centre 3....14
    3.3.1 Foyaite (aegirine nepheline syenite)....14
    3.3.2 Sodalite nepheline syenite....16
    3.3.3 Titanite melteigite....17
    3.3.4 Ijolite....17
    3.3.5 Urtite....18
    3.3.6 Phonolite....18
    3.3.7 Fenite....18
  3.4 Centre 4--The carbonatites....19
    3.4.1 The calcite carbonatite....19
    3.4.2 The dolomite carbonatite....20
    3.4.3 The Big Spruce Island carbonatite pegmatite....20
  3.5 Centre 5--The Moose Island satellite rocks....20
    3.5.1 Melanocratic syenite....20
    3.5.2 Biotite pyroxenite....21

3.5.3 Biotite peridotite....22
3.5.4 Minette....22
3.5.5 Lamprophyre....22
4. Mineral chemistry....24
4.1 Pyroxene....24
4.2 Amphibole....37
4.3 Mica....51
4.4 Feldspar....56
4.5 Olivine....60
4.6 Nepheline....63
4.7 Accessory phases....66
4.7.1 Rare element and REE-bearing minerals....66
4.7.2 Iddingsite....66
4.7.3 Chlorite....67
4.7.4 Opaque minerals....67
5. Minerals as indicators of temperature and oxidation-reduction conditions....74
6. Mass-balance calculations of the magma differentiation processes....75
7. Discussion....81
7.1 Fractional crystallization processes....81
7.2 The amphibole dissolution processes....82
7.3 The liquid immiscibility processes....84
7.4 Chemical evolution of alkaline magmas as a consequence of differentiation of rock-forming minerals....86
7.5 Inferred parental magma....87
7.6 Physical process of the magma evolution of the Big Spruce Lake alkaline complex....88
8. Conclusion....93
Bibliography....94

* *

Appendices....102
1. Photomicrographs....102
2. Estimation of modal mineral proportions (volume %)....118

3. Experimental method....119
4. Method of calculation of the structural formulae for pyroxenes....121
5. Method of calculation of the structural formulae for amphiboles and abbreviations for amphibole nomenclature...122
6. The principle of the calculations by least-squares approximation....124

List of Tables

Page

Table

1. Average pyroxene compositions: in magnetite pyroxenite & gabbro.........27
2. Average pyroxene compositions: in diorite & centre 5.........28
3. Average pyroxene compositions: in alkaline syenite & nepheline syenite.........29
4. Average pyroxene compositions: in nepheline syenite.........30
5. Average amphibole compositions: in centres 1 & 5.........41
6. Average amphibole compositions: in gabbro.........42
7. Average amphibole compositions: in diorite & comendite.........43
8. Average amphibole compositions: in quartz-free & quartz syenite.........44
9. Average amphibole compositions: in quartz syenite & nepheline syenite.........45
10. Average mica compositions: in centres 1 & 5.........52
11. Average mica compositions: in centres 2, 3 & 4.........53
12. Average feldspar compositions: in centres 1 & 5.........58
13. Average feldspar compositions: in centres 2 & 3.........59
14. Average olivine compositions: in centres 1 & 5.........61
15. Average nepheline compositions: in centre 3.........64
16. Average oxide & accessory phase compositions.........72
17. Mass balance fractionation/resorption calculations by the least-squares approximation method.........77
18. Mineral compositions for the mass-balance calculations.........79
19. Calculated percentages of rock types of the Big Spruce Lake alkaline complex by mass balance calculations.........80

List of Figures

Page

Figure

1. Geology and location map of the Big Spruce Lake alkaline complex, Northwest Territories......6
2. Q-J diagram for pyroxene classification......31
3. Compositional ranges of calcic clinopyroxenes in the quadrilateral enstatite-diopside-hedenbergite-ferrosilite (En-Di-Hd-Fs)......32
4. Na-Ca and Na-clinopyroxene compositions from the foyaite, melteigite and ijolite, plotted in terms of QUAD-Jd-Ae......33
5. Compositional variation of clinopyroxenes plotted in terms of aegirine-diopside-hedenbergite (Ae-Di-Hd) components......34
6. Element variations (Si, Al, Ca & Na) as referred to Mg# in clinopyroxenes of the Big Spruce Lake alkaline complex......35
7. Element variations (Mg, Ti, Fe^{2+} & Fe^{3+}) as referred to Mg# in clinopyroxenes of the Big Spruce Lake alkaline complex......36
8. Amphibole compositional variation, plotted in terms of cationic ($Ca+Al^{IV}$) vs. (Si+Na+K)......46
9. Amphibole $Mg/(Mg+Fe^{2+})$ vs. (Na+K) diagram......47
10. Composition and classification of the calcic amphiboles of the Big Spruce Lake complex......48
11. Composition and classification of sodic-calcic amphiboles in quartz syenite......49
12. Composition and classification of sodic amphiboles in nepheline syenites......50
13. Biotite plotted in terms of Al, Mg & Fe cations......54
14. Biotite Al_2O_3 vs. MgO & FeO (in wt.%)......55
15. Feldspar compositions plotted in terms of albite (Ab), anorthite(An) and orthoclase (Or) end-members......57
16. Compositions of olivines plotted as Mg# vs. SiO_2, CaO and MnO content (in wt.%)......62
17. Nepheline compositions plotted in Ne-Ks-Qz (nepheline-kalsilite-quartz) in wt.%, in Si-undersaturated rocks

of the Big Spruce Lake complex..65
18. EDS spectrum of Nb-, Ta-, U-perovskite in melteigite....................68
19. EDS spectrum of allanite in carbonatite..69
20. EDS spectrum of pyrochlore in carbonatite..70
21. EDS spectrum of carbocernaite in foyaite...71
22. EDS spectrum of cobalt-pentlandite in olivine of melanocratic syenite..73
23. Relations between $Fe^T/(Fe^T+Mg)$ (wt.) ratios in clinopyroxenes and in host rocks..90
24. Relations between SiO_2 (wt.%) in amphiboles and in host rocks...91
25. Flow chart of the magma types and intrusive processes of the Big Spruce Lake alkaline complex..92

List of Plates

Page

Plate

1. Gabbro. Titanian augite (aug) is replaced by greenish amphibole (am). Feldspar (fsp) is partly altered. Opaque minerals include titanian magnetite and ilmenite. Magnification 51x. Plane polarized light......................103
2. Gabbro, containing titanian augite (aug), and subhedral kaersutite (brown) which also occurs as inclusions in augite. Greenish ferro-hornblende rims augite and kaersutite. Biotite (bi) and magnetite (opaque) are present. Magnification 51x. Plane polarized light........................103
3. Olivine magnetite pyroxenite. Olivine (ol) is traversed by serpentine veinlets (blue grey). Titanian augite (aug) and opaque oxides (titanian magnetite & ilmenite) are other major phases. Magnification 41x. Crossed Nicols..104
4. Magnetite pyroxenite. Kaersutite (brown) is resorbed in an augite groundmass, new augite is formed around the kaersutite. The original augite contains exsolution blebs which consist of Ti, Fe-bearing oxide. The fracture is filled by Fe, Ti oxide in augite. Magnification 128x. Plane polarized light..................104
5. Kaersutite (brown) occurring as a vein in magnetite pyroxenite. Magnification 51x. Plane polarized light..................105
6. An amphibole vein intruding magnetite pyroxenite which consists of augite (aug) and titanian magnetite and ilmenite. The vein consists of hastingsite (has) and apatite (ap) which contains subhedral hastingsitic hornblende inclusions. Magnification 51x. Plane polarized light..105
7. The augite (aug) and opaque minerals (titanian magnetite and ilmenite) are replaced and rounded alongside a hastingsite (blue green)-apatite (ap) vein. Magnification 51x. Plane polarized light..106
8. Diorite. Augite is rimmed by edenitic hornblende (hn)

which is surrounded by biotite (brown). Apatite (ap) and opaque phases (ilmenite & titanian magnetite) are commonly associated with the mafic minerals. Magnification 51x. Plane polarized light......................106

9. Quartz-free syenite, containing alkali feldspar (fsp), augite (aug), primary ferro-hornblende (hn), biotite (bi) and opaque magnetite. Secondary actinolite (act) has replaced augite. Magnification 51x. Plane polarized light........107

10. Quartz syenite, containing edenite (am), alkali feldspar (fsp) and quartz (qz). Magnification 51x. Crossed Nicols..........107

11. Foyaite, containing aegirine augite (green), nepheline which is altered to cancrinite (cac), and alkali feldspar (fsp). Biotite (bi) is present in minor amount. Magnification 51x. Crossed Nicols.....................................108

12. Carbocernaite (brown) included in aegirine augite (green) of foyaite. Magnification 128x. Plane polarized light................108

13. Foyaite, containing carbonate ocelli (cat) which are interstitial to aegirine augite (green). Magnification 128x. Crossed Nicols..109

14. Riebeckite-metasomatized rock. Radiating riebeckite (blue) grows on aegirine augite (green). Magnification 41x. Plane polarized light..109

15. Titanite melteigite, containing titanite (tan) and aegirine augite (green). Magnification 41x. Plane polarized light...........110

16. Pyrochlore (brown) included in aegirine augite (green) of melteigite. Magnification 128x. Plane polarized light.........110

17. Ijolite, containing nepheline (nep), aegirine augite (greyish green) and sodalite (dark). Magnification 128x. Crossed Nicols..111

18. Urtite, consisting dominantly of nepheline (nep) which is partly altered to cancrinite (cac). Minor aegirine augite (green) is present. Magnification 41x. Crossed Nicols...............111

19. Phonolite. The phenocryst is orthoclase and the groundmass contains aegirine augite, alkali feldspar and nepheline. Magnification 41x. Crossed Nicols.................................112

20. Apatite carbonatite. Apatite forms grey, hexagonal

grains. Magnification 128x. Crossed Nicols.....................................112
21. Silicate carbonatite, containing alkali feldspar aggregates (fsp) and epidote (ep). Magnification 128x. Crossed Nicols.....113
22. Fluorite carbonatite, consisting of purple fluorite and calcite. Magnification 41x. Plane polarized light.........................113
23. Carbonatite, containing biotite (brown) and aegirine augite (green) in calcite groundmass. Magnification 128x. Plane polarized light.......................................114
24. Allanite (dark brown) forms discrete bands in carbonatite. Magnification 128x. Plane polarized light.............114
25. Melanocratic syenite, containing olivine (ol), diopside (dio), biotite (brown) and alkali feldspar (fsp). Magnification 51x. Plane polarized light..115
26. Biotite pyroxenite, consisting of augite (aug) and biotite (brown). Augite is stained by greenish chlorite phase. Magnification 128x. Plane polarized light..........................115
27. Biotite peridotite, containing biotite (brown), olivine (ol), carbonate (cat) and opaque phases (titanian magnetite). Magnification 128x. Plane polarized light..............116
28. Minette. Zoned phlogopite phenocrysts (brown) occur in fine-grained groundmass. Magnification 41x. Plane polarized light..116
29. Lamprophyre, containing a carbonate-epidote globule. The matrix contains the opaque mineral ilmenite & magnetite, chlorite, sericite and uralite. Magnification 51x. Crossed Nicols..117

Chapter 1.
Introduction.

The magmas of the Big Spruce Lake complex span the plagioclase-olivine-clinopyroxene thermal divide. According to Yoder and Tilley (1962), this divide separates the two principal magma types--tholeiite and alkali basalt that crystallize to form quartz normative and nepheline normative rocks respectively. However, basalt magmas close to the thermal divide may fractionate to residual liquids of different degree of silica saturation depending on how the pressure and volatile content affects the stability or compositions of the fractionating phases (Coombs and Wilkinson, 1969; Giret and Lameyre, 1980).

Bowen (1928) initially suggested that the 'fractional resorption of accumulated hornblende' would lead to 'a switching over of tholeiitic magma into an alkaline line of descent'. According to Bowen's mechanism, the amphibole crystals sink into a higher temperature environment and are dissolved there and result in a change of magma composition. This suggestion was supported by experimental studies (Yoder and Tilley, 1962). However, the composition of the amphibole species is crucially important, if its resorption is to cause a transformation of magma composition from tholeiite to alkali basalt.

There have been some discussions of the mechanism by which silica-undersaturated and oversaturated rock types can form from a common parent magma. One mechanism for bridging the thermal divide is by fractional crystallization or resorption of different mineral assemblages (Giret *et al.*, 1980; Bonin & Giret, 1985; Henderson *et al.*, 1989), in particular, hastingsitic amphibole and biotite (Foland *et al.*, 1993), leading to diverging liquid lines of descent. Through amphibole fractionation, a previously Si-undersaturated melt can enter the oversaturated field in silicate systems (Maury, 1976). Conversely, breakdown and oxidation of amphibole can lead to the production of highly silica-undersaturated liquids (Giret, 1979). One example is the Montagnes Vertes complex, which shows a chilled gabbro outer zone and a progressive petrographic evolution towards a nepheline-bearing syenite core. The formation of nephelinitic rocks was interpreted as resulting from the destabilization of the hastingsitic amphibole (Giret, 1979).

In the Big Spruce Lake alkaline complex, the mineral chemistry shows a continuous alkaline differentiation trend from silica-saturated and oversaturated rocks to silica-undersaturated rocks and indicates a genetic relationship between the contrasting rock types. Isotopic evidence is consistent with such an interpretation because both of the rock types have identical isotopic signatures (Cavell, 1986). Fractional crystallization evidently played a major rôle during the evolution of the two rock series. It is observed that in the Big Spruce Lake complex, amphibole is a common primary phase in the silica-saturated to oversaturated rocks but is lacking in nepheline-bearing rocks. This absence may suggest that early crystallized amphiboles were dissolved. Amphibole-apatite segregations were found as veins within magnetite pyroxenite. The occurrence of the veins suggests that there have been amphibole accumulation at depth in the early stage of magma evolution. The compositions of these amphiboles are hastingsite and kaersutite. Their compositions would decrease the magma Si content if they were melted in the magma. Therefore, amphibole fractionation and destabilization may account for the change in magma silica levels in the Big Spruce Lake alkaline complex.

Igneous fractionation trends in minerals relate to the distribution of various elements between minerals and melts. The mineral chemistry thus reflects the different stages of magma evolution. The study of major rock-forming minerals is central to tracing the liquid line of descent. In addition, minerals are participants during the fractionation of magmas, they influence the chemical variation of the remaining liquids during the magmatic evolutionary processes. Therefore, knowledge of mineral compositions is essential in evaluating the magma differentiation trends.

Another reason for studying the Big Spruce Lake complex is related to the occurrence of carbonatite that is closely associated with the nepheline-bearing rocks. The petrogenesis of carbonatites has been a subject of controversy. Various models have been put forward: (1) direct partial melting of mantle (Gittins, 1989), (2) crystal fractionation from carbonated silicate melts (Wyllie, 1987; Wyllie *et al.*, 1990), or (3) carbonate-silicate liquid immiscibility (Le Bas, 1977, 1989; Freestone & Hamilton, 1980).

This thesis presents the results of a detailed study of the mineral chemistry and petrography of the Big Spruce Lake alkaline complex, looks for textural evidence for carbonate-silicate liquid immiscibility and for amphibole resorption and then combines mass balance calculations to account for the magma differentiation processes.

Thus, the purpose of the present work may be summarized as follows:

(1) To study the petrography of the various rock types and the major rock-forming and accessory minerals systematically, and thereby to characterize the petrographic and mineral compositional variation in the Big Spruce Lake alkaline complex.

(2) To determine the crystallization histories of the magmas as recorded by rock-forming minerals and their chemistry; to elucidate the petrological relationship between the coexisting silica-undersaturated and silica-saturated to oversaturated magmas, and between the silicate rocks and carbonatites, and therefore to provide new insights into the petrogenesis of the spectrum of the rock types of the Big Spruce Lake alkaline complex.

(3) To constrain the nature of the parental magma from which the Big Spruce Lake alkaline complex was formed.

Chapter 2.
General Geology.

The field geological relationships and rock nomenclature used in the thesis are based on the work of Martineau (1970), Lambert (1964), Cavell (1986) and the IUGS classification (IUGS, 1989). Sample numbers are after Cavell (1986).

The Big Spruce Lake alkaline and carbonatite complex (Fig. 1), Northwest Territories (latitude 63°33'N; longitude 115°55'W), covers an area of 3.5x9.0 km^2 and intrudes Precambrian granodiorite gneiss that is 2500-2600 Ma old (Cavell, 1986). The complex has an average crystallization age at 2183 ± 75 Ma based on Sm-Nd whole rock data (Cavell, 1986).

Five intrusive centres were involved in the formation of the complex, which consists of a remarkable diversity of rock types (Martineau, 1970). Centres 1, 2, 3 and 4 are the main intrusive bodies, and are designated in the order of intrusive sequence and are emplaced in a linear direction from NE to SW. Centre 5 (the Moose Island satellite centre) lies 5 km south of the main intrusion and was assumed to be coeval with the main intrusions or younger at 1800-1900 Ma (Cavell, 1986).

Centres 1 and 2 are silica saturated to oversaturated and define a trend from (olivine) magnetite pyroxenite through gabbro, diorite, quartz-free syenite to quartz syenite. The magnetite pyroxenite occurs both as an arcuate mass with a diorite margin, and as numerous dykes and small masses cross-cutting gabbro (Martineau, 1970). The gabbro is an inner intrusion central to the diorite, and both of them are layered cumulus bodies. The quartz-free and quartz syenites occur in ring dykes and rim a portion of the diorite. Comendite is an associated hypabyssal rock and occurs in a dyke swarm in centre 2.

Centres 3 and 4 include nepheline-bearing rocks and carbonatites. They are closely related in occurrence and define a rock series of foyaite (nepheline syenite, layered), melteigite and ijolite (stock or breccia pipe), urtite, and carbonatite. Associated hypabyssal activity is represented by phonolite dykes. The main carbonatite activity intruded the centre of the main foyaite body in Big Spruce Island and formed a concentric carbonatite-foyaite-ijolite zoned intrusion. Carbonatites also intrude as dykes and pipes.

Along the eastern side of centre 3, post-crystallization shear and metasomatic activity created an elongate zone of riebeckite-bearing foyaites. Fenite developed around the intrusions of foyaite and carbonatite. Several elliptical gas escape vents are associated with carbonatite pipes.

Centre 5 consists of a series of mafic potassium-rich rocks. Rock types include melanocratic syenite, biotite pyroxenite, biotite peridotite, minette and other strongly altered lamprophyres. Although these rocks are nepheline-normative (Cavell, 1986), melanocratic syenite and biotite pyroxenite may contain quartz xenoliths. The central zone includes intrusive melanocratic syenite occurring as broader dykes or as small elliptical breccia pipes (30-100m), and biotite pyroxenite occurring as pipes, or as schlieren within syenite. Narrow dykes of minette and melanocratic syenite occur in a broad marginal belt (Martineau, 1970). Fenite is developed around the biotite pyroxenite. The relationship between the potassic satellite body and the main intrusions cannot be established in the field.

There are abundant intermediate intrusions of dyke rocks between the intrusion of the silica-saturated and silica-undersaturated rock series. These dyke rocks include both silica-saturated and silica-undersaturated types and include porphyritic gabbro, porphyritic quartz syenite, biotite peridotite, comendite, porphyritic nepheline syenite, *etc.*

All the rocks from centres 1, 2, 3, 4 and centre 5 have mantle-derived initial $^{87}Sr/^{86}Sr$ ratios in the range 0.688-0.703 (Cavell, 1986). The similarity in isotopic signatures is consistent with these rocks being comagmatic.

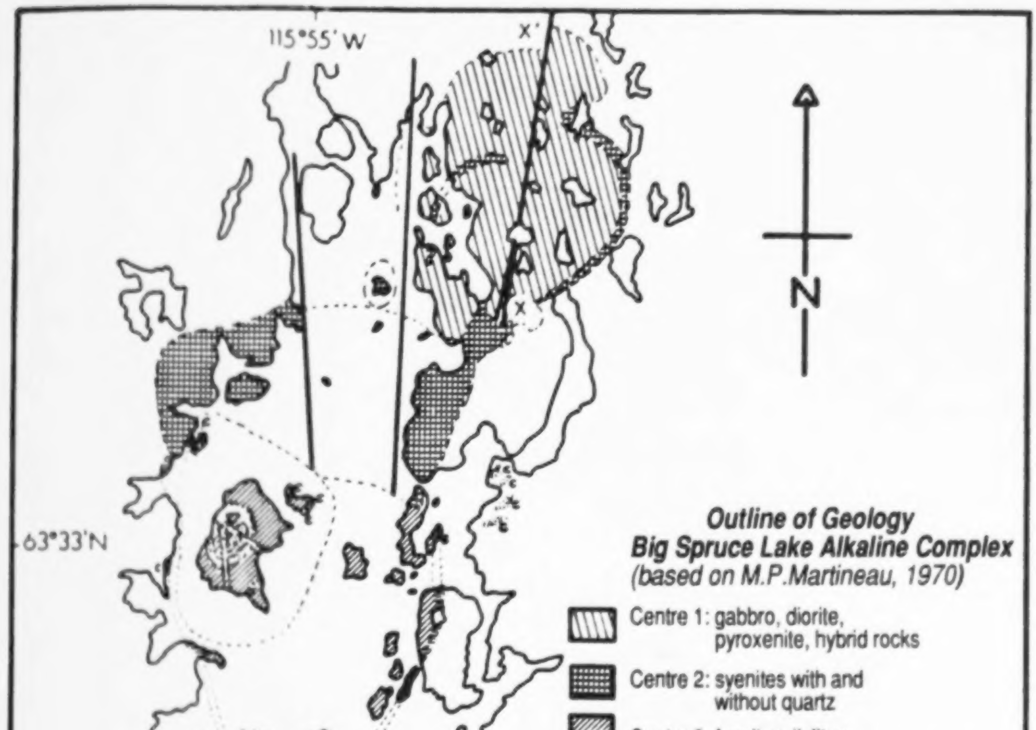
115°55' W
63°33'N
X'
X
N
Outline of Geology
Big Spruce Lake Alkaline Complex
(based on M.P.Martineau, 1970)
Centre 1: gabbro, diorite, pyroxenite, hybrid rocks
Centre 2: syenites with and without quartz
Centre 3: foyaites, ijolites, riebeckite-metasomatized rock
Centre 4: carbonatites and radial fracture pattern
Centre 5: melanocratic syenite and pyroxenite
Fenite
Fault
LOCATION
1 km

Fig.1: Geology and location map of the Big Spruce Lake alkaline complex, Northwest Territories, after Cavell (1986).

Chapter 3.
Petrography.

Photomicrographs of representative rock types are shown in Appendix 1. Estimation of mineral contents in various rocks are listed in Appendix 2.

3.1 Centre 1

3.1.1 The gabbros

According to Martineau (1970), the intrusion can be subdivided in the field into a marginal, coarse grained Big Feldspar Gabbro, a central, medium grained, Leucocratic Laminated Gabbro and an upper, Rhythmic Banded Gabbro. The major minerals include clinopyroxene, kaersutite, hastingsitic and edenitic amphiboles, and plagioclase. Biotite is minor. Accessory minerals include ilmenite, titanian magnetite, apatite, and titanite.

3.1.1.1 The Big Feldspar Gabbro

The rock is porphyritic, with large euhedral plagioclase crystals (3-7 mm) occurring as phenocrysts in a medium-grained matrix that consists of clinopyroxene, amphibole, biotite, ilmenite, magnetite and apatite. The plagioclase phenocrysts are commonly zoned. Cores are broader than rims and have compositions of An_{32-34}. Discrete alkali feldspars are not seen, but narrow coronas of alkali feldspars occasionally rim plagioclase phenocrysts. In the matrix, clinopyroxene is the most abundant phase. It forms subhedral to rounded grains and shows pinkish pleochroism. Microprobe analyses show that these are titanian augites that are often mantled by green amphiboles (plate 1), biotite and oxides.

Three amphibole populations are present, with absorption colors varying from brown to blue green and green. Greenish amphiboles commonly occur as rims on titanian augites. Microprobe analysis showed that they range from edenite through edenitic hornblende to actinolite, forming a continuous solid solution series. The dark brown pleochroic amphibole is kaersutite. It occurs in the rock as individual subhedral grains, as coronas overgrowing titanian augite, and as small inclusions in titanian augites (plate 2). This texture indicates that kaersutite crystallized over a relatively longer time than the clinopyroxene. Greenish blue amphiboles are largely hastingsitic amphiboles as determined by microprobe analysis. They occur both as discrete grains, and as rims on kaersutite (plate 2).

Large brown biotite plates form the outermost rims of the pyroxene cores and greenish amphibole coronas. This observation is consistent with the melt becoming increasingly alkali- and volatile-rich as it evolved. Here Bowen's discontinuous series where 'liquid reacts with olivines to produce pyroxenes, with pyroxenes to produce amphiboles and with amphiboles to produce biotites' (Bowen, 1922), is well illustrated.

Olivine is rarely seen and this suggests that it may have been an early formed phase but was subsequently replaced by other minerals; or it may have been fractionated out at depth.

Zoning in early-formed mafic phases is lacking and this may reflect a slow cooling. Although discontinuous reaction relationships are present, most rock-forming minerals appear to re-equilibrate during slow magmatic cooling. This observation also applies to other plutonic rocks throughout the entire complex.

Abundant titanian magnetite, ilmenite and apatite occur in the rock. Titanian magnetite and ilmenite form subhedral to anhedral grains occurring in glomeroporphyritic aggregates or as inclusions in augite, amphibole and biotite. The magnetite and ilmenite are heterogeneous mixtures and are often surrounded by coronas of biotite and titanite or are veined by biotite.

Titanite is commonly observed in all the basic and intermediate rocks as skeletal crystals rimming titanian magnetite and manganian ilmenite. Apatite forms stubby prisms and is usually enclosed within amphiboles, biotites and oxides.

3.1.1.2 The Leucocratic Laminated Gabbro

This rock consists of two distinct parts, the felsic part, which is composed mainly of plagioclase, and the mafic part, which is composed of oxides and mafic minerals. Platy plagioclase crystals make up the major part of the rock. The size of the crystals ranges from fine to coarse with well-developed polysynthetic twinning. Zoning is not observed.

Mafic minerals form aggregates that are interstitial to plagioclase. Titanian augites and amphiboles (kaersutite, hastingsite, pargasitic hornblende and edenite) are dominant. As in the Big Feldspar Gabbros, kaersutite has three modes of occurrences. The first occurrence is as small inclusions within augite. The second type forms primary discrete grains interstitial to the other major minerals. The third forms rims on augite. Hastingsite is commonly intergrown with, or rims augite and brown kaersutite. Greenish edenite also occurs as rims on augite.

Oxides are abundant within the mafic mineral aggregates and are commonly traversed or rimmed by amphibole, biotite and chlorite, reflecting late-stage volatile activity in the rock. Biotite crystallized after the amphiboles and forms a platy outer layer on the amphiboles. Apatite occurs as stubby crystals and is frequently enclosed by augite, and biotite.

3.1.1.3 The Rhythmic Banded Gabbro

This rock is made up of rhythmic layers (5-10cm thick) of dark minerals and layers of plagioclase (Martineau, 1970). Minerals in the mafic bands include titanian augite, amphibole, magnetite, ilmenite and apatite.

There is a higher proportion of amphibole in the Rhythmic Banded Gabbro than in the Big Feldspar and Leucocratic Laminated Gabbros. Amphiboles are mostly greenish and blue green species (in thin section) that include hastingsite, and members of edenite-actinolite solid solution. They are medium-grained, granular and interstitial to the feldspar. Brown kaersutite occurs as anhedral interstitial grains, veinlets and rims of augite.

The feldspar has a composition of An_{45}. In many cases, however, the grains have been partially altered or weathered to clay minerals.

3.1.2 The olivine magnetite clinopyroxenite

These rocks are cumulates and vary from olivine magnetite pyroxenite to plagioclase-bearing magnetite pyroxenite. Olivine magnetite pyroxenite (*e.g.*, #1004) contains 10% modal olivine, 70% pyroxene and 20% (magnetite + ilmenite). Magnetite pyroxenite (#1001) contains little olivine and clinopyroxene is the major cumulus phase.

Generally, the rock is medium to coarse grained and shows typical sideronitic texture. Major minerals are titanian augite, olivine, ilmenite and titanian magnetite. Euhedral olivine and augite grains preceded the crystallization of the large patches of oxides which filled the interstices between the cumulus augite and olivine (plate 3). Fresh olivine (Fo_{70}) occurs as granular grains, but most of the olivine has altered to pseudomorphs containing tremolite, talc, serpentine, titanian magnetite, and sometimes cobalt-pentlandite.

The clinopyroxene is pale pinkish titanian augite. It is subhedral, sometimes showing polysynthetic twinning. Sector zoning is characteristic of the clinopyroxenes in the rock. The augites also show fine exsolution lamellae (plate 4). In a back-scattered electron image, the lamellae appear to be fine needles and are made up of Ti, Fe, Mn. According to Wass (1979), the lamellae in clinopyroxenes of alkali basalt may be titanian magnetite and ilmenite. Sometimes the augite contains small inclusion of kaersutite, which appears to have been partly resorbed (plate 4), or the augite is rimmed by kaersutite. Biotite and plagioclase are seen occasionally but apatite is absent.

Locally the rock contains kaersutite veinlets (plate 5). The rock was also invaded by apatite-bearing amphibole veins that are composed dominantly of bluish green hastingsite (plates 6 & 7). Euhedral to subhedral hastingsitic hornblende is included in apatite. The vein indicates injection of magma from depth. The interaction between the magmas of magnetite pyroxenite and amphibole vein resulted in the complex mineral assemblages in the rock.

3.1.3 The diorite

The diorite is a medium to coarsely crystalline rock (plate 8). The texture of the rock is similar to that of gabbros. Alkali feldspars appear and amphibole and biotite are the dominant mafic phases. Plagioclase An_{27-33} is the major phase of the rock. Mafic minerals include clinopyroxene, amphibole, biotite and oxides. They occur in dark clusters together with apatite that is interstitial to poikilitic feldspars.

Plagioclase shows albite twinning. Zoning is not developed and the crystals are often saussuritized and occasionally rimmed by narrow alkali feldspar. A granophyric intergrowth of quartz and alkali feldspar is occasionally seen in the diorite.

The clinopyroxene is augite. It is much less abundant than in the gabbros and often occurs as an altered core rimmed by amphibole and biotite.

Microprobe analyses show that the amphiboles include hastingsitic hornblende, edenitic hornblende, ferro-hornblende and edenite. They are mostly primary and occur as euhedral to subhedral grains in the rock. Secondary amphiboles rimming augite are mainly actinolite. Minor brown kaersutite also occurs and is commonly rimmed by hastingsitic hornblende or edenite. Further alteration of the amphiboles produced light green actinolite and chlorite.

Biotite occurs as hexagonal plates interstitial to the feldspar and amphibole, and often rims the amphibole and magnetite. The biotite probably formed by subsolidus reactions.

Ilmenite and titanian magnetite are major oxides. Very minor amounts of pyrite, sphalerite and hematite are also present. The oxides occur within the mafic aggregates and are commonly rimmed or traversed by fine-grained amphiboles and biotite. The increasing amount of biotite and amphibole is consistent with a higher volatile content in the diorite compared to the gabbros.

Modal quartz is found in the diorite and forms interstitial granophyric intergrowths with alkali feldspars. Zircon is occasionally seen. Abundant stubby apatite crystals are enclosed within the amphibole and biotite.

3.2 Centre 2

3.2.1 The alkali syenites

According to Martineau (1970), the syenites were numbered 1-4 in order of intrusion. Syenite 1 and syenite 3 are quartz-free syenite and occur in the area of centre 1. Syenite 2 and 4 are quartz-bearing syenite and occur in centre 2.

3.2.1.1 Quartz-free syenite

This rock is composed of platy or rhombic feldspars with interstitial agglomerates of mafic minerals, oxides and accessories. The feldspar is mostly oligoclase with composition of $An_{17}Ab_{82}Or_1$, whereas the alkali feldspar is in less amount.

The mafic mineral content is characterized by aggregates of amphibole, biotite, clinopyroxene that is often altered to amphibole, chlorite, opaque minerals, zircon and apatite (plate 9). Minor pyroxene with colourless cores and green rims can be found. The core is augite, while the rim is an actinolitic amphibole.

Amphibole is the dominant mafic mineral in the syenites with several types present. The principal type is a greenish brown ferro-horblende and greenish blue hastingsitic hornblende. They occur as primary, euhedral to subhedral interstitial grains. Greenish edenite and actinolite are present and often occur as reaction rims around pyroxene and oxides.

Biotite is black-brown and often contains exsolution lamellae (probably rutile). Paler brown or green biotite occurs sporadically. Biotite often occurs with, and encloses amphibole.

Opaque minerals include magnetite and ilmenite, and occur within mafic mineral aggregates. Zircon is a common accessory and occurs as euhedral crystals that are square in cross section. Apatite is less abundant than in the gabbros and diorites, and is usually prismatic in shape. Minor titanite occurs in the rock as euhedral crystals.

3.2.1.2 Quartz syenite

The quartz syenite is a coarse grained pinkish rock. The major minerals include alkali feldspar and oligoclase. Finer grained amphibole, biotite, clinopyroxene (minor), quartz, alkali feldspar, oxide and apatite are disseminated between the coarse alkali feldspar crystals (plate 10).

The alkali feldspar shows coarsely perthitic exsolution structure with composition $Ab_{61}Or_{38}An_1$. Oligoclase ($An_{16}Ab_{77}Or_7$) and albite is also present.

Amphiboles include ferro-hornblende, edenite and actinolite, as well as katophorite and winchite. The sodic-calcic amphiboles (katophorite and winchite) occur as subhedral grains and are pleochroic from deep brown to greenish brown. The winchite is often zoned with a deeper brown core and a lighter greenish brown rim.

Biotite forms small plates that often replace oxides and amphibole. Ilmenite and titanian magnetite are closely associated with mafic minerals in occurrence. Quartz is medium to fine grained, and occurs as interstitial grains, and as granophyric intergrowths with perthitic alkali feldspars. Coarse zircon is a common accessory mineral and shows square outline in cross section with strong zoning. The quartz syenites are poor in apatite.

3.2.2 The porphyritic dykes

There had been intrusions of many dyke rocks before and after the crystallization of the alkali syenites in centre 2. Comendite, and porphyritic nepheline-sanidine syenite samples are found and their petrography are outlined below.

3.2.2.1 Porphyritic quartz syenite dyke

This is a porphyritic quartz syenite dyke and has a similar mineral assemblage to the main body of quartz syenite. Phenocrysts are alkali feldspar and quartz.

3.2.2.2 Comendite

It is a porphyritic peralkaline rhyolite. Oligoclase and alkali feldspar phenocrysts are embedded in a fine-grained matrix which is composed of fibrous ferro-edenite, small platy perthite, quartz and oxides. Biotite occurs as an alteration product of the amphibole and oxides. Minor carbonate ocelli occur in the rock. The comendite is interpreted as an end crystallization product of the silica-oversaturated magma.

3.2.2.3 Porphyritic nepheline-sanidine phonolite dykes

These are the most abundant dykes occurring throughout the complex. They are composed of very coarse (10mm±) nepheline and feldspar (probably sanidine) phenocrysts in a dark groundmass that is made up of microlites of perthite, nepheline, aegirine augite, biotite, magnetite, apatite and fluorite. The sanidine occurs as euhedral coarse platy crystals. Nepheline occurs as green hexagonal tablets with oscillatory zoning and is sometimes altered to fine-grained aggregates of clay minerals including sericite. Aegirine-augite and biotite are present in minor amounts as small flakes. Magnetite is partly altered to titanite and hematite.

The occurrence of peralkaline porphyritic phonolite dykes indicates that magmatic activity became increasingly more alkaline and more silica-undersaturated.

3.3 Centre 3

Centre 3 contains strongly silica undersaturated intrusive rocks. Petrographically they are divided into foyaite (aegirine nepheline syenite), sodalite nepheline syenite, melteigite, ijolite and urtite. Thick fenites occur around the foyaite and ijolite.

3.3.1 Foyaite (aegirine nepheline syenite)

This is the major nephelinitic rock type exposed in the Big Spruce Lake complex. It is a medium to coarse grained cumulate rock (plate 11). Alkali feldspar and nepheline are the cumulus phases. The interstices are filled by aegirine augite, alkali feldspar and nepheline grains. As a result of the subparallel orientation of tabular alkali feldspars, the rock shows a trachytoid texture and thus may be referred to by the varietal name “foyaite”.

Accessory minerals are more abundant in the foyaite than in the quartz-free and quartz syenites and include titanite, fluorite, apatite, oxides, pyrochlore, carbocernaite (plate 12), perovskite, allanite, calcite and dolomite. The amount of oxide and apatite decreases, and the fluorite and carbonate content increases relative to that in the centre 1 and 2 rocks. Allanite, carbocernaite, pyrochlore and perovskite are not present in the rocks of centres 1 and 2 but do appear in the nepheline syenites.

The marginal, chilled foyaite is porphyritic. Alkali feldspar, nepheline and aegirine augite phenocrysts occur in a groundmass of small laths of alkali feldspar, aegirine, biotite and nepheline.

The feldspars are all alkali feldspars ($Ab_{43-9}Or_{57-91}$) and albite, ($Ab_{98}Or_2$) which are sometimes stained red. Plagioclase is not present. The alkali feldspar is mostly patchy with intergrowths of vague cryptoperthite to well-defined albite exsolution lamellae. There are two generations of feldspars, the first being coarse tablets, and the second, smaller laths. The laths produce a local trachytoid structure when they occur around coarse feldspar and aegirine augite.

The nepheline is euhedral with hexagonal or rectangular outlines. It is often altered to a mixture of sericite and clay minerals. Where there has been carbonate metasomatism, the nepheline is characterized by alteration to cancrinite. This forms veins crosscutting the nepheline or clusters around nepheline. Coarse nepheline crystals often contain lamellae of aegirine which also persists in the cancrinite when nepheline is altered. Bailey and Schairer (1966) demonstrated that there exists a solid solution of aegirine in nepheline and the texture suggests that the aegirine may crystallize in equilibrium with nepheline.

The aegirine augite is pleochroic from light green to deep green. There are usually two generations of pyroxene. The first consists of coarse to medium grained dipyramidal crystals interstitial to the framework of alkali feldspars. The second generation forms fibrous needles that occur in streaks or ragged fringes next to the alkali feldspars and nephelines.

Pyrochlore is found in biotite as small inclusions. It occurs as small (<50μm) reddish brown rounded crystals and is also found in the melteigite, ijolite and carbonatites.

Titanian magnetite is often altered to titanite or hematite. Sodalite occurs as poikilitic crystals with nepheline, or as veins. Nepheline is embayed by sodalite, indicating that sodalite was formed later. Fluorite and apatite occur as grains that are interstitial to, or inclusions in, aegirine and nepheline.

Calcite occurs as interstitial polycrystalline ocelli in the foyaite (plate 13). Such ocelli are generally interpreted as having formed by the solidification of immiscible drops of a carbonatite magma contained within a silicate magma (Roedder, 1979). Rounded blebs of calcite are also found in the alkali feldspar. The texture of the interstitial carbonate is very common in the nepheline syenite and probably represents immiscible carbonate droplets crystallized from a melt that was possibly composed of CO_2-rich nepheline syenite melt and a carbonatite melt (Andersen, 1988).

Locally, foyaite pegmatite occurs, and is rich in aegirine augite (> 50%). The aegirine augite is coarse to fine grained, and prismatic to fibrous and densely packed. The interstices are occupied by alkali feldspar, nepheline and carbonate ocelli.

Blue riebeckite is locally present. It occurs as stellate or fibrous clusters and grows into aegirine (plate 14) and occasionally into feldspar. Tiny brown biotite is also present. Also, red-brown biotite is present as veinlets and rims on aegirine-augite. The amphibole and mica are probably late subsolidus products, formed at the expense of the aegirine-augite by alkali and volatile metasomatism.

The characteristic minerals cancrinite, carbonate, fluorite and sodalite indicate that CO_2 and halogens were the dominant volatiles during crystallization of the nepheline syenites.

3.3.2 Sodalite nepheline syenite

Alkali feldspar, nepheline, sodalite and cancrinite make up the bulk of this rock. The alkali feldspar is patchy perthite. Nepheline is often rimmed or veined by cancrinite or is otherwise homogeneous.

Sodalite either occurs as a primary liquidus phase in association with nepheline, or occupies fractures as masses or veinlets. It has been suggested that the late stage masses of sodalite could be the product of crystallization from a Na- and Cl-enriched fluid that separated immiscibly from silicates (Woolley & Platt, 1988).

There are two generations of cancrinite. The first occurs as elongate clusters rimming nepheline. The second is contained in sodalite patches as small flakes.

Biotite is a minor mineral. It occasionally contains U-bearing perovskite (determined by microprobe) that produces radioactive halos.

3.3.3 Titanite melteigite

This rock is melanocratic and composed of aegirine-augite (> 50%), abundant nepheline (mostly altered to cancrinite), titanite and minor amounts of opaque minerals and perthitic alkali feldspar. The cumulus phases are aegirine-augite, titanite and opaque phases (plate 15). Nepheline and alkali feldspar are intercumulus phases. The titanite often contains apatite inclusions. Pyrochlore is locally abundant in aegirine augite (plate 16).

3.3.4 Ijolite

The ijolite (plate 17) is composed essentially of equal amounts of blocky nepheline and aegirine augite with minor alkali feldspar, sodalite, biotite, titanite, opaque phase, calcite, and apatite.

Fresh nepheline contains abundant needles of aegirine, which form parallel lamellae along the cleavage in nepheline. Clusters of cancrinite frequently rim nepheline. The aegirine-augite contains abundant inclusions of apatite, purple fluorite, titanite, perovskite and carbocernaite. The carbocernaite is deep brown, anisotropic and has high relief.

The ijolite intruded the Northern Foyaite as 4 small masses and the contact between foyaite and ijolite is gradational (Martineau, 1970).

3.3.5 Urtite

This is a coarse grained leucocratic rock containing over 70% nepheline and 10-20% aegirine-augite, with biotite and alkali feldspar in very minor amounts. The nepheline is mostly altered to cancrinite in veins and clusters (plate 18).

3.3.6 Phonolite

This dark-green, fine-grained rock occurs as dyke swarms in foyaite and ijolite (Martineau, 1970). The dominant constituents are microperthite, aegirine-augite and nepheline (plate 19). The aegirine-augite occurs as tiny prisms in the interstices of poikilitic alkali feldspar and nephelines. Titanite, apatite, fluorite, and cancrinite are present in small amounts. The phonolite is interpreted as an end crystallization product of the silica-undersaturated plutonic rock series.

3.3.7 Fenite

Fenitization around carbonatite dyke margins is weak and marginal effects are largely confined to the shattering of the country rock, the introduction of calcite and dolomite and saussuritization of feldspars (Martineau, 1970).

However, fenites developed strongly around the larger intrusive foyaite bodies and are composed dominantly of medium grained perthite with some microcline and plagioclase. Aegirine-augite, biotite, epidote, calcite, magnetite and ilmenite are fine to medium grained and are enclosed by the feldspar. Minor quartz is present. The feldspar is often reddish. Plagioclase contains disseminated sericite and usually has perthite rims.

The fenite around the biotite pyroxenite pipes is a quartz-poor, aegirine syenite. The feldspar includes albite and microcline which are extensively altered to sericite, and stained brick-red by hematite. Aegirine occurs as large elongate prisms or fibres. Biotite, hematite, calcite, talc, apatite and unidentified oxides are present.

3.4 Centre 4 -- The carbonatites

According to Martineau (1970), these rocks were intruded as dykes and pipes, and are represented by dolomitic and calcitic carbonatites. The calcite carbonatites are centred on the radial fracture pattern of the Big Spruce Island. The dolomite-ankerite carbonatites are arranged in a radial and cone-sheet pattern around the ankerite silica-carbonatite breccia pipe.

3.4.1 The calcite carbonatite

This rock is coarse grained with calcite as the major mineral. Various types of calcite carbonatites are present, however in terms of their accessory mineral assemblage:

(1) Apatite carbonatite. This rock is characterized by an abundance of apatite up to 20%(plate 20).

(2) Silicate carbonatite. This rock type is characterized by presence of various amounts of silicate minerals, mainly alkali feldspars (albite and K-feldspar) which are fine-grained and form rounded aggregates enclosed in a calcite groundmass. Epidote is present in various amount. This texture indicates immiscible separation between carbonates and silicates and suggest that the rock is essentially a silica-carbonatite (plate 21).

(3) Fluorite carbonatite. This rock is characterized by an abundance of fluorite up to 30% (plate 22).

The carbonatites are often foliated with strings of biotite (plate 23) and purple fluorite. Fluorite also occurs as scattered crystals. Other accessory minerals contained in the carbonatite include aegirine-augite, nepheline, pyrochlore, carbocernaite, allanite, zircon, ilmenite, titanian magnetite, hematite, pyrite, and sphalerite.

Allanite is present as numerous small grains and forms necklaces of grains, or appears as streaks within the carbonatite (plate 24). Apatite forms euhedral stubby prisms which are disseminated interstitially between calcites. Apatite in most rock types in the Big Spruce Lake complex contains abundant primary aqueous fluid inclusions. Epidote is a late mineral and is distributed in clots in the rock. Titanian magnetite occurs as small cubes. Barite was found in small quantities. Its paragenetic relationship is not clear because of the lack of a distinctive petrographic texture.

3.4.2 The dolomite carbonatite

This rock is composed dominantly of brown, interlocking dolomite crystals. Ankerite, magnetite, ilmenite, biotite, serpentine, apatite, barite, pyrite, and fluorite are present in various amounts.

3.4.3 The Big Spruce Island carbonatite pegmatites

According to Martineau (1970), the northern foyaite at Big Spruce Island is regarded as the centre of calcite carbonatite activity by virtue of its fracture pattern, the intense metasomatism and zoned pegmatites. The following zonation is seen outwards from the center of the zoned pegmatite:

core: carbonatite

rim zone outwards from core: foyaite -> ijolite -> magnetite-rich foyaite.

According to Martineau (1970), the carbonatite pegmatites are essentially calcite, containing also minor aegirine, biotite, and magnetite.

3.5 Centre 5 -- The Moose Island satellite rocks

These rocks are characteristically rich in potassium and contain abundant biotite. Rock types include melanocratic syenite, biotite pyroxenite, biotite peridotite and lamprophyres occurring in distinct dykes or pipe-like bodies. Of the lamprophyres, only the minettes are fresh; other types are extensively hydrothermally altered and difficult to identify.

3.5.1 Melanocratic syenite

This rock has a deep color due to the presence of abundant augite. The texture of the rock varies from porphyritic to coarsely crystalline. In coarsely crystalline rocks, the mafic minerals include augite, biotite, olivine, and magnetite, which are embedded in a poikilitic groundmass of perthitic feldspar (plate 25). Apatite occurs commonly as stubby inclusions in biotite, or as slender prisms.

The feldspar is a coarse-grained microperthite. It is anhedral, lacks twinning and presumably crystallized late in the sequence.

The augite is euhedral to subhedral, and is embayed by the surrounding microperthite. It often has rims containing biotite, actinolite and chlorite. Lamellar twinning and sector zoning are common in augites.

Olivine, if present, is mostly fresh. It is somewhat altered to networks of presumed greenish 'bowlingite', an alteration product consisting of smectite, sericite and other phyllosilicates.

The biotite is reddish-brown and occasionally enclosed by augite. Coarse biotite also occurs as megacrysts in the rock. Actinolitic amphibole occurs as subsolidus rims surrounding augite.

Chilled marginal melanocratic syenite is porphyritic. Clinopyroxene phenocrysts are euhedral, medium to coarse grained in a groundmass of fine grained laths of microperthite, clinopyroxene, biotite and accessory minerals.

3.5.2 Biotite pyroxenite

This is a medium grained rock composed dominantly of clinopyroxene and biotite (plate 26). Biotite forms dark brown, poikilitic crystals that commonly contain exsolution lamellae, which are assumed to be ilmenite or rutile.

The clinopyroxene is diopside. It forms subhedral to euhedral prisms and is rimmed by a thin secondary green amphibole. Diopside phenocrysts are also enclosed by biotite forming a corona texture.

Apatite, titanite, alkali feldspar, calcite, and magnetite are interstitial to the major minerals.

Some biotite pyroxenites contain abundant country rock (granite) and quartz xenoliths. The xenoliths are clearly not stable for they are rounded and corroded by reaction rims that consist of biotite laths. The granite xenoliths contains quartz, microcline, and plagioclase. The quartz macrocrysts must be crustal xenoliths because the host rock is nepheline-normative (Cavell, 1986) and could not precipitate quartz.

3.5.3 Biotite peridotite

The biotite peridotite is highly carbonated. It contains abundant carbonate ocelli or the peridotite occurs as xenolith in carbonatite matrix. The rock is fine grained and consists of granular olivine, biotite, diopside and opaque minerals (plate 27). Accessory minerals include calcite, apatite, titanite, fluorite and epidote.

3.5.4 Minette

The minette contains phenocrysts of red-brown phlogopite and clinopyroxene set in a matrix that consists of fine-grained phlogopite, clinopyroxene, alkali feldspar, albite, apatite, carbonate, titanite and oxides (titanian magnetite and ilmenite) (plate 28).

The tabular mica phenocrysts (5-10 mm) are pseudohexagonal. Zoning is ubiquitous and includes sharp zoning from a pale yellow core (Mg-rich) surrounded by a narrow deep brown rim (slightly Fe-rich). Trellis lamellae are common in the phlogopite crystals. Phlogopite in the matrix is fine grained and often forms parallel growths around the oxides.

Clinopyroxene shows a pinkish (Ti-rich) absorption colour, and is mantled by actinolite and chlorite. Zeolite occurs in the groundmass as radiating sheafs. Opaque minerals include titanian magnetite, pyrite and chalcopyrite. Carbonate, apatite and alkali feldspar ocelli occur occasionally in the rock. A quartz xenocryst was found in the minette and was presumed to be a xenocryst from the country rock.

3.5.5 Lamprophyre

The rock (#2265) contains phenocrysts of clinopyroxene (augite) and amphibole (tschermakatic hornblende) and probably olivine set in a thoroughly altered groundmass which is composed of greenish chlorite, uralite and fine-grained oxides.

The augite and hornblende are typically uralitized and chloritized. Lamellar twinning and sector zoning are frequently seen in the augite. Fresh augite is zoned with a colourless core and greenish margin. The fresh core is augite, the rim is altered augite or uralite. Feldspar is not seen in the rock and is assumed to be altered.

Globular ocelli are abundant in lamprophyre #2272 (similar to #2265). The ocelli include a carbonate-epidote type (plate 29) and a quartz-bearing ocelli type. The minerals within the ocelli occur in clusters and include calcite, epidote, quartz, chlorite and a zeolite. The origin of the ocelli (especially the quartz ocelli) is enigmatic. Mitchell *et al.* (1991) ascribed the formation of ocelli in lamprophyres to liquid immiscibility. However, the quartz ocelli must be a crustal xenolith in the lamprophyre because the rock is nepheline-normative.

Chapter 4.
Mineral Chemistry.

4.1 Pyroxene

Compositions of pyroxenes analyzed by the electron microprobe are presented in Tables 1-4. The experimental methods used for mineral analyses are presented in Appendix 3. The nomenclature, structural formulae and end-members were determined by the computer program PX (Gomez, 1990) which is based on the new IMA classification and nomenclature for pyroxene minerals (Morimoto, 1989). The procedure for this classification is shown in Appendix 4.

The clinopyroxenes in the Big Spruce Lake alkaline complex range from calcic through sodic calcic to sodic species (Fig. 2). The calcic pyroxenes are further plotted on En-Fs-Di-Hd quadrilateral diagram (Fig. 3). They are essentially calcic titanian augite to ferroaugite in the silica-saturated and oversaturated rocks, and diopside in some of the centre 5 rocks. The sodic-calcic and sodic clinopyroxenes are shown in QUAD-Jd-Ae triangular diagram (Fig. 4). They include aegirine-augite and aegirine, the latter of which occurs in nepheline-bearing rocks. The variation of the pyroxene compositions follows a typically alkaline trend (Rock, 1978) from diopside through titanian augite, augite, aegirine-augite to aegirine (Fig. 5). The trend is characterized by a large increase in aegirine content after crystallization of quartz syenite without significant enrichment in hedenbergite.

Cation variation in terms of Mg# (=100xMg/(Mg+Fe^T)) of the pyroxenes is plotted in Figs. 6 and 7. In the magnetite pyroxenite and gabbro, the clinopyroxene has relatively high Al, Ca, Mg and Ti, and markedly low Fe^{2+}, Fe^{3+} and Na contents. The Mg# in these pyroxenes ranges from 74-68.

Pyroxenes in diorites and quartz-free syenites evolve with slightly decreasing Mg, Ti, Al and slightly increasing Fe^{2+} contents with Mg# ranging from 64-48. Ca, Fe^{3+}, and Na contents remain constant in gabbros, diorite and quartz-free syenite. Therefore the major substitution in the gabbro, diorite and quartz-free syenite is of the $CaMg=CaFe^{2+}$ type.

Pyroxenes in quartz syenites show some hedenbergite enrichment (Fig. 5) relative to quartz-free syenite. Concentrations of Mg, Ca, Ti and Al decrease while Fe^{2+} increases to the highest level in all the clinopyroxenes of the complex without showing Na and Fe^{3+} enrichment (Figs. 6 & 7). Also, Si has increased slightly while Al decreases, indicating minor substitution of Si=Al in the tetrahedral site. Mg# decreases to the range of 48-41. The variation of pyroxene compositions in the silica-saturated rocks reflects a gradual Mg, Ca depletion and Fe enrichment and this may be caused by a fractional crystallization process.

Pyroxenes in centre 5 rocks (biotite pyroxenite, biotite peridotite and lamprophyre) are the least evolved species in the whole complex as shown by their high Mg# (77-81). The pyroxene in biotite pyroxenite is diopside, which is rich in Mg and Ca but poor in Fe^T, Al and Na compared with augites in gabbros. The diopside is sometimes zoned with an altered augite rim that has relatively higher Na, Fe and lower Ca and Mg (Table 2). The pyroxene in lamprophyre (#2265) is augite. However, most pyroxenes in the lamprophyres are substantially altered to actinolite and chlorite.

Sector zoning is characteristic of the clinopyroxenes in the magnetite pyroxenite and in the centre 5 rocks. Dowty (1976) proposed that cation absorption into some proto sites on the growing faces of crystals favours small, highly charged ions (Al^{3+}, Fe^{3+} and Ti^{4+}) and resulted in the metastable phenomenon of sector zoning.

In the foyaite-ijolite rock series, the pyroxenes are aegirine-rich species including sodic calcic aegirine-augite and sodic aegirines. Fe^{3+} and Na enrichment characterizes the trend of these pyroxenes (Figs. 6 & 7) and indicates enhanced alkali contents in the silica-undersaturated liquids at this stage. Mg, Ca and Fe^{2+} contents decrease drastically whereas Ti shows marked variation. The Mg# ranges from 0.9 to 25. These pyroxenes are all nearly Si-saturated ($Si \geq 2.00$) and this precludes significant substitution in the tetrahedral sites. The Fe^{3+} enrichment is probably at the expense of Mg and Fe^{2+} and indicates that the aegirine augite represents an extension of precipitation of the augite trend. The solid solutions between Ca-clinopyroxenes, Na-Ca clinopyroxenes and Na-clinopyroxenes are thus controlled by CaMg=CaFe^{2+} and Ca(Mg,Fe^{2+}) = NaFe^{3+} substitutions. The substitutions show variation with the degree of silica content of the magma. CaMg=CaFe^{2+} is predominant in the silica-saturated and oversaturated environment prior to NaFe^{3+} enrichment. However, in the silica-undersaturated environment, the substitution is Ca(Mg,Fe^{2+})=NaFe^{3+} as Na and Fe^{3+} become enriched.

According to Woolley & Jones (1992), the degree of peralkalinity, the stage at which the peralkalinity first develops and the fO_2 of the evolving liquids have a profound effect on the trend of pyroxene evolution. They propose that the diopside - aegirine-augite - aegirine trend is a function of a higher fO_2 associated with a development of peralkaline liquids (Platt and Woolley, 1986). The sodium enrichment is enhanced when fO_2 rises above QFM buffer (Stephenson & Upton, 1982). The Fe^{3+}/Fe^{2+} ratio tends to be increased by increasing alkalinity (Carmichael *et al.*, 1974; Fudali, 1965). Thus, the aegirine enrichment in the silica-undersaturated rocks reflects the onset of peralkalinity and higher fO_2 conditions in the melt.

Two generations of clinopyroxenes are present in some nepheline syenites. The early generation is aegirine augite, whereas the late generation is aegirine. The crystallization of aegirine reflects significant fractionation of augite and aegirine-augite. The coexistence of aegirine-augite and aegirine in the nepheline-bearing rocks reflects a complex history of liquid-crystal fractionation and reaction.

The partitioning of Ca into early calcic pyroxenes and Na and Fe^{3+} into the liquid for the Big Spruce Lake magma is evidenced by the pyroxene compositions. The early pyroxenes are Na- and Fe^{3+}-poor, Ca rich augites. The fractionation of these pyroxenes provides a mechanism to drive the liquid to more alkaline and Fe^{3+}-rich compositions. The variation from augite to aegirine-augite and aegirine becomes pronounced at a later stage in nepheline syenites because of the onset of peralkalinity in the liquid. Thus, a continuous variation from augite to aegirine augite and aegirine is produced. The trend of decreasing Mg and Fe^{2+} and increasing Na and Fe^{3+} in clinopyroxenes is a result of fractional crystallization.

Table 1. Average pyroxene compositions: in magnetite pyroxenite and gabbro.

Rock #	pc-81001	pc-81130	pc-82193	pc-82207	pc-82196	pc-81275	pc-82198	pc-81492	pc-82116
SiO2	50.79	51.24	50.75	51.20	51.51	51.09	51.51	50.77	51.36
TiO2	1.20	1.06	0.93	0.96	0.84	1.11	0.96	1.39	0.78
Al2O3	3.06	3.38	2.38	2.61	2.27	2.79	2.16	3.05	2.3
Cr2O3	0.06	0.28	0.01	0.02	0.02	0.01	0.01	0.01	0.05
FeO*	9.02	8.17	11.19	10.32	9.83	10.49	11.54	10.32	11.19
MnO	0.19	0.16	0.27	0.27	0.25	0.24	0.3	0.24	0.34
MgO	14.45	14.40	12.94	13.52	13.78	13.64	13.31	13.38	13.46
CaO	20.67	21.43	20.38	21.56	20.69	20.86	20.58	20.82	20.18
Na2O	0.52	0.51	0.53	0.48	0.48	0.50	0.48	0.56	0.53
Total	99.96	100.63	99.38	100.94	99.67	100.73	100.85	100.54	100.19
Structural formulae based on 4 cations and 6 oxygens									
Si	1.886	1.887	1.915	1.895	1.927	1.895	1.916	1.888	1.919
AlIV	0.114	0.113	0.085	0.105	0.073	0.105	0.084	0.113	0.081
T site	2.000	2.000	2.000	2.000	2.000	2.000	2.000	2.001	2.000
Ti	0.034	0.029	0.026	0.027	0.024	0.031	0.027	0.039	0.022
AlVI	0.020	0.034	0.021	0.009	0.027	0.017	0.011	0.021	0.020
Fe2+	0.217	0.203	0.304	0.244	0.275	0.263	0.306	0.267	0.296
Fe3+	0.064	0.049	0.050	0.076	0.032	0.062	0.053	0.054	0.054
Mn	0.006	0.005	0.009	0.008	0.008	0.008	0.009	0.008	0.011
Mg	0.800	0.790	0.728	0.746	0.768	0.754	0.738	0.741	0.750
Ca	0.822	0.846	0.824	0.855	0.830	0.829	0.820	0.829	0.808
Na	0.037	0.036	0.039	0.034	0.035	0.036	0.035	0.040	0.038
M site	2.000	1.992	2.001	1.999	1.999	2.000	1.999	1.999	1.999
Total	4.000	3.992	4.001	3.999	3.999	4.000	3.999	4.000	3.999
no. of anal. pts.	8	7	5	6	7	6	5	5	10
classification	augite	augite	augite	augite	augite	augite	augite	augite	augite

Note: pc-81001, pc-81130 & pc-82193: magnetite pyroxenite; pc-82207, pc-82196 & pc-81275: Leucocratic Laminated Gabbro; pc-82198 & pc-82116: Big Feldspar Gabbro.

pc-81492: Rhythmic Banded Gabbro.

* = total iron as FeO.

no. of anal. pts. = number of analytical points (the same in the subsequent tables).

Table 2. Average pyroxene compositions: in diorite and centre 5.

Rock #	pc-81126a	pc-81272	pc-82118	pc-81065 core	pc-81065 rim	pc-82262	pc-82265
SiO2	51.85	51.36	51.71	52.72	52.10	52.02	49.89
TiO2	0.62	0.67	0.56	0.87	0.76	0.70	1.77
Al2O3	1.55	2.22	1.45	1.25	1.48	1.32	3.68
Cr2O3	0.01	0.04	0.02	0.00	0.04	0.12	0.09
FeO*	12.86	12.4	11.55	6.79	9.77	6.83	8.18
MnO	0.38	0.35	0.28	0.16	0.22	0.14	0.15
MgO	12.91	13.14	12.8	14.98	12.79	16.56	15.03
CaO	19.7	19.59	21.57	22.28	19.77	22.74	21.51
Na2O	0.4	0.71	0.54	0.84	1.74	0.32	0.58
Total	100.28	100.48	100.48	99.89	98.67	100.75	100.88
Structural formulae based on 6 oxygens							
Si	1.950	1.917	1.933	1.944	1.958	1.897	1.828
AlIV	0.050	0.083	0.064	0.054	0.042	0.057	0.159
Fe3+	0.000	0.000	0.003	0.000	0.000	0.046	0.013
T site	2.000	2.000	2.000	1.998	2.000	2.000	2.000
Ti	0.018	0.019	0.016	0.024	0.021	0.019	0.049
AlVI	0.019	0.015	0.000	0.000	0.024	0.000	0.000
Fe2+	0.380	0.305	0.285	0.140	0.207	0.078	0.124
Fe3+	0.025	0.082	0.074	0.070	0.101	0.084	0.113
Mn	0.012	0.011	0.009	0.005	0.007	0.004	0.005
Mg	0.724	0.731	0.713	0.823	0.716	0.900	0.821
Ca	0.794	0.783	0.864	0.880	0.796	0.889	0.844
Na	0.029	0.051	0.039	0.060	0.127	0.023	0.041
M site	2.001	1.997	2.000	2.002	1.999	1.997	1.997
Total	4.001	3.997	4.000	4.000	3.999	3.997	3.997
no. of anal. pts.	8	6	5	4	4	7	5
classification	augite	augite	augite	diopside	augite	diopside	augite

Note: pc-81126a, pc-81272 & pc-82118: diorite; pc-81065: biotite pyroxenite; pc-82262: biotite peridotite; pc-82265: lamprophyre.
* = total iron as FeO.

Table 3. Average pyroxene compositions: in alkali syenite and nepheline syenite.

Rock #	pc-81006	pc-81005b	pc-81083	pc-81289	pc-81289	pc-81082	pc-81082
SiO2	51.00	53.03	51.62	51.01	50.58	51.06	52.37
TiO2	0.93	0.13	0.19	1.39	0.67	0.91	0.57
Al2O3	2.03	0.89	0.40	0.80	0.88	0.87	1.04
Cr2O3	0.00	0.00	0.00	N/D	N/D	N/D	N/D
FeO*	12.24	20.34	19.40	25.59	24.86	25.08	26.84
MnO	0.40	0.45	0.60	0.55	0.66	0.60	0.17
MgO	12.37	10.76	7.74	1.03	1.42	1.20	0.90
CaO	19.66	11.70	20.03	6.90	9.92	9.31	2.50
Na2O	0.53	0.23	0.46	9.33	7.65	8.10	12.24
Total	99.16	97.53	100.44	96.60	96.64	97.13	96.63
Structural formulae based on 4 cations and 6 oxygens							
Si	1.933	2.109	2.002	2.003	2.002	2.008	2.007
AlIV	0.067	0.000	0.000	0.000	0.000	0.000	0.000
T site	2.000	2.109	2.002	2.003	2.002	2.008	2.007
Ti	0.027	0.004	0.006	0.041	0.020	0.027	0.016
AlVI	0.024	0.042	0.018	0.037	0.041	0.040	0.047
Fe2+	0.345	0.676	0.617	0.255	0.322	0.317	0.045
Fe3+	0.042	0.000	0.012	0.585	0.502	0.507	0.815
Mn	0.013	0.015	0.020	0.018	0.022	0.020	0.006
Mg	0.699	0.638	0.447	0.060	0.084	0.070	0.051
Ca	0.798	0.499	0.832	0.290	0.421	0.392	0.103
Na	0.039	0.018	0.035	0.710	0.587	0.617	0.909
M site	1.987	1.892	1.987	1.996	1.999	1.990	1.992
Total	3.987	4.001	3.989	3.999	4.001	3.998	3.999
no. of anal. pts.	5	5	4	7	5	5	7
classification	augite	augite	augite	aegirine-augite	aegirine-augite	aegirine-augite	aegirine

Note: pc-81006: quartz-free syenite; pc-81005b & pc-81083: quartz syenite;
pc-81289 & pc-81082: nepheline syenite.
In pc-81005, the augite is partly altered.
* = total iron as FeO. N/D = Not/Determined.

Table 4. Average pyroxene compositions: in nepheline syenite.

Rock #	pc-81223	pc-81223	pc-81169	pc-81194	pc-81418	pc-81418
SiO2	54.00	52.05	51.97	52.27	52.96	53.05
TiO2	0.21	0.62	0.34	0.27	0.62	0.58
Al2O3	4.00	0.97	0.95	1.11	1.00	0.96
FeO*	25.83	25.16	22.31	25.18	28.89	29.60
MnO	0.03	0.64	0.79	0.77	0.07	0.06
MgO	0.12	2.17	4.20	2.33	0.34	0.27
CaO	0.28	8.50	13.60	8.05	0.75	0.53
Na2O	13.90	8.78	5.76	9.02	13.22	13.53
Total	98.37	98.89	99.92	99.00	97.85	98.58
Structural formulae based on 4 cations and 6 oxygens						
Si	2.001	1.990	1.986	1.989	2.003	1.990
AlIV	0.000	0.010	0.014	0.011	0.000	0.010
T site	2.001	2.000	2.000	2.000	2.003	2.000
Ti	0.006	0.018	0.010	0.008	0.018	0.016
AlVI	0.175	0.034	0.029	0.039	0.045	0.033
Fe2+	0.000	0.214	0.321	0.177	0.030	0.000
Fe3+	0.801	0.591	0.392	0.624	0.884	0.928
Mn	0.001	0.021	0.026	0.025	0.002	0.002
Mg	0.007	0.124	0.239	0.132	0.019	0.015
Ca	0.011	0.348	0.557	0.328	0.030	0.021
Na	0.999	0.651	0.427	0.665	0.969	0.984
M site	2.000	2.001	2.001	1.998	1.997	1.999
Total	4.001	4.001	4.001	3.998	4.000	3.999
no. of anal. pts.	5	3	5	7	6	5
classification	aegirine	aegirine-augite	aegirine-augite	aegirine-augite	aegirine	aegirine

Note: pc-81223: nepheline syenite; pc-81169: melteigite; pc-81194: urtite;
pc-81418: riebeckite-metasomatized nepheline syenite.
* = total iron as FeO.

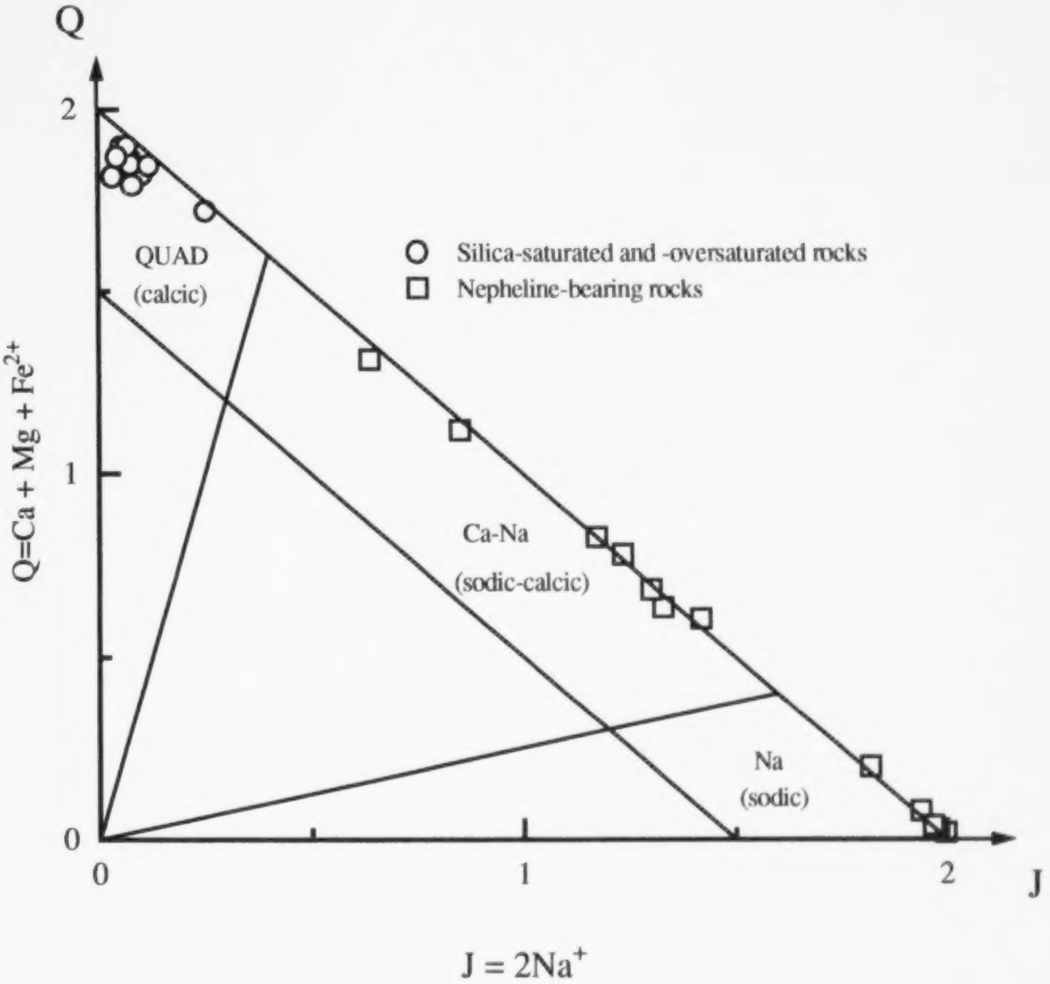

Fig. 2: Q-J diagram for clinopyroxene classification, after Morimoto and Kitamura (1983).

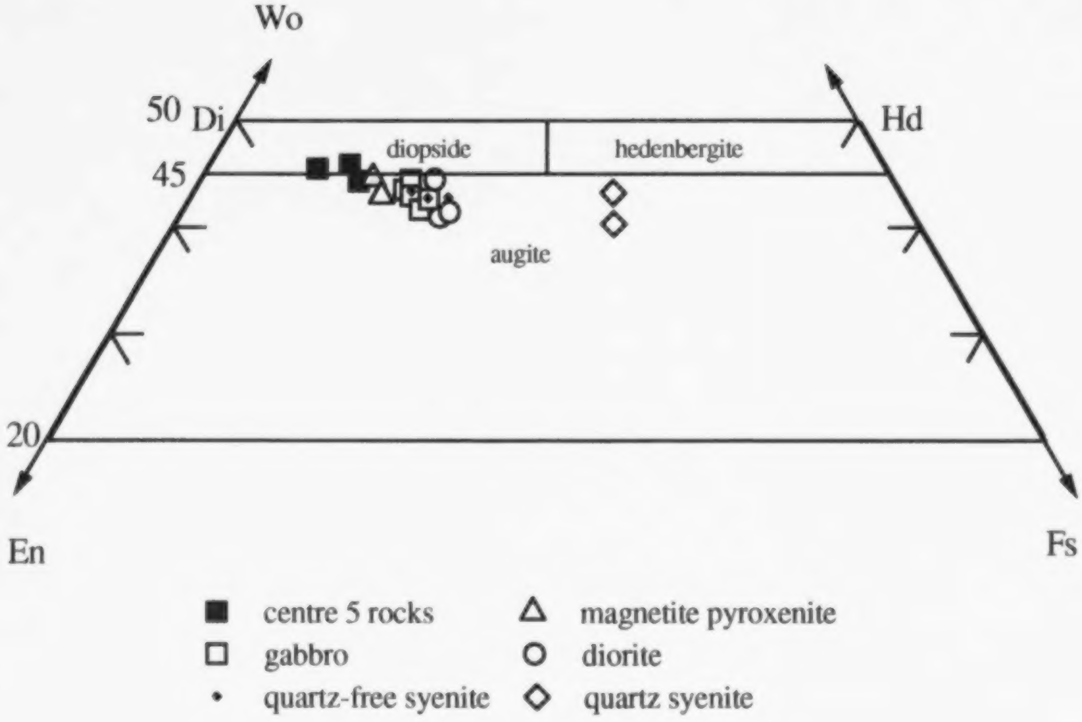

Fig. 3: Compositional ranges of calcic clinopyroxenes in the quadrilateral enstatite - diopside - hedenbergite - ferrosilite (En - Di - Hd - Fs), based on Morimoto (1989).

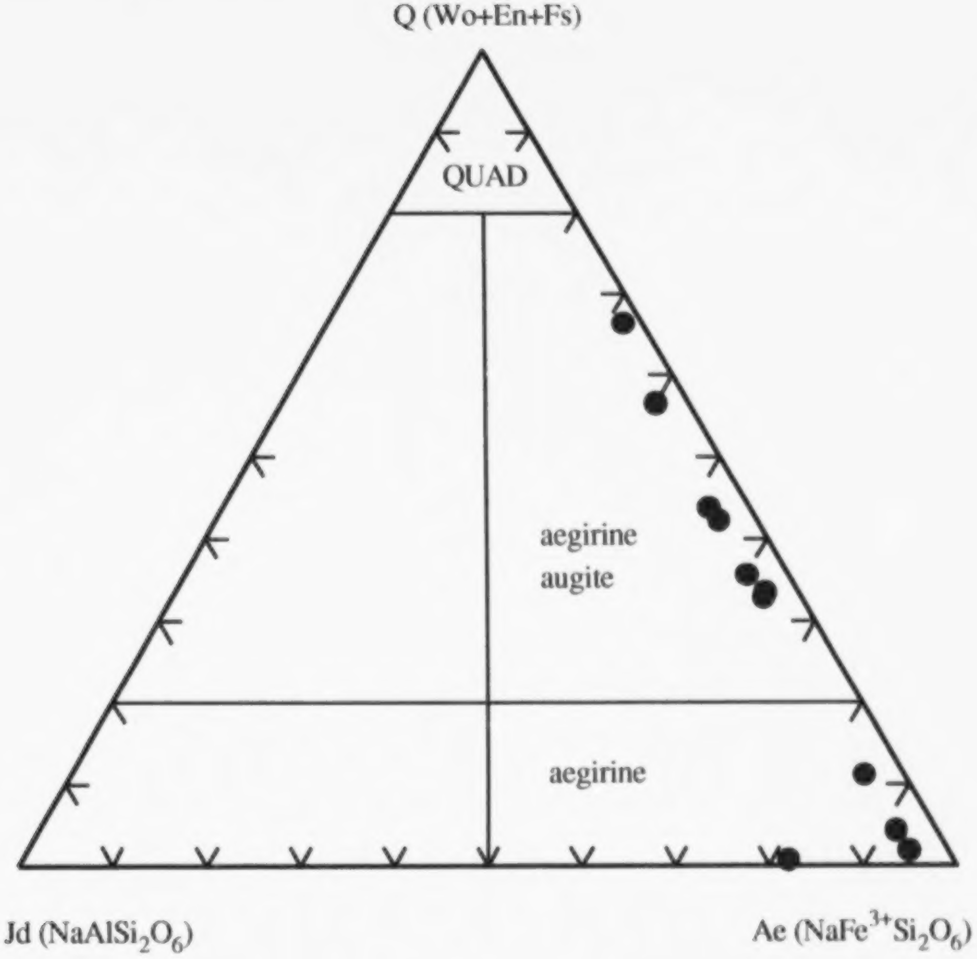

Fig. 4: Na-Ca and Na-clinopyroxene compositions from the foyaite, melteigite and ijolite, plotted in terms of QUAD - Jd - Ae. QUAD represents the calcic pyroxene area, the diagram is after Morimoto (1989).

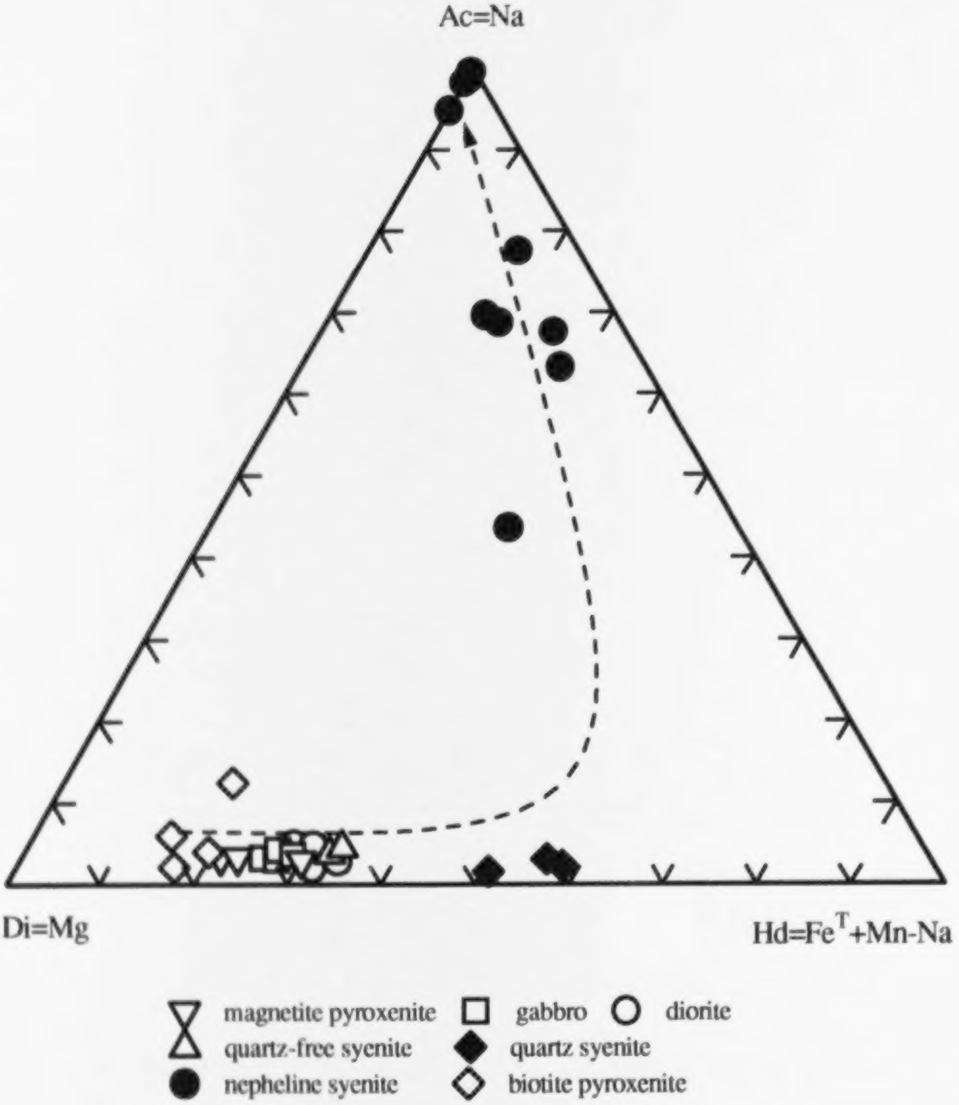

Fig. 5: Compositional variation of clinopyroxenes plotted in terms of aegirine-diopside-hedenbergite (Di-Ac-Hd) components, after Bedard *et al*. (1988). The arrowed and dashed line indicates the pyroxene trend in the Big Spruce Lake complex .

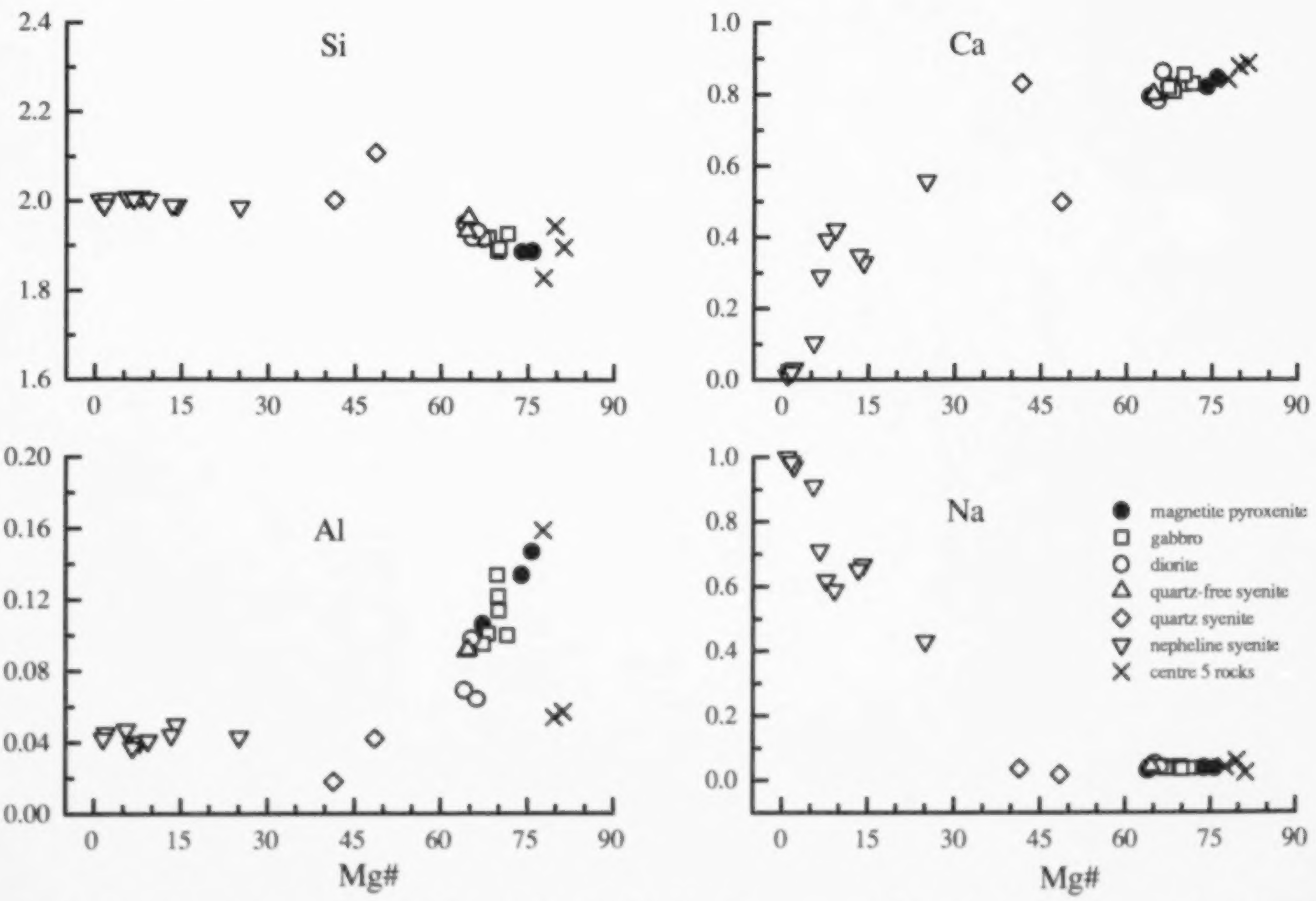

Fig. 6: Element variations (Si, Al, Ca, Na) as refered to Mg# in clinoproxenes of the Big Spruce Lake alkaline complex. Note: one point, sample pc-81005, lies off trends for Si, Ca & Al. This is probably a reflection of its alteration (see Table 3).

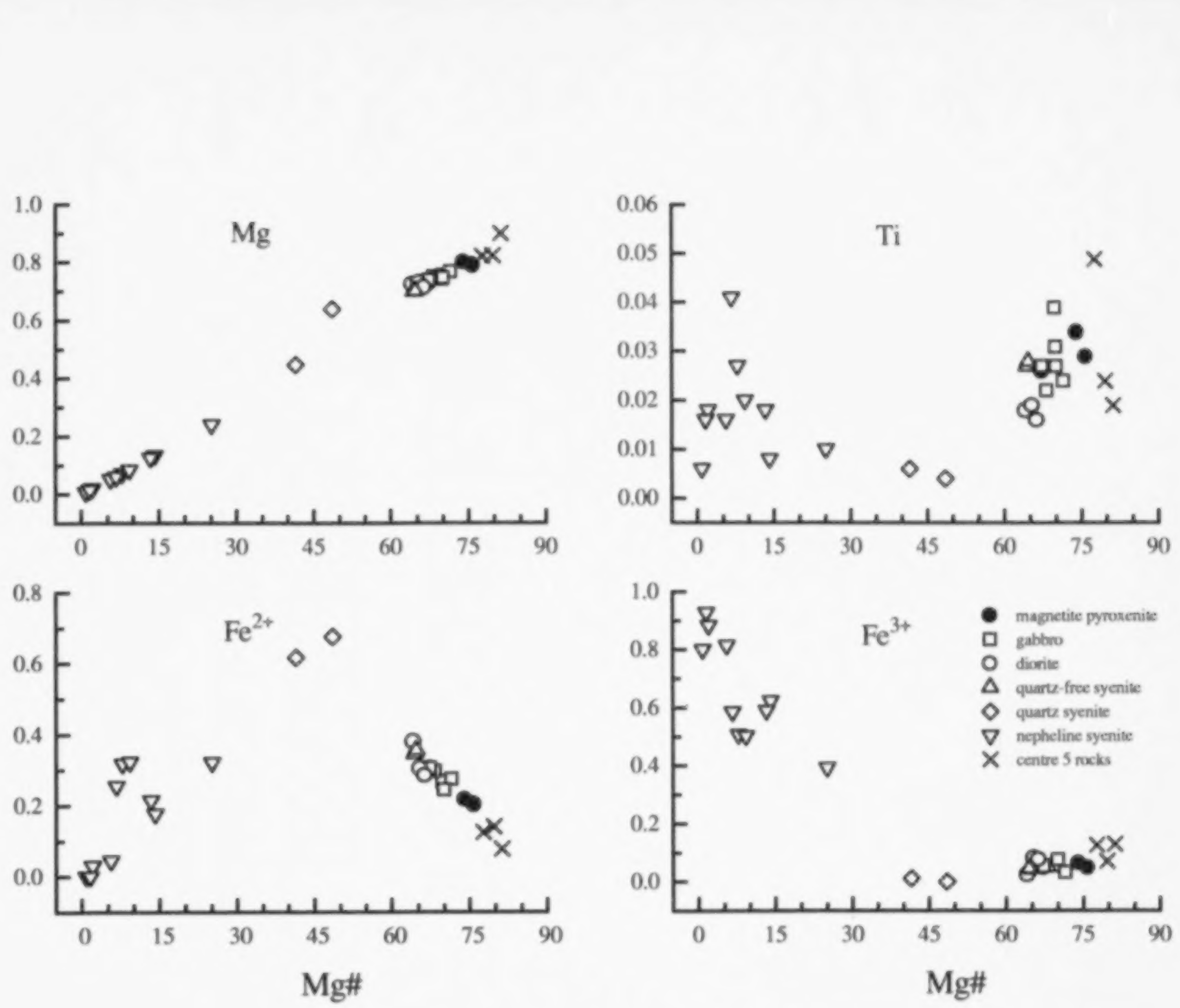

Fig. 7: Element variations (Mg, Ti, Fe^{2+}, Fe^{3+}) as referred to Mg# in clinopyroxenes in the Big Spruce Lake alkaline complex.

4.2 Amphibole

Amphiboles are one of the dominant constituent minerals in the saturated rocks. Their compositions and structural formulae are presented in Table 5-9. Individual amphibole grains are generally chemically homogeneous. The calculation of amphibole formulae is based on 23 oxygens and is produced by a computer program EMP-AMPH which is based on IMA classification (Leake, 1978) and written by Mogessie *et al.* (1988). The method and procedures for the calculation and classification are shown in Appendix 5.

In the Big Spruce Lake complex, amphibole covers an extensive range of species from calcic, sodic-calcic to sodic species, including kaersutite, hastingsite, hastingsitic-hornblende, edenitic-hornblende, edenite, ferro-hornblende, actinolite, ferro-winchite, katophorite and riebeckite, according to the IMA classification (Leake, 1978). A typical feature of the complex is that primary amphiboles are absent from nepheline-bearing rocks and carbonatites in centres 3 and 4. Only subsolidus riebeckite is found in the locally metasomatized zone in centre 3. In centre 5 rocks, a tschermakitic-hornblende is found in the lamprophyres.

The complete range of amphiboles is shown in Fig. 8 in terms of (Al^{IV}+Ca) and (Si+Na+K) cations, after Giret (1980). The general evolutionary trend of the amphiboles is kaersutite -> hastingsitic amphibole -> hornblendic amphibole -> edenitic amphibole -> katophorite -> winchite -> riebeckite as the rock types vary from magnetite pyroxenite -> gabbro -> diorite -> quartz-free syenite -> quartz syenite -> nepheline syenite. The amphibole trend is parallel to the coexisting pyroxene evolutionary trend towards Mg depletion and alkali and Fe^{3+}/Fe^{2+} enrichment (Fig. 9). They followed a path from initially alkali-poor toward increasing Fe^{2+}:Mg ratio, similar to the calcic clinopyroxene trend, and then towards increasing alkalinity corresponding to the aegirine-augite trend. The sequential crystallization of calcic, sodic-calcic and sodic amphiboles is defined as the primary magmatic trend and reflects decreasing temperature and increasing oxygen fugacity (Mitchell, 1990).

In the magnetite pyroxenite, gabbros and diorites, the amphiboles are all calcic species and include kaersutite, hastingsite, pargasitic- and hastingsitic-hornblende to edenitic-hornblende, edenite and actinolite (Fig. 10). Primary phases are mainly kaersutite, pargasitic and hastingsitic amphiboles. They have high contents of Ti, K, Al and relatively low contents of Si. The uralitized phases are tremolite and actinolite and have low Ti, K and Al contents but high Si contents. Kaersutite phenocrysts have a very constant composition ($Mg\#=Mg/(Mg+Fe^T)=0.55-0.6$); rims of hastingsite and hastingsitic hornblende are more Fe-enriched ($Mg\#=0.25-0.35$). Hastingsite-apatite veins are found in the magnetite pyroxenite. Euhedral hastingsite and hastingsitic hornblende occur as inclusions in the apatite. These amphiboles have very low silica contents. However, they have high Al^{IV} contents, possibly reflecting a relatively high crystallization temperature (Gilbert *et al.*, 1982).

In the quartz-free syenite, amphiboles range from hastingsite to edenitic-hornblende, edenite and actinolitic-hornblende. They are more silicic and iron-rich. Kaersutite is found in minor amounts in augite.

The compositional variations of the calcic amphiboles correspond to a continuous solid solution series characterized by a decrease in Ti, Al and Mg content and $Mg/(Mg+Fe^{2+})$ ratio, as well as an increase in Si and Fe. Ca remains virtually constant. The series is dominated by (Na,Al)=Si and $Mg=Fe^{2+}$ substitutions that are similar to the substitution mechanisms in the clinopyroxenes of the complex.

In quartz syenite, amphiboles vary from end-member calcic species including titanian-magnesio hornblende, edenite, actinolitic-hornblende and actinolite (Fig. 10) to sodic-calcic species including katophorite and winchite (Fig. 11). Edenite occur in the groundmass of comendite. These amphiboles define a clear trend from ferro-edenite to ferro-winchite. The variation is characterized by decreasing Mg, Ti and Al and increasing Si, Fe. Also, the Ca content decreases and Na correspondingly increases, indicating substitution of $Ca(Mg,Fe^{2+})=NaFe^{3+}$ and CaAl=NaSi.

Within the rocks of centres 1 and 2, the amphiboles show continuous compositional variations consistent with progressive increase in the magma's silica activity, alkali activity and fO_2 as a result of continuing fractionation of calcic amphiboles. Amphibole trends reflect the different stages of liquid differentiation.

Growths of dendritic blue riebeckite in a local sheared metasomatized zone in centre 3 indicate sodium vapor build-up at a postmagmatic stage. In foyaite pegmatites, riebeckite occurs in acicular and radiating sheafs on larger crystals of aegirine-augite or along fractures in rocks. The textures are consistent with an origin by subsolidus reactions, presuming a secondary development for the riebeckite. This process is correlated with the magmatic/subsolidus trend of hydrothermal origin from katophorite to arfvedsonite defined by Strong and Taylor (1984). Riebeckite is Na and Fe^{3+} rich (Fig. 12) and has generally been ascribed to late stage subsolidus precipitation (Mitchell, 1990) or replacement due to the action of a low temperature (500-600^{0}C) fluid or vapor phase (Strong and Taylor, 1984).

The contrast of amphiboles between the silica-saturated and undersaturated rock series is a reflection of differing magma silica activity and magmatic conditions. The ($Ca+Al^{IV}$)-rich amphiboles are absent in nepheline-bearing rocks. This absence may result from the breakdown of such amphiboles. This could occur when differentiated liquids become peralkaline as P_{H_2O} decreases or P_{O_2} increases (Ferguson, 1978). In the same way, the general absence of sodic amphiboles in the silica-saturated and oversaturated rocks indicates that crystallization of sodic amphiboles occurred only in late peralkaline magmas as suggested by Giret *et al.* (1980).

As mentioned before, intrusive hastingsite-apatite and kaersutite veins occur in magnetite pyroxenite. The occurrence of amphibole veins may suggest that the mantle beneath the Big Spruce Lake region was rich in Fe-rich, Si-poor hastingsite and kaersutite amphiboles with abundant volatiles. The compositions of the hastingsitic amphiboles (hastingsite and hastingsitic hornblende in rock pc-82193) approximate compositions of nephelinitic melt (melanephelinite in Le Bas, 1977, p.289). There is a possibility of localized partial melting of the postulated amphibole-rich zone providing a possible source for the formation of silica-undersaturated alkaline melt. It has been proposed that kaersutite may form at a considerable range of depths. Melting of upper mantle kaersutite can yield alkali olivine basalts and nephelinites (Varne, 1968; Forbes and Starmer, 1974).

The major intrusive bodies of the Big Spruce Lake complex are cumulates. The chemical compositions of the minerals of the cumulates can be used to estimate the composition of the liquid in which they were formed (Bonin and Giret, 1985).

The estimations of liquid $Mg/(Mg+Fe)_{liq}$ ratios from amphiboles are shown in table 5-9. The experimental distribution coefficient K_D for hornblendic amphibole is from Helz (1982) where: $K_D=(Mg/Fe)_{am}/(Mg/Fe)_{liq}=2.7$. The Mg/Fe ratio of liquid for gabbroic rocks calculated from kaersutites range from 0.3 to 0.39 which corresponds to a differentiated liquid of intermediate composition (Bonin and Giret, 1985). Hastingsite, edenitic hornblende and actinolite give lower liquid Mg/(Mg+Fe) ratios (0.12-0.32) and suggest some of these amphiboles may have undergone subsolidus modification and been reequilibrated. Also, the calculated liquid Mg/(Mg+Fe) ratio could be influenced by the K_D value chosen for the calculation. Tremolite altered from olivines gives a high ratio of 0.76. The high Mg concentration was inherited from olivine crystals.

The liquid Mg/(Mg+Fe) ratios estimated from diorite amphiboles range from 0.14 to 0.32. The primary hastingsitic hornblende (#2160) gives a high ratio of 0.32 while the rim hastingsitic-hornblende gives low value of 0.20 (#1272). The ratios estimated from quartz-free syenites range from 0.11 to 0.31, from quartz syenites are around 0.06 - 0.22, and from comendite is 0.073.

The Mg/(Mg+Fe) ratios of liquids decrease continuously from gabbro to diorite, quartz-free syenites and quartz syenites and suggests a Mg depletion and Fe enrichment process for the formation of these rocks.

The ratios estimated from undersaturated nepheline syenites are all very low and fall in the range of 0.05 to 0.1, suggesting that these amphiboles are subsolidus products and that the magmas from which the amphiboles crystallized had low Mg/(Mg+Fe) ratios.

Table 5. Average amphibole compositions: in centres 1 and 5.

Rock #	pc-81001	pc-81001	pc-81130	pc-82193	pc-82193	pc-82193	pc-82265
SiO2	41.19	57.35	41.68	41.63	38.50	41.36	42.97
TiO2	5.72	0.02	4.36	4.60	0.18	0.19	1.07
Al2O3	11.60	0.42	11.59	10.87	14.41	10.99	11.53
Cr2O3	0.02	0.00	0.10	0.03	0.01	0.01	0.01
FeO*	13.90	4.15	12.51	13.33	24.80	23.27	15.53
MnO	0.13	0.09	0.11	0.15	0.20	0.17	0.22
MgO	10.97	22.60	12.18	11.74	4.83	6.87	12.28
CaO	11.01	12.80	11.50	11.43	11.32	11.33	12.35
K2O	0.75	0.00	1.33	1.19	0.64	0.43	1.38
Na2O	2.82	0.14	2.36	2.48	2.58	2.18	1.04
Total	98.11	97.57	97.72	97.45	97.47	96.80	98.38
Structural Formulae based on 13 cations and 23 oxygens							
Si	6.129	7.843	6.199	6.233	5.980	6.383	6.293
AlIV	1.871	0.066	1.801	1.767	2.020	1.617	1.707
Fe3+IV	0.000	0.091	0.000	0.000	0.000	0.000	0.000
T site	8.000	8.000	8.000	8.000	8.000	8.000	8.000
AlVI	0.166	0.000	0.226	0.149	0.620	0.387	0.282
Ti	0.643	0.000	0.491	0.522	0.019	0.019	0.114
Fe3+VI	0.000	0.351	0.002	0.000	0.676	0.696	0.754
Fe2+	1.724	0.035	1.552	1.673	2.542	2.309	1.147
Mn	0.018	0.008	0.018	0.018	0.028	0.019	0.026
Mg	2.430	4.613	2.697	2.618	1.119	1.577	2.685
Cr	0.000	0.000	0.009	0.000	0.000	0.000	0.000
Y site	4.981	5.007	4.986	4.980	5.004	5.007	5.008
CaB	1.751	1.875	1.831	1.835	1.885	1.874	1.936
NaB	0.249	0.041	0.169	0.165	0.115	0.126	0.064
X site	2.000	1.916	2.000	2.000	2.000	2.000	2.000
NaA	0.564	0.000	0.510	0.555	0.659	0.523	0.235
KA	0.143	0.000	0.250	0.225	0.131	0.083	0.255
A site	0.707	0.000	0.760	0.780	0.790	0.606	0.490
Total	15.688	14.923	15.755	15.760	15.794	15.613	15.498
no. of anal. pts.	6	6	4	4	6	7	4
Mg/(Mg+Fe)liq.	0.34	0.78	0.39	0.37	0.12	0.16	0.34
classification	kae	Trem	Ti Fo Pg	Kae	Mgn Has	Mgn Has Hn	Fan Pts Tsch Hn

Note: pc-82265: lamprophyre; pc-82193: amphibole vein; others: magnetite pyroxenite.

* = total iron as FeO.

Table 6. Average amphibole compositions: in gabbro.

Rock #	pc-82207	pc-81275	pc-82116	pc-82116	pc-82198	pc-81492	pc-81492	pc-82196
SiO2	41.05	41.91	43.18	43.41	42.14	41.35	43.69	41.19
TiO2	4.94	0.29	4.12	0.34	4.40	4.77	0.32	4.70
Al2O3	11.36	13.95	9.73	10.26	10.32	11.11	9.10	11.35
Cr2O3	0.01	0.02	0.09	0.01	0.01	N/D	N/D	N/D
FeOT	14.73	22.45	14.21	23.77	15.69	14.97	23.25	14.51
MnO	0.15	0.15	0.22	0.21	0.22	0.16	0.19	0.17
MgO	10.61	5.40	11.81	6.94	11.30	10.93	7.51	10.71
CaO	11.52	11.64	11.69	11.76	11.24	11.08	10.95	11.07
K2O	1.23	1.43	1.00	0.50	1.24	1.27	0.51	1.29
Na2O	2.22	0.71	2.27	1.75	2.37	2.28	1.68	2.24
Cl	N/D	N/D	N/D	N/D	N/D	0.12	0.10	0.12
Total	97.82	97.95	98.32	98.95	98.93	98.04	97.20	97.35
Structural Formulae based on 23 oxygens								
Si	6.164	6.363	6.412	6.556	6.251	6.177	6.647	6.199
AlIV	1.836	1.637	1.588	1.444	1.749	1.823	1.353	1.801
Fe3+IV	0.000	0.000	0.000	0.000	0.000	0.000	0.000	0.000
T site	8.000	8.000	8.000	8.000	8.000	8.000	8.000	8.000
AlVI	0.176	0.860	0.115	0.381	0.052	0.135	0.274	0.214
Ti	0.560	0.037	0.464	0.036	0.490	0.539	0.037	0.533
Fe3+VI	0.000	0.465	0.000	0.550	0.218	0.162	0.838	0.076
Fe2+	1.850	2.379	1.766	2.455	1.725	1.706	2.124	1.749
Mn	0.018	0.018	0.027	0.027	0.027	0.018	0.027	0.018
Mg	2.374	1.221	2.613	1.561	2.497	2.433	1.700	2.404
Cr	0.000	0.000	0.009	0.000	0.000	N/D	N/D	N/D
Y site	4.978	4.980	4.994	5.010	5.009	4.993	5.000	4.994
CaB	1.850	1.896	1.855	1.907	1.783	1.778	1.783	1.780
NaB	0.150	0.104	0.145	0.093	0.217	0.222	0.217	0.220
X site	2.000	2.000	2.000	2.000	2.000	2.000	2.000	2.000
NaA	0.500	0.106	0.506	0.415	0.461	0.443	0.277	0.431
KA	0.235	0.274	0.187	0.100	0.232	0.243	0.101	0.244
A site	0.735	0.380	0.693	0.515	0.693	0.686	0.378	0.675
Total	15.713	15.360	15.687	15.525	15.702	15.679	15.378	17.669
no. of anal. pts.	6	4	7	8	7	6	6	9
Mg/Mg+Fe)liq.	0.32	0.14	0.35	0.16	0.32	0.33	0.18	0.33
classification	Kae	Pts Fo Tsch Hn	Ti Fon Pg Hn	Fo Ed Hn	Mgn Has	Kae	Fan Fo Hn	Kae

Note: pc-82207, pc-81275 & pc-82196: Leucocratic Laminated Gabbro; pc-82116 & pc-82198: Big Feldspar Gabbro; pc-81492: Rhythmic Banded Gabbro.

* = total iron as FeO. N/D = Not/Determined.

Table 7. Average amphibole compositions: in diorite and comendite.

Rock #	pc-82160	pc-82160	pc-81272	pc-81126a	pc-82118	pc-82118	pc-82119
SiO2	42.14	42.23	44.23	45.76	43.07	47.62	42.45
TiO2	4.45	4.30	0.32	0.16	3.73	0.21	0.47
Al2O3	9.92	10.09	8.78	6.94	9.74	7.02	7.67
Cr2O3	0.00	0.00	0.02	0.01	0.03	0.01	0.02
FeO*	15.50	15.36	21.81	25.24	17.58	21.83	28.74
MnO	0.24	0.21	0.22	0.32	0.21	0.20	0.60
MgO	10.55	10.99	8.33	6.07	10.03	8.86	3.40
CaO	10.88	10.82	11.09	11.56	10.74	11.20	11.39
K2O	1.13	1.16	0.28	0.74	1.12	0.39	1.14
Na2O	1.85	2.39	2.31	0.84	2.59	1.51	1.10
Cl	0.12	0.12	N/D	N/D	N/D	N/D	N/D
Total	96.78	97.67	97.39	97.64	98.84	98.85	96.98
Structural formulae based on 13 cations and 23 oxygens							
Si	6.358	6.325	6.708	7.039	6.421	7.049	6.785
AlIV	1.642	1.675	1.292	0.961	1.579	0.951	1.215
Fe3+IV	0.000	0.000	0.000	0.000	0.000	0.000	0.000
T site	8.000	8.000	8.000	8.000	8.000	8.000	8.000
AlVI	0.127	0.106	0.276	0.296	0.131	0.276	0.227
Ti	0.508	0.486	0.036	0.018	0.421	0.027	0.058
Fe3+VI	0.222	0.208	0.604	0.432	0.194	0.581	0.378
Fe2+	1.738	1.717	2.166	2.810	2.000	2.121	3.466
Mn	0.027	0.027	0.027	0.046	0.027	0.027	0.077
Mg	2.377	2.456	1.887	1.395	2.230	1.956	0.807
Cr	0.000	0.000	0.000	0.000	0.000	0.000	0.000
Y site	4.999	5.000	4.996	4.997	5.003	4.988	5.013
CaB	1.760	1.736	1.805	1.903	1.719	1.778	1.951
NaB	0.240	0.264	0.195	0.097	0.281	0.222	0.049
X site	2.000	2.000	2.000	2.000	2.000	2.000	2.000
NaA	0.304	0.429	0.489	0.152	0.471	0.214	0.287
KA	0.218	0.225	0.055	0.148	0.215	0.071	0.230
A site	0.522	0.654	0.544	0.300	0.686	0.285	0.517
Total	15.521	15.654	15.540	15.297	15.689	15.273	15.530
no. of anal. pts.	5	6	4	6	6	5	5
Mg/(Mg+Fe)liq.	0.31	0.32	0.20	0.14	0.27	0.21	0.073
classification	Kae	Ti Mgn Has Hn	Fo Ed Hn	Fo Hn	Ti Mgn Has Hn	Fo Hn	Fo Ed

Note: pc-82119: comendite; others: diorite.

* = total iron as FeO.

Table 8. Average amphibole compositions: in quartz-free and quartz syenite.

Rock #	pc-81006	pc-82351	pc-81332	pc-81333	pc-81326	pc-81083	pc-81083	pc-81005
SiO2	48.92	44.26	39.91	41.05	39.91	45.10	51.62	51.42
TiO2	1.09	2.08	3.06	2.41	3.24	1.30	0.10	0.23
Al2O3	4.57	6.48	9.51	8.97	9.86	5.32	0.21	2.07
Cr2O3	0.00	0.01	0.02	0.01	0.01	0.00	0.00	0.00
FeO*	18.61	24.98	25.15	23.79	23.28	28.55	32.47	21.48
MnO	0.40	0.52	0.60	0.57	0.53	0.51	0.52	0.40
MgO	11.10	5.98	4.78	6.49	5.79	5.08	2.80	9.37
CaO	10.59	10.48	10.65	10.60	10.90	6.85	5.13	11.36
K2O	0.28	1.05	1.31	1.35	1.35	2.52	0.94	0.16
Na2O	0.57	1.47	2.24	1.87	1.83	2.82	4.84	0.33
Cl	0.03	N/D	N/D	N/D	N/D	0.10	0.03	0.04
Total	96.16	97.31	97.23	97.11	96.70	98.15	98.66	96.86

Structural formulae based on 13 cations and 23 oxygens

Si	7.253	6.878	6.320	6.391	6.286	6.974	8.026	7.742
AlIV	0.747	1.122	1.680	1.609	1.714	0.966	0.000	0.258
Fe3+IV	0.000	0.000	0.000	0.000	0.000	0.060	0.000	0.000
T site	8.000	8.000	8.000	8.000	8.000	8.000	8.026	8.000
AlVI	0.054	0.063	0.100	0.038	0.113	0.000	0.037	0.113
Ti	0.125	0.243	0.362	0.281	0.388	0.148	0.009	0.027
Fe3+VI	0.883	0.440	0.280	0.642	0.324	1.103	0.540	0.298
Fe2+	1.424	2.808	3.052	2.456	2.744	2.524	3.683	2.406
Mn	0.053	0.065	0.076	0.075	0.066	0.065	0.065	0.054
Mg	2.450	1.381	1.133	1.507	1.363	1.170	0.644	2.099
Cr	0.000	0.000	0.000	0.000	0.000	0.000	0.000	0.000
Y site	4.989	5.000	5.003	4.999	4.998	5.010	4.978	4.997
CaB	1.684	1.745	1.808	1.769	1.837	1.133	0.850	1.836
NaB	0.160	0.255	0.192	0.231	0.163	0.845	1.150	0.100
X site	1.844	2.000	2.000	2.000	2.000	1.978	2.000	1.936
NaA	0.000	0.184	0.493	0.331	0.396	0.000	0.308	0.000
KA	0.053	0.205	0.266	0.271	0.275	0.501	0.187	0.027
A site	0.053	0.389	0.759	0.602	0.671	0.501	0.495	0.027
Total	14.886	15.389	15.762	15.601	15.669	15.489	15.499	14.960
no. of anal. pts.	5	8	5	9	5	5	5	5
Mg/(Mg+Fe)liq.	0.28	0.14	0.11	0.21	0.140	0.110	0.054	0.220
classification	Fan Ac Hn	Fo Hn	Pts Ti Has Hn	Pts Ti Mgn Has Hn		Fi Pts Kat	Fo Win	Fo Act

Note: pc-81006, pc-82351, pc-81332 & pc-81333: quartz-free syenite; others: quartz syenite.

* = total iron as FeO. N/D = Not/Determined.

Table 9. Average amphibole compositions: in quartz syenite and nepheline syenite.

Rock #	pc-82519	pc-82519	pc-82388	pc-82226	pc-82109	pc-81416	pc-81082	pc-81418
SiO2	42.27	49.92	44.84	43.48	45.64	52.15	51.37	51.59
TiO2	1.75	0.19	1.68	1.60	1.34	0.09	0.23	0.05
Al2O3	7.41	1.31	6.63	4.58	4.11	0.84	1.18	1.36
Cr2O3	0.01	0.01	0.00	0.01	0.01	0.00	0.00	0.03
FeO*	27.75	29.12	23.63	31.17	30.13	35.16	32.42	32.63
MnO	0.62	0.79	0.51	0.71	0.87	0.19	0.68	0.10
MgO	3.49	4.14	6.99	3.00	2.67	2.14	3.37	2.62
CaO	10.13	10.11	10.23	8.93	8.45	0.10	1.75	0.09
K2O	1.10	0.34	1.03	0.98	1.01	0.36	1.23	0.44
Na2O	2.51	1.07	1.60	2.23	2.32	7.14	6.67	6.81
Cl	N/D	N/D	N/D	N/D	N/D	0.01	0.00	N/D
Total	97.04	97.00	97.14	96.69	96.55	98.18	98.90	95.72
Structural formulae based on 13 cations and 23 oxygens								
Si	6.764	7.843	6.900	6.958	7.287	7.894	7.798	7.934
AlIV	1.236	0.157	1.100	0.864	0.713	0.106	0.202	0.066
Fe3+IV	0.000	0.000	0.000	0.178	0.000	0.000	0.000	0.000
T site	8.000	8.000	8.000	8.000	8.000	8.000	8.000	8.000
AlVI	0.159	0.088	0.102	0.000	0.063	0.039	0.008	0.183
Ti	0.212	0.019	0.194	0.192	0.163	0.009	0.027	0.009
Fe3+VI	0.152	0.226	0.546	0.725	0.524	1.841	1.363	1.725
Fe2+	3.562	3.596	2.497	3.267	3.494	2.606	2.751	2.468
Mn	0.087	0.104	0.065	0.096	0.115	0.027	0.091	0.009
Mg	0.837	0.972	1.601	0.712	0.633	0.482	0.766	0.601
Cr	0.000	0.000	0.000	0.000	0.000	0.000	0.000	0.000
Y site	5.009	5.005	5.005	4.992	4.992	5.004	5.006	4.995
CaB	1.741	1.699	1.684	1.528	1.448	0.018	0.283	0.018
NaB	0.259	0.301	0.316	0.472	0.552	1.982	1.717	1.982
X site	2.000	2.000	2.000	2.000	2.000	2.000	2.000	2.000
NaA	0.520	0.029	0.165	0.220	0.168	0.110	0.244	0.050
KA	0.221	0.066	0.203	0.202	0.201	0.073	0.237	0.083
A site	0.741	0.095	0.368	0.422	0.369	0.183	0.481	0.133
Total	15.750	15.100	15.373	15.414	15.361	15.187	15.487	15.128
no. of anal. pts.	8	5	9	8	8	5	5	4
Mg/Mg+Fe)liq.	0.077	0.086	0.16	0.062	0.055	0.098	0.065	0.051
classification	Fo Ed	Fo Act	Fo Hn	Fan Fo Hn	Fo Ac Hn	Rie	Rie	Rie

Note: pc-81416, pc-81418 & pc-81082: riebeckite metasomatized nepheline syenite; others: quartz syenite.

* = total iron as FeO. N/D = Not/Determined.

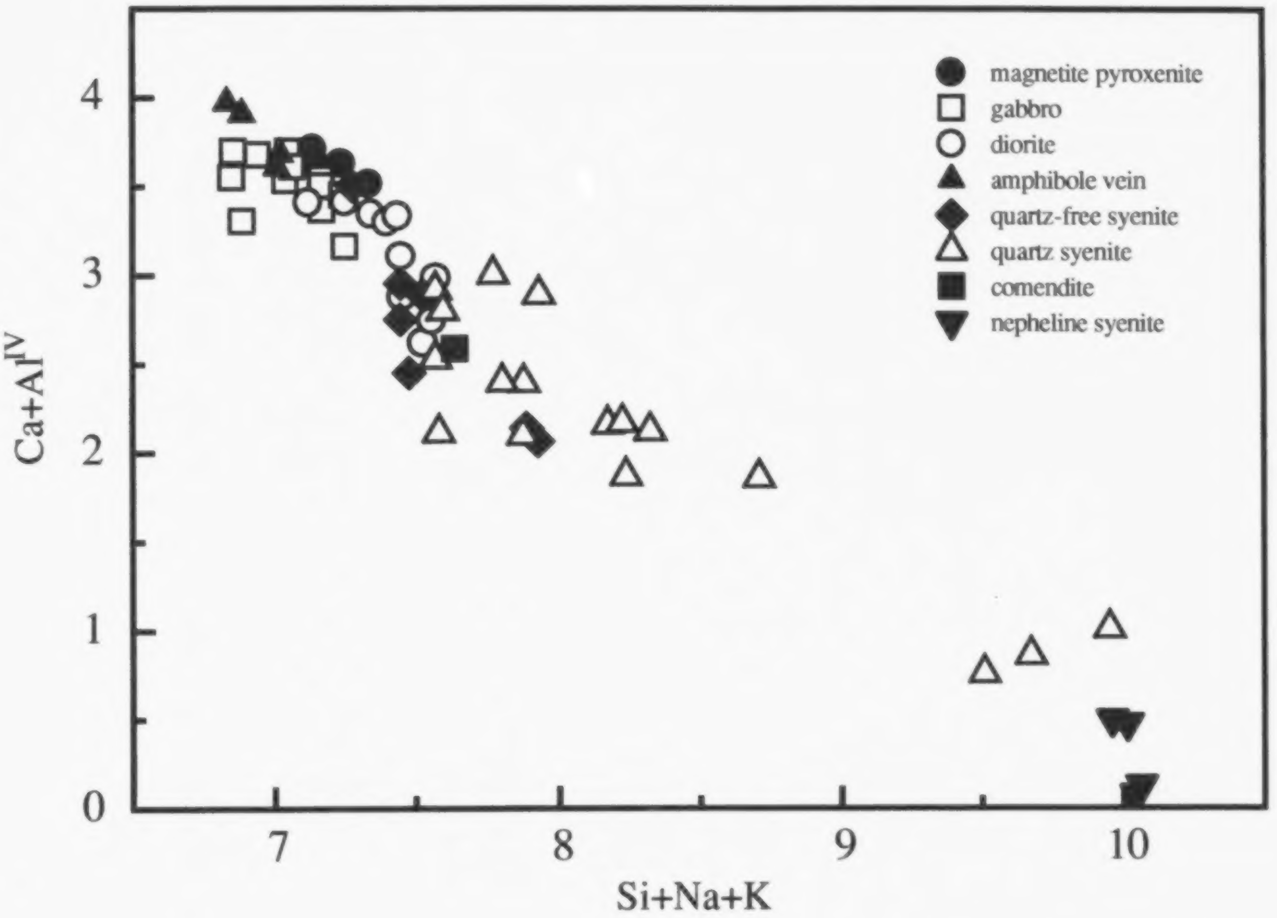

Fig. 8: Amphibole compositional variations, plotted in terms of cationic (Ca + Al^{IV}) vs. (Si + Na + K).

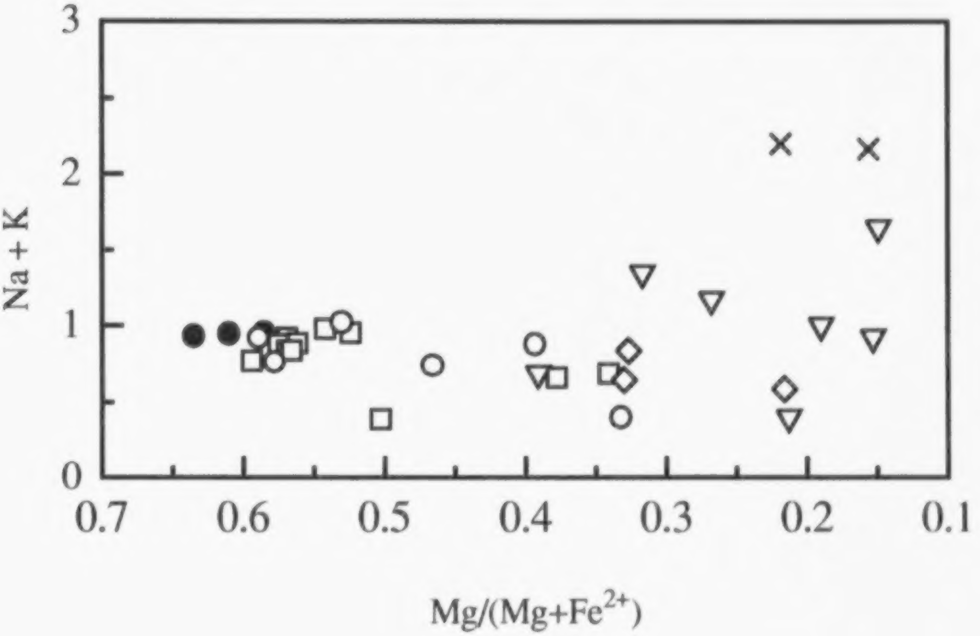

Fig. 9: Amphibole Mg/(Mg+Fe^{2+}) vs. (Na+K) diagram, symbols as in figure 10 & 12.

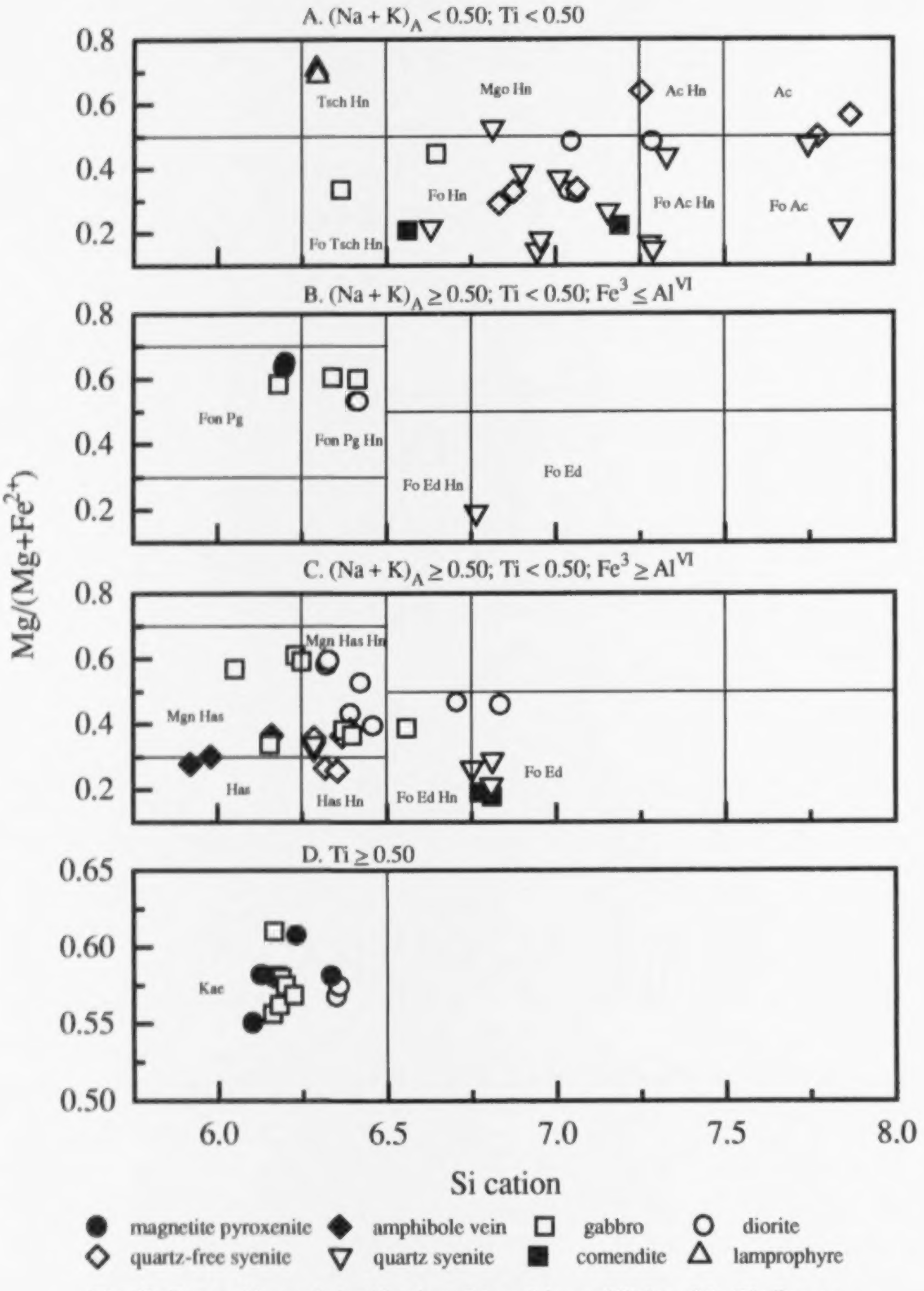

Fig. 10: Composition and classification of the calcic amphiboles of the Big Spruce Lake complex (after Leake, 1978). For amphibole abbreviations, see Appendix 5.

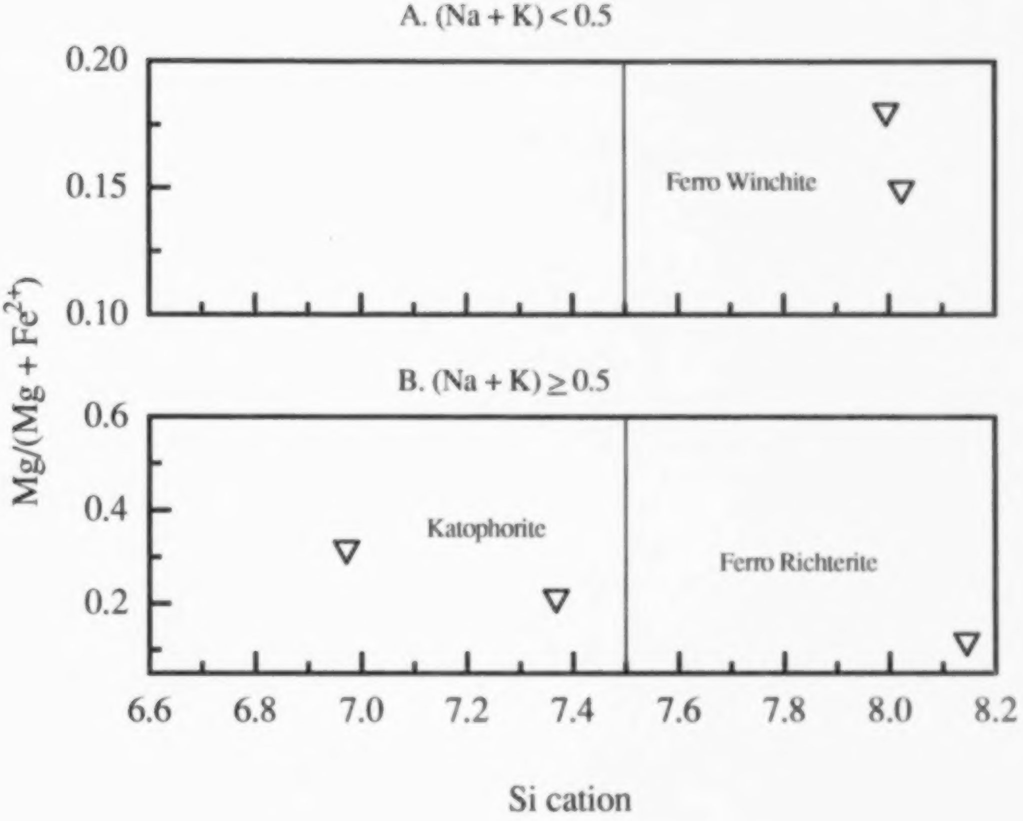

Fig. 11: Composition and classification of sodic-calcic amphiboles in quartz syenite, after Leake (1978), symbols as in Fig. 10.

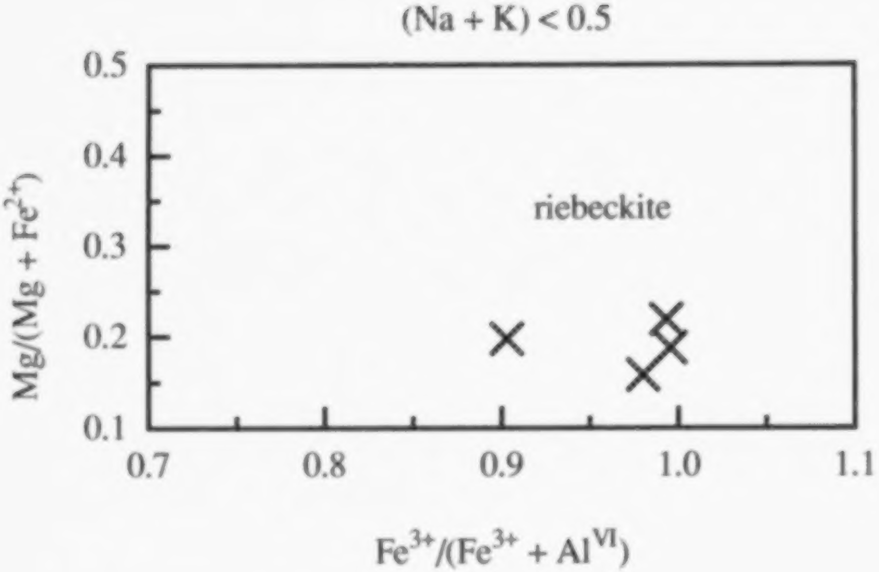

Fig. 12: Composition and classification of sodic amphibole in nepheline syenites, after Leake (1978).

4.3 Mica

Representative analyses of micas from the complex are listed in Table 10-11. The totals of mica compositions range from 92-96. It is suggested that the low totals resulted largely from absence of analyses of H_2O and F. The structural formulae are calculated to 22 oxygens. Primary micas are trioctahedral species. Muscovite occurs as a secondary phase in some of the nepheline syenites.

Compositions of trioctahedral micas are plotted in Fig. 13 in terms of Mg-Fe-Al cation contents. These micas include phlogopite in minette, Mg-rich biotite and Fe-rich biotites in other rock types.

The Mg# (=Mg/(Mg+Fe)) of biotite in gabbros ranges from 0.36 to 0.38; in diorite the Mg# is 0.30; in quartz-free and quartz syenites it ranges from 0.25-0.26; in foyaite and melteigite from 0.06-0.25. As Mg decreases from gabbro through diorite, alkali syenites to nepheline syenites, FeO increases and Al_2O_3 decreases slightly (Fig. 14), and the micas show a compositional variation towards annite (Fig. 13).

In carbonatite, melanocratic syenite and biotite pyroxenite, biotites are relatively Mg-rich with Mg# ranging from 0.39 to 0.57. Phlogopite in minette shows slight variations in core and rim compositions (Table 10), the Mg# of the core being 0.74 and that of the rim 0.69.

Wones and Eugster (1965) have shown experimentally that increasing annite (Fe) content of micas is a function of falling temperatures. Mitchell (1981, 1985) proposed that lamproite micas high in FeO^T and/or Fe^{3+} formed at low temperatures and low pressures. Thus, the decreasing MgO and increasing FeO in micas in the Big Spruce Lake complex suggests a decreasing temperature process. The most annite-rich biotite occurs in the peralkaline foyaite and melteigite, indicating that these rocks are the most evolved and formed at relatively lower temperatures.

Table 10. Average mica compositions: in centres 1 and 5.

Rock #	pc-82196	pc-82198	pc-81126a	pc-82468	pc-81065	pc-81070	pc-81070
						core	rim
SiO2	35.41	33.12	34.59	36.07	35.53	38.58	37.93
TiO2	1.47	6.00	2.58	3.88	4.19	2.49	2.45
Al2O3	16.28	12.92	13.37	13.52	12.11	13.02	12.70
Cr2O3	0.00	0.00	0.00	0.00	0.00	0.00	0.00
FeO*	23.28	25.24	26.72	17.47	22.82	11.14	12.88
MnO	0.08	0.22	0.14	0.12	0.32	0.11	0.18
MgO	7.91	7.84	6.44	12.90	9.46	18.16	16.16
K2O	8.89	8.25	8.90	9.27	8.50	9.83	9.59
Na2O	0.56	0.06	0.06	0.20	0.51	0.04	0.07
Cl	0.12	0.14	0.26	0.08	0.02	0.02	0.02
Total	94.00	93.79	93.06	93.51	93.46	93.39	91.98
Structural formulae based on 22 oxygens							
Si	5.589	5.339	5.647	5.593	5.663	5.790	5.832
AlIV	2.411	2.451	2.353	2.407	2.271	2.210	2.168
T site	8.000	7.790	8.000	8.000	7.934	8.000	8.000
Ti	0.174	0.726	0.316	0.452	0.502	0.281	0.283
AlVI	0.612	0.000	0.215	0.059	0.000	0.089	0.129
Cr	0.000	0.000	0.000	0.000	0.000	0.000	0.000
Fe2+	3.062	3.391	3.635	2.257	3.031	1.393	1.650
Mn	0.011	0.030	0.019	0.016	0.043	0.014	0.023
Mg	1.856	1.879	1.563	2.973	2.242	4.051	3.694
O site	5.715	6.026	5.749	5.757	5.817	5.828	5.779
K	1.791	1.698	1.855	1.835	1.730	1.883	1.882
Na	0.171	0.019	0.019	0.060	0.157	0.012	0.021
A site	1.962	1.717	1.874	1.895	1.887	1.895	1.903
Cl	0.029	0.035	0.065	0.019	0.005	0.005	0.005
Total	15.706	15.568	15.689	15.670	15.643	15.728	15.687
Mg#=Mg/(Mg +Fe)	0.38	0.36	0.30	0.57	0.43	0.74	0.69
no. of anal. pts.	3	6	4	5	7	3	3
classification	biotite	biotite	biotite	biotite	biotite	phlogopite	

Note: pc-2196 & pc-82198: gabbro; pc-81126a: diorite; pc-82468: olivine melanocratic syenite; pc-81065: biotite pyroxenite; pc-81070: minette.

T site: tetrahedral site; O site: octahedral site; A site: 12-fold coordinated site;

* = total iron as FeO.

Table 11. Average mica compositions: in centres 2, 3 and 4.

Rock #	pc-82351	pc-81326	pc-82119	pc-81082	pc-81289	pc-81169	pc-81176
SiO_2	35.00	34.25	33.39	35.41	32.65	35.34	35.82
TiO_2	2.35	1.53	1.40	3.23	1.70	2.71	1.52
Al_2O_3	12.55	13.21	13.08	9.00	11.95	10.93	12.50
Cr_2O_3	0.00	0.00	0.00	0.00	0.01	0.00	0.00
FeO*	29.08	30.85	30.99	33.40	35.65	30.03	24.75
MnO	0.21	0.42	0.49	0.71	0.84	1.08	0.71
MgO	5.78	5.66	4.74	3.46	1.35	5.52	9.01
K_2O	8.60	9.19	8.22	8.85	8.82	7.99	9.08
Na_2O	0.14	0.07	0.04	0.04	0.06	0.12	0.12
Cl	0.00	0.17	0.00	0.04	0.01	0.01	0.03
F	N/D	0.84	N/D	N/D	N/D	0.27	N/D
Total	93.71	96.19	92.58	94.20	93.04	94.00	93.54
Structural formulae based on 22 oxygens							
Si	5.733	5.483	5.637	5.949	5.644	5.791	5.771
AlIV	2.267	2.488	2.363	1.779	2.356	2.209	2.229
T site	8.000	7.971	8.000	7.728	8.000	8.000	8.000
Ti	0.289	0.184	0.178	0.408	0.221	0.333	0.184
AlVI	0.152	0.000	0.235	0.000	0.074	0.000	0.140
Cr	0.000	0.000	0.000	0.000	0.000	0.000	0.000
Fe^{2+}	3.970	4.115	4.360	4.676	5.136	4.100	3.323
Mn	0.029	0.057	0.070	0.101	0.123	0.150	0.097
Mg	1.408	1.347	1.190	0.864	0.347	1.345	2.158
O site	5.847	5.703	6.032	6.049	5.900	5.928	5.901
K	1.798	1.878	1.772	1.898	1.946	1.671	1.867
Na	0.044	0.022	0.013	0.013	0.020	0.038	0.037
A site	1.843	1.900	1.785	1.911	1.967	1.709	1.905
Cl	0.000	0.042	0.000	0.010	0.003	0.003	0.007
F	N/D	0.425	N/D	N/D	N/D	0.140	N/D
Total	15.690	16.040	15.817	15.699	15.869	15.779	15.813
Mg#=Mg/(Mg+Fe)	0.26	0.25	0.21	0.16	0.06	0.25	0.39
no. of anal. pts.	4	6	3	7	10	4	4
classification	biotite	biotite	biotite	biotite	biotie	biotitet	biotie

Note: pc-82351: quartz-free syenite; pc-81326: quartz syenite; pc-82119: comendite;
pc-81082 & pc-81289: foyaite; pc-81169: melteigite; pc-81176: carbonatite.
* = total iron as FeO. N/D = Not/Determined.

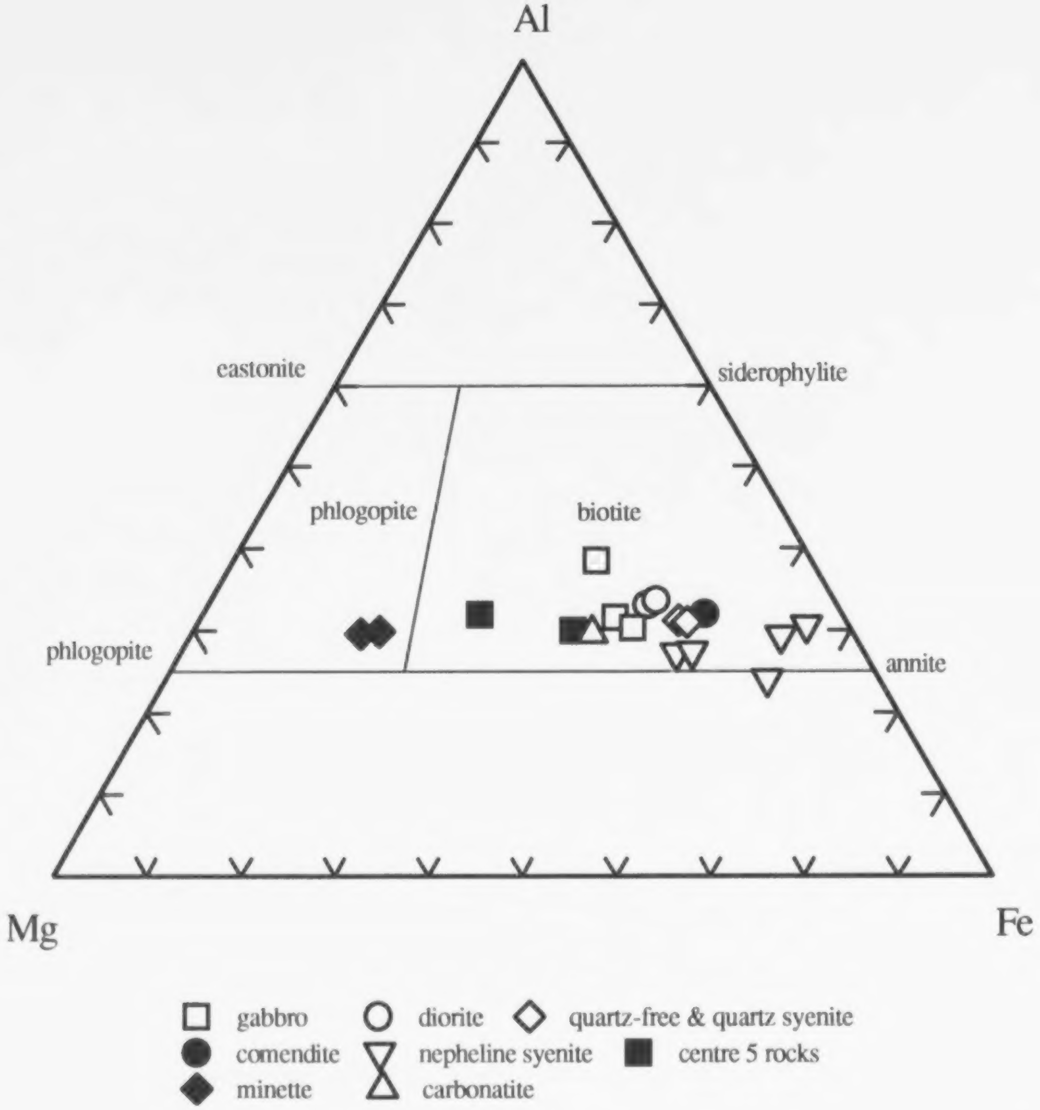

Fig. 13: Biotite plotted in terms of Al, Mg & Fe cations.

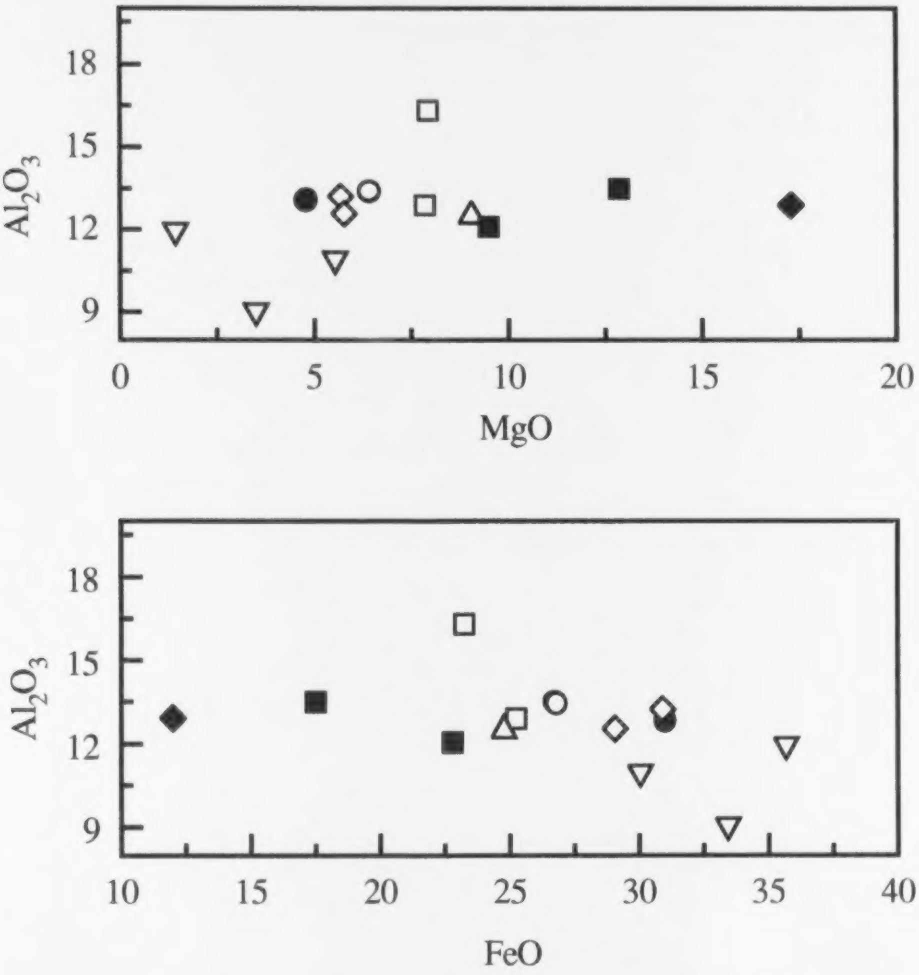

Fig. 14: Biotite Al_2O_3 vs. MgO and FeO (in wt.%), rock symbols as in Fig. 13.

4.4 Feldspar

The feldspars define the following ranges of compositions (Fig. 15; Tables 12-13): plagioclases vary from An_{32-45} in gabbros, An_{27-33} in diorite to An_{16-17} in the quartz-free and quartz syenite. Alkali feldspar is present in the quartz syenite and foyaite. In quartz syenite, the alkaline feldspar has a composition of $Or_{38}Ab_{62}$. In foyaites, patchy perthite containing albite lamellae ($Ab_{98}Or_2$) in orthoclase ($Or_{57}Ab_{43}$) is present. Late stage albite also occurs as single grains. Evidently, subsolidus re-equilibration has affected the compositions of the feldspars. The BaO contents in all feldspars are low ranging from 0-0.2wt.%. FeO contents range from 0.1-1.9% wt%.

The evolution of feldspars from intermediate plagioclase (andesine), oligoclase, albite, to Na-K feldspar and K-feldspar follows a trend of Ca depletion, Na enrichment in plagioclase and Na decrease and K enrichment in alkali feldspars (Fig. 15) and reflects fractionation from An-rich to An-poor plagioclase and to alkali feldspar. The fractionation of the feldspars contributed to producing residual peralkaline liquids (see Chapter 7.4).

In centre 5 rocks, feldspars include labradorite (An_{68}) and K-feldspar. The highly calcic plagioclase probably reflects initial high content of anorthite in the magma of this satellite intrusion.

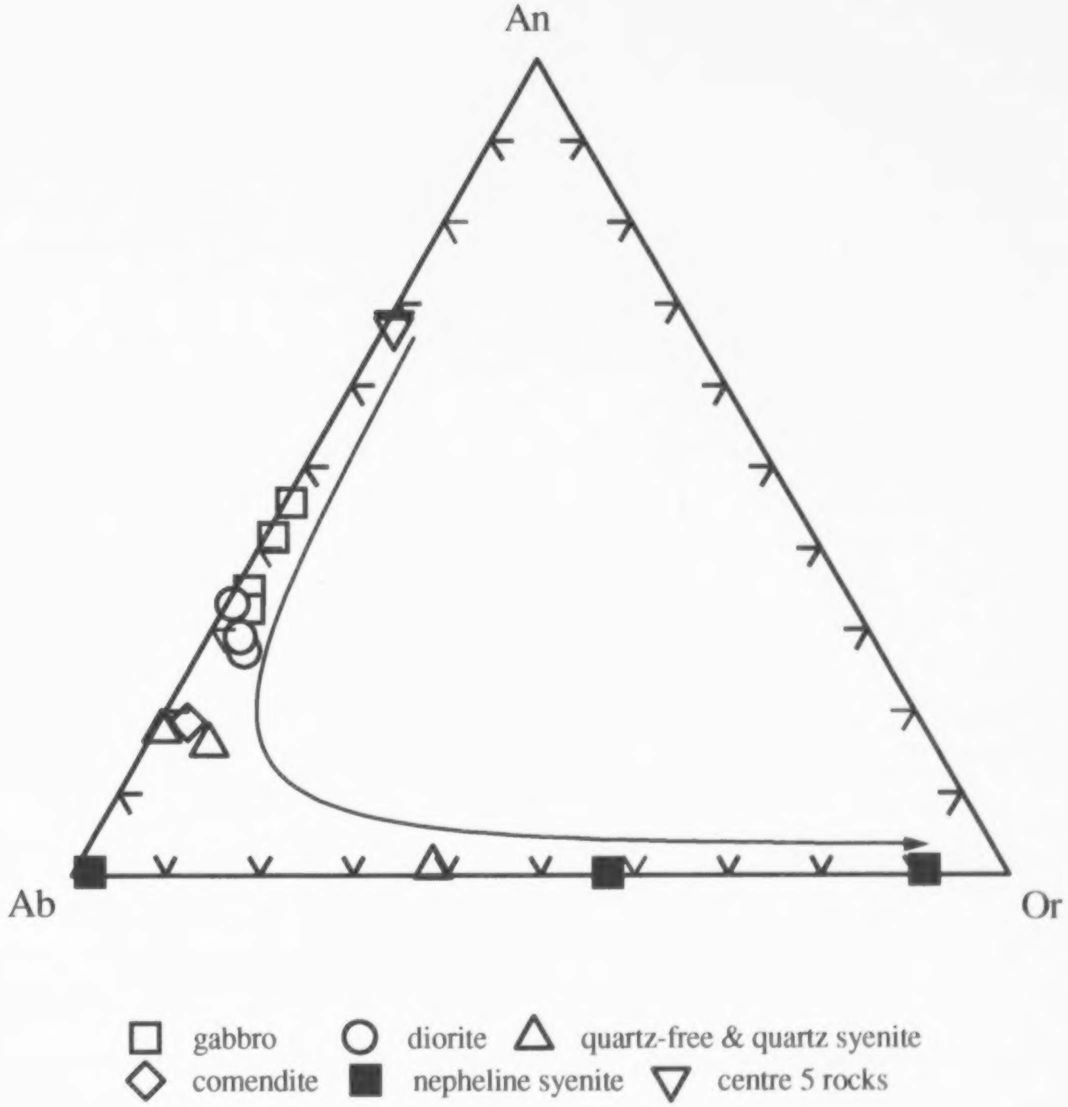

Fig. 15: Feldspar compositions plotted in terms of albite (Ab), anorthite (An) and orthoclase (Or) end-members. Arrowed line indicates the feldspar trend.

Table 12. Average feldspar compositions: in centres 1 and 5.

Rock #	pc-82198	pc-81275	pc-81492	pc-82116	pc-81126a	pc-81272	pc-81068
SiO2	59.72	56.04	57.14	58.50	60.54	59.44	50.81
Al2O3	25.74	27.96	27.28	26.02	24.85	25.89	31.04
FeO*	0.25	0.30	0.27	0.35	0.25	0.26	0.72
MnO	0.01	0.01	0.01	0.01	0.01	0.00	0.02
MgO	0.08	0.08	0.06	0.04	0.07	0.04	0.27
BaO	0.08	0.05	0.05	0.10	0.12	0.10	0.02
CaO	6.78	9.32	8.66	7.15	5.72	6.85	13.74
Na2O	7.51	6.04	6.56	7.15	7.79	7.48	3.51
K2O	0.36	0.12	0.07	0.21	0.75	0.16	0.05
Total	100.53	99.92	100.10	99.53	100.10	100.22	100.18
Structural formulae based on 8 oxygens							
Si	2.654	2.523	2.562	2.629	2.699	2.648	2.315
Al	1.346	1.481	1.439	1.376	1.303	1.357	1.664
Fe2+	0.009	0.011	0.010	0.013	0.009	0.010	0.027
Mn	0.000	0.000	0.000	0.000	0.000	0.000	0.001
Mg	0.005	0.005	0.004	0.003	0.005	0.003	0.019
Ba	0.001	0.001	0.001	0.002	0.002	0.002	0.000
Ca	0.323	0.450	0.416	0.344	0.273	0.327	0.671
Na	0.646	0.526	0.569	0.622	0.672	0.645	0.310
K	0.020	0.007	0.004	0.012	0.043	0.009	0.003
Total	5.006	5.004	5.006	5.000	5.007	5.001	5.009
An	32.6	45.8	42.1	35.2	27.7	33.3	68.2
Ab	65.3	53.6	57.6	63.6	68.0	65.7	31.5
Or	2.1	0.7	0.4	1.2	4.3	0.9	0.3
no. of anal. pts.	8	4	5	4	7	6	5

Note: pc-82198, pc-81275, pc-81492 & pc-82116: gabbro.
pc-81126a & pc-81272: diorite; pc-81068: melanocratic syenite.
* = total iron as FeO.

Table 13. Average feldspar compositions: in centres 2 and 3.

Rock #	pc-81006	pc-81005b	pc-82109	pc-82119	pc-81418	pc-81082	pc-81082
SiO2	63.01	63.00	65.88	62.16	66.41	68.82	63.30
Al2O3	23.10	22.76	19.66	21.10	19.33	19.75	18.68
FeO*	0.20	0.18	0.21	1.92	0.42	0.21	0.09
MnO	0.02	0.00	0.01	0.02	0.04	0.00	0.02
MgO	0.04	0.07	0.03	0.04	0.01	0.03	0.02
BaO	0.05	0.12	0.23	0.02	0.00	0.01	0.08
CaO	3.66	3.38	0.15	4.18	0.00	0.02	0.03
Na2O	9.42	8.88	6.92	9.67	4.86	11.28	0.99
K2O	0.16	1.17	6.45	0.54	9.83	0.34	14.81
Total	99.66	99.56	99.54	99.65	100.90	100.46	98.02
Structural formulae based on 8 oxygens							
Si	2.798	2.809	2.965	2.803	2.980	2.994	2.763
Al	1.207	1.194	1.041	1.119	1.020	1.011	0.959
Fe2+	0.007	0.007	0.008	0.072	0.016	0.008	0.003
Mn	0.001	0.000	0.000	0.001	0.002	0.000	0.001
Mg	0.003	0.005	0.002	0.003	0.001	0.002	0.001
Ba	0.001	0.002	0.004	0.000	0.000	0.000	0.001
Ca	0.174	0.162	0.007	0.202	0.000	0.001	0.001
Na	0.810	0.766	0.603	0.844	0.422	0.950	0.084
K	0.009	0.067	0.371	0.031	0.563	0.019	0.825
Total	5.009	5.011	5.001	5.075	5.003	4.985	4.640
An	17.5	16.3	0.7	18.8	0.0	0.1	0.1
Ab	81.6	77.0	61.5	78.4	42.8	97.9	9.2
Or	0.9	6.7	37.8	2.9	57.2	1.9	90.7
no. of anal. pts.	5	5	5	4	3	4	4

Note: pc-81006: quartz-free syenite; pc-81005b & pc-82109: quartz syentie.
pc-82119: comendite; pc-81418 & pc-81082: nepheline syenite.
* = total iron as FeO.

4.5 Olivine

Olivines are present in the olivine magnetite pyroxenite, melanocratic syenite and the biotite peridotite. They are absent in most of the plutonic rocks.

The olivine grains have homogeneous compositions that fall within the range Fo_{60} to Fo_{92} (Table 14). The Mg# (Mg#=Mg/(Mg+Fe)) in olivines correlates negatively with CaO and MnO, but, as would be anticipated, positively with the SiO_2 contents (Fig. 16). The compositions of olivines do not correlate with rock types however, and are of little use in determining the petrogenetic relationships.

The NiO content of olivines in magnetite pyroxenite is relatively low (0.07%) compared with those in centre 5 rocks (Table 14), suggesting lower Ni content in the original magma of magnetite pyroxenite.

The major compositional ranges of olivines (Fo_{60-85}) in the complex are Fe-rich compared with values of Fo_{88-92} in olivine of most upper-mantle peridotites and spinel lherzolites (Hervig *et al.*, 1986) and they suggest crystallization from a fractionated basaltic liquid (Azambre *et al.*, 1992).

Table 14. Average olivine compositions: in centres 1 and 5.

Rock #	pc-81004	pc-82262	pc-82464	pc-82468	pc-82478
SiO2	37.55	36.78	41.64	40.32	36.17
TiO2	0.02	0.01	0.01	0.01	0.02
Al2O3	0.06	0.09	0.08	0.06	0.07
Cr2O3	0.01	0.01	0.05	0.03	0.01
FeO*	26.99	32.22	7.34	14.13	34.36
MnO	0.37	0.59	0.08	0.15	0.62
MgO	34.65	30.33	49.87	44.77	28.82
CaO	0.12	0.17	0.05	0.08	0.19
NiO	0.07	0.13	0.37	0.22	0.12
Total	99.84	100.33	99.49	99.77	100.38
Structural formulae based on 4 oxygens					
Si	1.000	1.002	1.011	1.007	0.997
Ti	0.000	0.000	0.000	0.000	0.000
Al	0.002	0.003	0.002	0.002	0.002
Cr	0.000	0.000	0.001	0.001	0.000
Fe	0.599	0.731	0.148	0.294	0.789
Mn	0.008	0.014	0.002	0.003	0.014
Mg	1.384	1.239	1.815	1.678	1.191
Ca	0.003	0.005	0.001	0.002	0.006
Ni	0.002	0.003	0.007	0.004	0.003
Total	2.999	2.997	2.988	2.991	3.002
Fo=Mg/(Mg+Fe)	0.70	0.63	0.92	0.85	0.60
no. of anal. pts.	7	9	5	5	8

Note: pc-81004: olivine magnetite pyroxenite; pc-82262: biotite peridotite.
pc-82464, pc-82468 & pc-82478: olivine melanocratic syenite.
* = total iron as FeO.

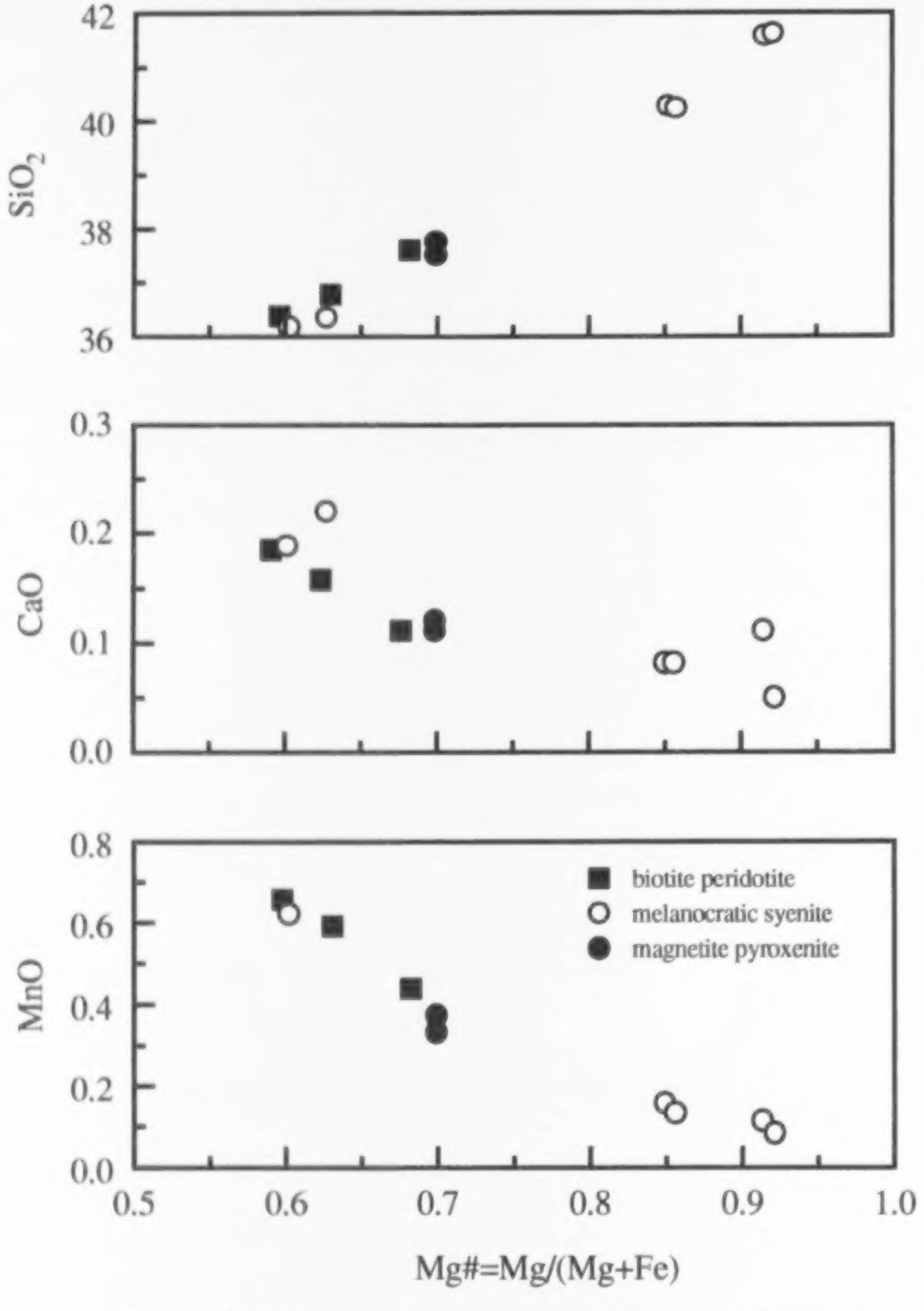

Fig. 16: Compositions of olivines plotted as Mg#=Mg/(Mg+Fe) vs. SiO$_2$, CaO and MnO contents (in wt.%). Data are from Table 14 and additional analyses of individual grains.

4.6 Nepheline

Nepheline is the dominant feldspathoid in the Big Spruce Lake alkaline complex and typical compositions are shown in Table 15. The nephelines do not display significant chemical variation (Fig. 17) and most of them fall within a crystallization temperature range of 700-750°C according to Hamilton (1961). One nepheline overlaps the Morozewicz-Buerger convergence field (Morozewicz, 1928; Buerger, *et al.*, 1947); others are adjacent to this field. This suggests that the nephelines in the Big Spruce lake complex are low temperature plutonic nephelines and that they were formed through a slow cooling process (Tilley, 1954; 1956). Thus, the nephelines reflect only the subsolidus temperature of magma consolidation.

Table 15. Average nepheline compositions: in centre 3.

Rock #	pc-81223	pc-81231	pc-82137	pc-82139	pc-81194
SiO_2	44.38	44.60	44.41	43.29	44.97
Al_2O_3	33.50	33.69	33.92	34.31	33.07
Fe_2O_3*	0.87	0.43	0.30	0.22	0.69
MnO	0.00	0.01	0.01	0.00	0.02
MgO	0.05	0.05	0.04	0.03	0.04
CaO	0.02	0.03	0.00	0.02	0.04
Na_2O	16.07	16.14	16.04	15.58	15.97
K_2O	5.54	5.52	5.51	6.16	5.25
Total	100.43	100.47	100.23	99.61	100.05
Structural formulae based on 32 oxygens					
Si	8.451	8.475	8.453	8.322	8.566
Al	7.505	7.532	7.595	7.760	7.411
Fe^{3+}	0.124	0.061	0.043	0.032	0.099
Mn	0.000	0.002	0.002	0.000	0.003
Mg	0.014	0.014	0.011	0.009	0.011
Ca	0.004	0.006	0.000	0.004	0.008
Na	5.923	5.936	5.909	5.797	5.888
K	1.347	1.339	1.339	1.512	1.277
Total	23.369	23.366	23.352	23.436	23.262
no. of anal. pts.	7	7	6	6	6
weight % end-member molecules					
Ne	74.77	74.83	74.72	73.31	74.52
Ks	18.92	18.78	18.84	21.27	17.98
Qz	6.32	6.39	6.44	5.42	7.50

Ne = $NaAlSiO_4$; Ks = $KAlSiO_4$; Qz = SiO_2

Note: pc-81223 & pc-81231: foyaite; pc-82137: ijolite.

pc-82139 & pc-81194: urtite.

* Fe_2O_3: total iron as Fe_2O_3.

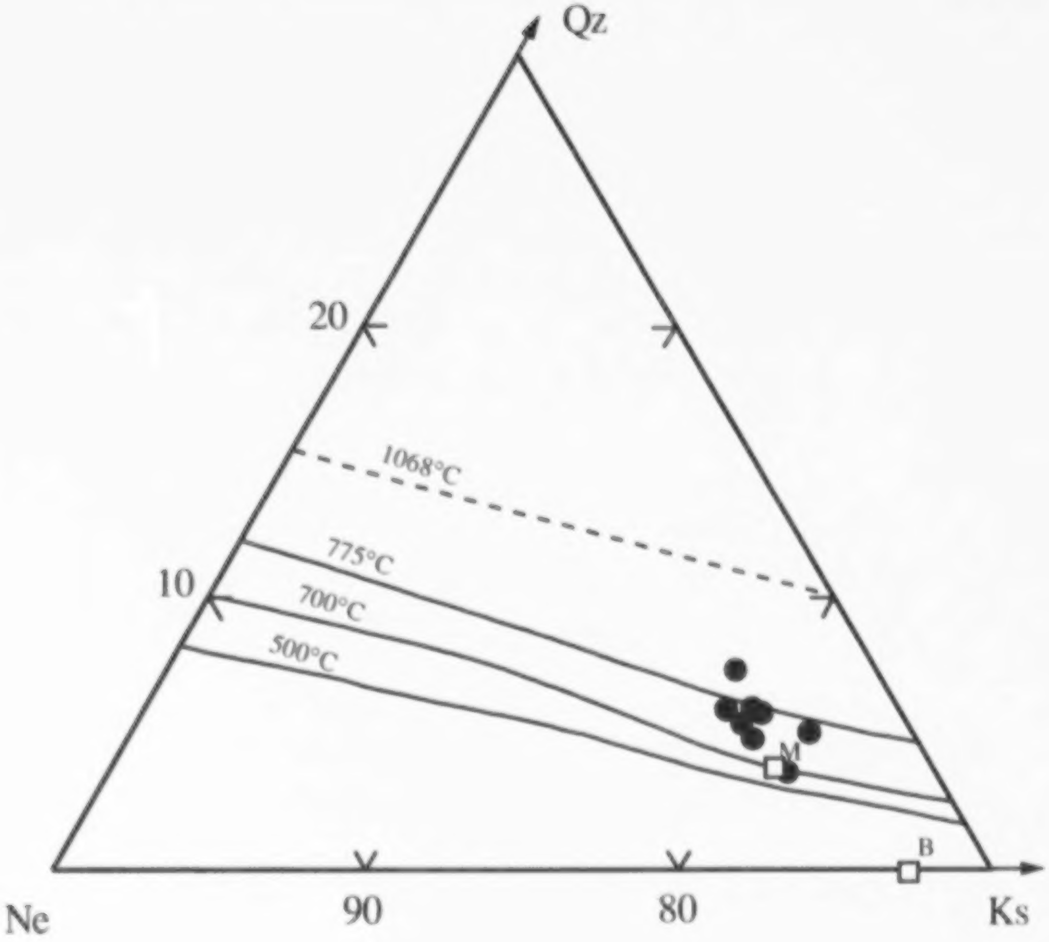

Fig. 17: Nepheline compositions plotted in Ne-Ks-Qz (nepheline-kalsilite-quartz) in wt.%, in Si-undersaturated rocks of the Big Spruce Lake complex. The isotherms indicates temperature ranges of nepheline solid solution, dashed line is inferred temperature boundary, after Hamilton (1961). M and B represent Morozewicz-Buerger convergence field.

4.7 Accessory Minerals

Common accessory minerals in various rocks of the complex include members of apatite and chlorite group, titanian magnetite, ilmenite, titanite and zircon. REE-, Nb-, Ta- and U-bearing minerals and fluorite occur in foyaite, melteigite, ijolite and carbonatites but are lacking in the silica-saturated to oversaturated rocks.

4.7.1 Rare element and REE-bearing minerals

EDS analyses of these minerals are shown in Figs. 18-21. They are determined to be perovskite, pyrochlore and allanite (Figs. 18-20), based on the MinIdent program (Smith and Leibovitz, 1986), and carbocernaite (Fig. 21) based on MinIdent (Smith and Leibovitz, 1986; Smith, 1989) and Wall *et al.* (1993).

The textures and compositions of these minerals indicate primary crystallization. They are related to the late stage crystallization, therefore by a high degree of fractionation.

The perovskite, allanite, and carbocernaite are light REE-enriched. This is characteristic of carbonatite-nephelinite rocks and suggests that the formation of these minerals is related to the degree of magma evolution.

Perovskite is probably formed by the reaction between nepheline and titanite according to Veksler and Teptelev (1990):

$$\underset{\text{nepheline}}{NaAlSiO_4} + \underset{\text{titanite}}{2CaTiSiO_5} = \underset{\text{perovskite}}{2CaTiO_3} + \underset{\text{albite}}{NaAlSi_3O_8}$$

An increase in alkali content diminishes the SiO_2 activity in the melt and increases the stability of perovskite. Therefore, a silica-undersaturated melt favours crystallization of perovskite, but prevents formation of titanite. Peralkaline residual magmas accumulate high concentrations of incompatible trace elements such as Nb, LREE, U, Ta and, therefore, perovskite crystallizing from the magmas is usually a complex Nb-, Ta-, U-, and LREE-bearing solid solution.

4.7.2 Iddingsite

This material appears as red brown grains in olivine-bearing melanocratic syenite and is evidently pseudomorphous after olivine.

The composition is shown in attached Table 16. According to Gay and Le Maitre (1961), iddingsite is neither a single mineral with a definite structure and chemical composition, nor a simple intergrowth of two or more minerals. The term "iddingsite" refers to any member of a continuous alteration series of olivine.

4.7.3 Chlorite

Chlorite is mostly associated with amphiboles and clinopyroxenes. One analysis of the composition is given in Table 16. Its composition is between clinochlore $(Mg_5,Al)(Si_3,Al)O_{10}(OH)_8$ and chamosite $(Fe^{2+}{}_5,Al)(Si_3,Al)O_{10}(OH)_8$ (Bayliss, 1975), and the chlorite is a chamosite.

4.7.4 Opaque minerals

The metallic minerals include Fe-Ti oxides and sulphides. Compositions of the oxide phases obtained by electron microprobe analyses are shown in Table 16. However, the oxide grains show varying degrees of exsolution and this makes it difficult to obtain their bulk compositions.

The oxides are titanian magnetite and Ilmenite which are magnetite-ulvospinel and ilmenite-hematite solid solutions. Both ilmenite and titanian magnetite coexist in most rocks.

The titanian magnetites contain (in wt%) 1.2-2.3% TiO_2, 0.05-1.3% MnO and 0.1% MgO. Ilmenites contain 49.3-53.5% TiO_2. MnO ranges largely between 1.1-4.8%. In the porphyritic foyaite, the MnO content of ilmenite reaches as high as 10.3%.

Sulphides include mainly pyrite and sphalerite. The sulphides are confined to nepheline-bearing rocks and carbonatites and reflect sulphur vapour accumulation at a late stage. Cobalt-pentlandite (Fig. 22) is found associated with olivine and is probably an alteration product within olivine. The Si, Mg peaks are interferences from the host olivine.

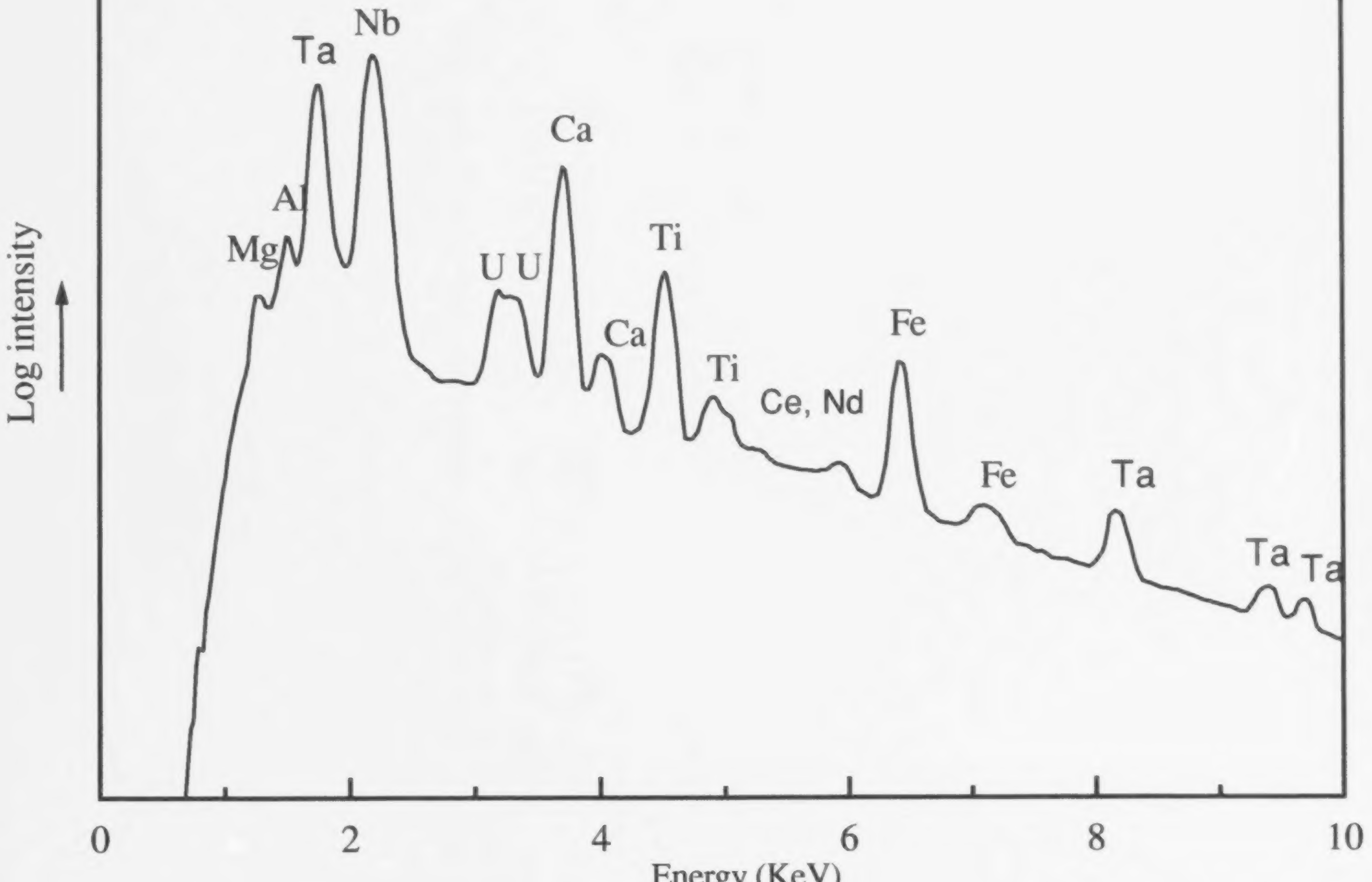

Fig. 18: EDS spectrum of Nb-, Ta-, U-perovskite in melteigite (pc-81169).

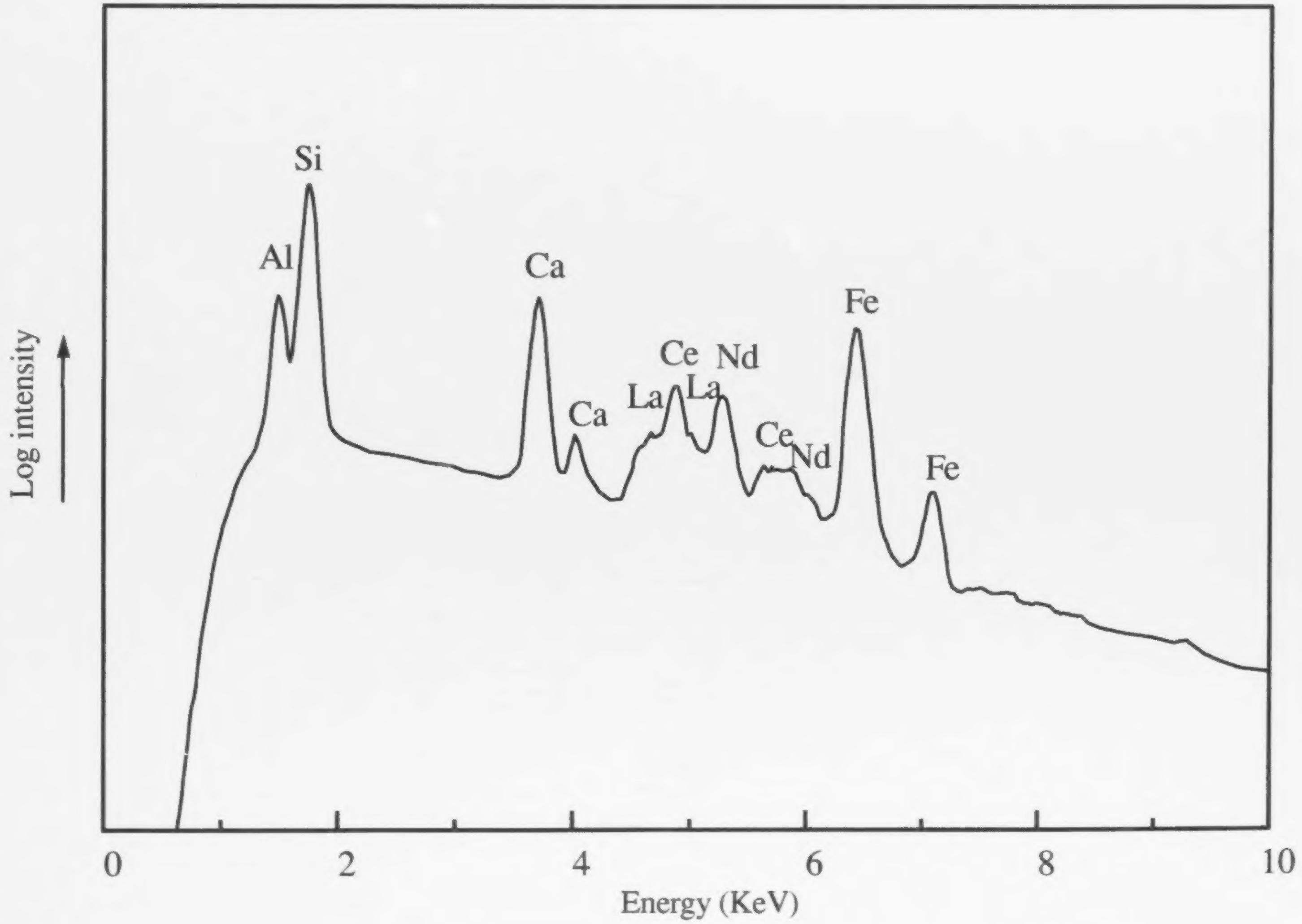

Fig. 19: EDS spectrum of allanite in carbonatite (pc-81471).

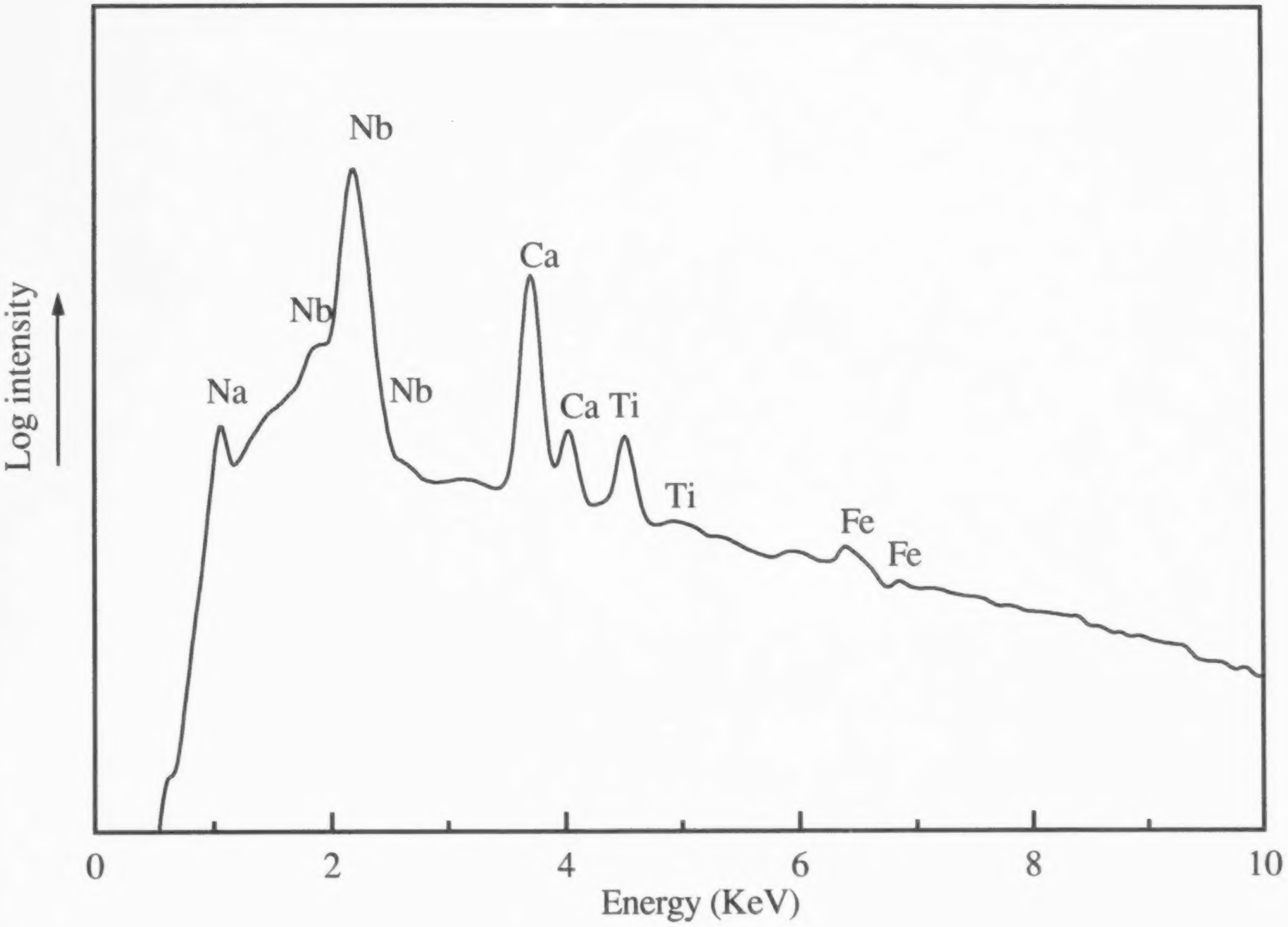

Fig. 20: EDS spectrum of pyrochlore in carbonatite (pc-81471).

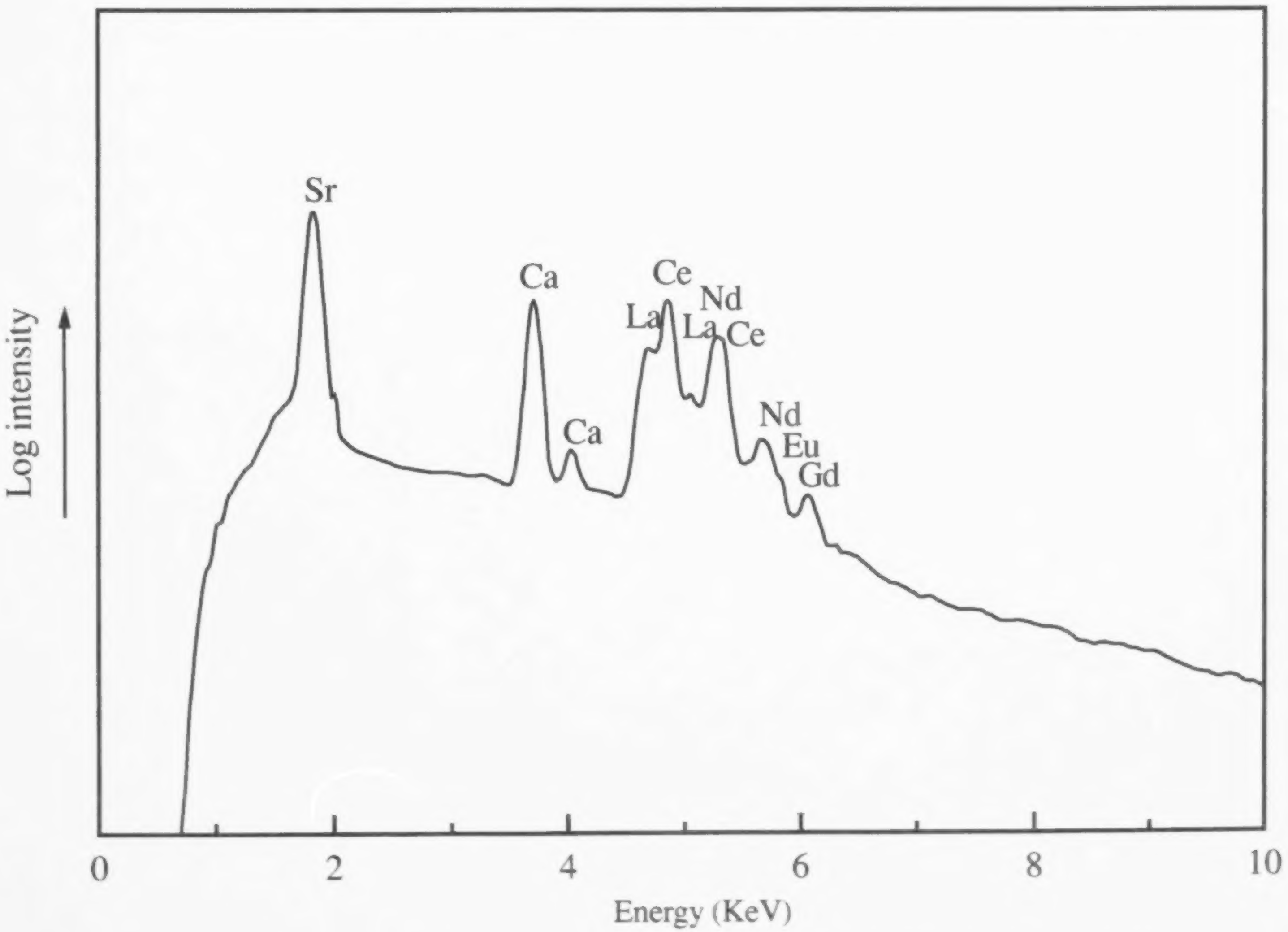

Fig. 21: EDS spectrum of carbocemaite in foyaite (pc-81223).

Table 16. Average oxide and accessory phase compositions.

Rock #	pc-81001	pc-82116	pc-81126a	pc-81126a	pc-81332	pc-81006
SiO2	0.10	0.14	0.11	0.26	0.21	0.10
TiO2	49.60	50.52	49.91	1.20	50.01	49.37
Al2O3	0.05	0.07	0.07	0.70	0.12	0.07
Cr2O3	0.01	0.01	0.02	0.32	0.02	0.02
FeO*	46.41	45.72	46.76	91.10	43.64	46.44
MnO	1.06	2.17	2.25	0.05	4.87	2.32
MgO	0.64	0.10	0.09	0.11	0.05	0.08
Na2O	0.03	0.03	0.02	0.03	0.03	0.03
Total	97.90	98.76	99.23	93.77	98.95	98.43
classification	ilmenite	ilmenite	ilmenite	magnetite	ilmenite	ilmenite
points of analysis	6	6	7	6	3	7

Rock #	pc-81005	pc-81223	pc-81289	pc-82116	pc-82262
SiO2	0.13	0.19	0.06	25.20	44.25
TiO2	50.62	2.36	53.47	0.02	0.04
Al2O3	0.08	0.10	0.07	20.16	0.55
Cr2O3	0.02	0.02	0.00	0.04	0.01
FeO*	45.95	88.24	35.50	31.21	35.23
MnO	2.69	1.27	10.37	0.21	0.29
MgO	0.06	0.06	0.03	11.81	6.93
CaO	N/D	N/D	N/D	0.03	0.43
Na2O	0.06	0.06	0.07	0.02	0.09
K2O	N/D	N/D	N/D	0.16	0.13
Total	99.61	92.30	99.57	88.86	87.95
classification	ilmenite	magnetite	ilmenite	chlorite	iddingsite
no. of anal. pts.	4	3	3	2	3

Note: pc-81001: magnetite pyroxenite; pc-82116: gabbro; pc-81126a: diorite;
pc-81332 & pc-81006: quartz-free syenite; pc-81005: quartz syenite.
pc-82262: olivine melanocratic syenite.
pc-81289: porphyritic foyaite; pc-81223: foyaite.
* = total iron as FeO.

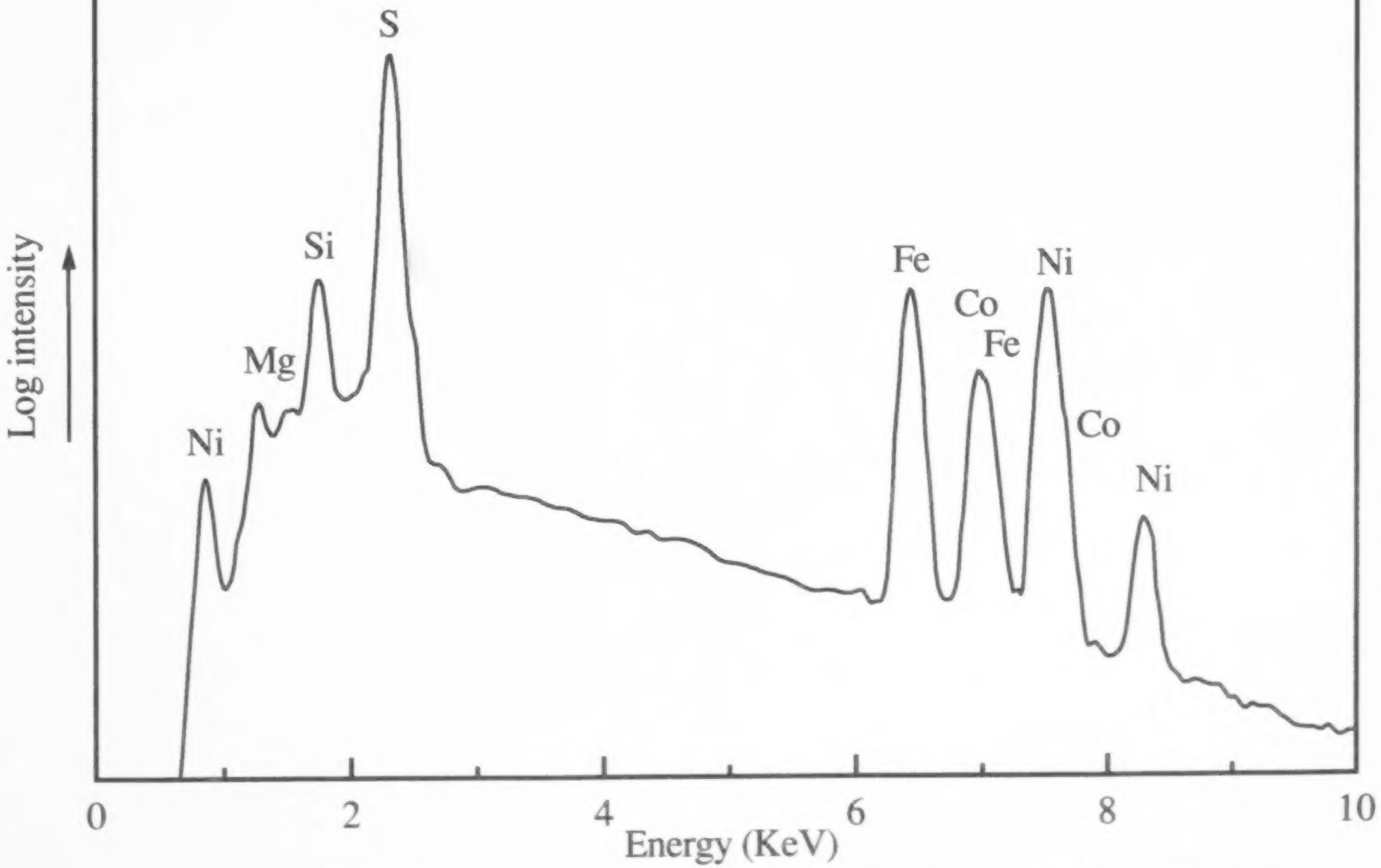

Fig. 22: EDS spectrum of cobalt-pentlandite in olivine of melanocratic syenite (pc-82478). Si and Mg are interference from hosting phase olivine.

Chapter 5.
Minerals as indicators of temperature and oxidation-reduction conditions.

Variation of crystallization temperature and oxidation-reduction conditions of the intrusions of the Big Spruce Lake alkaline complex are evaluated on the basis of the crystallizing mineral assemblage and mineral chemistry.

The rarity of mantle-derived xenoliths suggests a crustal environment for the formation of the various rocks in the Big Spruce Lake alkaline complex.

Temperature of magma crystallization, starting from magnetite pyroxenite through gabbro, diorite, quartz-free syenite, quartz syenite to nepheline syenite, is inferred to have decreased from the sequential crystallization trend of calcic, sodic-calcic and sodic amphiboles (Mitchell, 1990).

The silica-saturated rock series contain augitic pyroxenes (Fe^{2+}-rich). The silica-undersaturated series contain higher aegirine pyroxene (Fe^{3+}-rich). The presence of magnetite and lack of olivine in the nepheline-bearing rocks indicates relatively high fO_2 above QFM buffer (Wones and Gilbert, 1969). Therefore the fO_2 is inferred to have increased according to the increasing Fe^{3+}/Fe^T ratios in the clinopyroxene trend (Bonin and Giret, 1985; Bedard *et al.*, 1988).

In the silica-saturated to oversaturated series, water activity is important as is shown by the abundance of amphiboles. In the silica-undersaturated series, dissolution of amphibole and crystallization of aegirine pyroxenes suggest lower aH_2O (Ernst, 1968).

It is inferred that the silica-saturated rock series crystallized at higher T, aH_2O and more reducing conditions. Subsequent crystallization of the undersaturated rock series occurred at lower T, aH_2O and higher fO_2 conditions.

Chapter 6.
Mass balance calculations of the magma differentiation process.

The calculations of mass balance between rock and constituent minerals by a least square approximation method (Bryan *et al.*, 1969) can quantitatively account for the liquid evolution by removal or addition of mineral assemblages and can be used to evaluate the rôle of different mineral phases during magma evolution. An alkaline basalt from Hualalai, Hawaii (sample #18, in Yoder and Tilley, 1962, p.363) is assumed to represent the parental magma. Other magma and mineral compositions used for the calculations were taken from chemical analyses of the corresponding rocks and minerals of the Big Spruce Lake complex and the data is shown in Table 17 and 18. The calculations were carried out through a program IGPET (Carr, 1991) on an IBM-compatible computer. The procedure of the calculation is explained in Appendix 6. The result of the calculation is illustrated in Table 17.

The first step from alkali basalt (liquid fraction 100%) to gabbro consists of fractionation of 11.2% olivine, 21.4% clinopyroxene and 2.4% Titanian magnetite, resulting in a subtracted solid assemblage similar to magnetite pyroxenite.

The second step from gabboic melt (liquid fraction 65%) to alkali syenite melt is by subtracting 21.7% clinopyroxene, 6.4% hornblendic amphibole, 4.8% ilmenite, 11.8% plagioclase, 0.8% apatite and 3.1% biotite, forming cumulates of gabbros and diorites.

The third step from alkali syenite melt (liquid fraction 33.5%) to foyaite involves fractionation of 28.3% actinolitic amphibole (ferro-actinolite), 1.6% ilmenite, and 18.3% alkali feldspar, coupled with resorption of 11.4% hastingsite amphibole (as shown by the negative value), forming cumulates of alkali syenites and foyaite.

From the above calculations, it is apparent that amphiboles played contrasting rôles during liquid evolution. Fractionation of amphibole (ferro-hornblende) enhances Si enrichment in the residual liquid. Conversely, dissolution of hastingsitic amphibole results in a sharp increase of nepheline in the residual liquid. Thus, amphibole is a critical mineral that allows the magma to cross the olivine-diopside-plagioclase thermal barrier.

The continuing evolution of foyaitic melt (liquid fraction 21.2%) involves fractionation of 5.2% biotite, 17.4% aegirine, 57.4% nepheline and 0.7% titanite, forming cumulates of foyaite and titanite-rich melteigite and 4.1% residual liquid of ijolite composition. Evolution from the last liquid is inferred to have generated residual ijolite, urtite, phonolite and carbonatite.

The percentage of various rock differentiates formed is estimated from the calculation and is shown in Table 19.

Table 17. Mass balance Fractionation/resorption calculations by the least-squares approximation method. Negative amount indicates resorption of the phase. F: % of liquid fraction. r: total square residuum.

Compositions of magma		mineral	mineral per cent	cumulate rock
From alkali basalt, F=100%				
SiO_2 46.43		olivine	11.2	
TiO_2 2.59		clinopyroxene	21.4	magnetite
Al_2O_3 10.91		titanian magnetite		pyroxenite
Fe_2O_3 3.15		magnetite	2.4	
FeO 10.26				
MnO 0.09	r^2=5.099			
MgO 11.08				
CaO 10.09				
Na_2O 3.16				
K_2O 0.54				
P_2O_5 0.67				
To/from gabbro, F=65.0%				
SiO_2 48.43		clinopyroxene	21.7	
TiO_2 3.68		ferro-		
Al_2O_3 16.60		hornblende	6.4	gabbro and
Fe_2O_3 3.65		plagioclase	11.8	diorite
FeO 7.37		biotite	3.1	
MnO 0.13	r^2=6.134	ilmenite	4.8	
MgO 4.96		apatite	0.8	
CaO 8.57				
Na_2O 4.34				
K_2O 1.81				
P_2O_5 0.20				

(to be continued)

(continued from last page)

To/from Qz-free syenite, F=33.5%

SiO_2 55.23		hastingsite	-11.4	
TiO_2 1.47		ferro actinolite	28.3	alkali
Al_2O_3 16.59		ilmenite	1.6	syenite
FeO 9.24		alkali feldspar	18.3	
MnO 0.20				
MgO 1.36	r^2=7.666			
CaO 3.90				
Na_2O 6.26				
K_2O 3.18				
P_2O_5 0.00				

To/from foyaite, F=21.2%

SiO_2 51.38		aegirine augite	17.4	
TiO_2 0.39		biotite	5.2	foyaite &
Al_2O_3 20.93		nepheline	57.4	melteigite
FeO 5.76		titanite	0.7	
MnO 0.25				
MgO 0.65	r^2=16.216			
CaO 4.31				
Na_2O 10.57				
K_2O 5.19				
P_2O_5 0.05				

To ijolite, F=4.1%.

Table 18. Mineral compositions for the mass-balance calculations.

oxide	olivine	augite	aeg-aug	fo-hn	has am	actinolite	plag
SiO2	40.32	50.79	51.97	44.23	38.5	49.92	64.5
TiO2	0.01	1.2	0.34	0.16	0.18	0.19	0
Al2O3	0.06	3.06	0.95	6.94	14.41	1.31	20.81
Fe2O3	0	0	0	0	0	0	0
FeO	14.13	9.02	22.31	25.24	24.8	29.12	0.5
MnO	0.15	0.19	0.79	0.32	0.2	0.79	0
MgO	44.77	14.45	4.2	6.07	4.83	4.14	0.32
CaO	0.08	20.67	13.6	11.56	11.32	10.11	2.61
Na2O	0	0.52	5.76	0.84	2.58	1.07	9.36
K2O	0	0	0	0.74	0.64	0.34	1.41
P2O5	0	0	0	0	0	0	0
H2O	0	0		3			0
Total	99.52	99.9	99.92	99.1	97.46	96.99	99.51

oxide	biotite	alkali fsp	nepheline	titanite	apatite	Ti-mag
SiO2	35.41	64.08	43.29	33.14	7.55	0.11
TiO2	3.23	0.09	0	35.62	0	50.66
Al2O3	9	20.12	34.31	1.9	0	0.03
Fe2O3	0	0	0.22	0	0	0
FeO	33.4	0.12	0	1.51	0	45.48
MnO	0.71	0.03	0	0.11	0.07	1.13
MgO	3.46	0	0.03	0.01	0	0.58
CaO	0.06	0.31	0.02	27.69	52.7	0
Na2O	0.04	3.36	15.58	0.01	0	0.04
K2O	8.85	11.89	6.16	0	0	0
P2O5	0	0	0	0	39.68	0
H2O	4				0	0
Total	98.16	100	99.61	99.99	100	98.03

Note: aeg-aug: aegirine augite; ferro-hn: ferro hornblende;
has am: hastingsite; plag: plagioclase;
alkali fsp: alkali feldspar; Ti-mag: titanian magnetite.

Table 19. Calculated percentage of rock types of the Big Spruce Lake complex by mass balance calculations.

Rock type	mass per cent
olivine magnetite pyroxenite	35
gabbro, diorite	31.5
alkali syenites	12.3
foyaite, melteigite	17.1
ijolite, urtite, phonolite, carbonatite	4.1

Chapter 7.
Discussion.

7.1 Fractional crystallization process

Field relationships, petrography and mineral chemistry are consistent with fractional crystallization playing a dominant rôle in the origin of the Big Spruce Lake complex. Isotopic evidence permits such an interpretation because both the plutonic silica-undersaturated and silica-saturated to oversaturated rocks have identical isotopic signatures, the same intrusive age and were supposed to have formed from a common mantle source region (Cavell, 1986).

In the field, the five intrusive centres migrate in roughly linear alignment from north to south from centre 1 to centre 5. The development of several intrusive centres indicates that the formation of the complex has involved intrusion and differentiation of multiple magma pulses that gave rise to the spectrum of rock types. Migration of magma source and emplacement with time would account for the migration of individual intrusive centres (Mitchell *et al.*, 1993; Woolley and Platt, 1986). Periodic tapping of the magma from depth would account for the multiple intrusive character in each centre of the complex.

The petrographic characteristics of the plutonic intrusions indicate similar textures and gradual variation in mineral assemblages and suggest genetic links between the various rock types by fractional crystallization.

The distribution of rock-forming minerals in the complex defines a continuous evolutionary trend. The clinopyroxenes demonstrate a complete trend from Mg-rich augite through Fe-rich augite to aegirine augite and aegirine as the magma evolved from silica saturation and oversaturation to silica undersaturation. Similarly, the amphiboles vary from calcic species through sodic-calcic species to sodic species. The feldspars vary from Ca-rich to Na-rich plagioclase and alkali feldspar. Biotites vary from Mg-rich to Fe-rich biotites. The appearance of aegirinic pyroxenes, winchite, and alkali feldspar clearly indicate a trend of increasing peralkalinity.

Continuous mineral compositions from one rock unit to another have been cited as evidence of crystallization from genetically related magma (Dorais and Floss, 1992). From the mineral compositional variations in the Big Spruce Lake complex, it is conceivable that the magma was continuously evolved dominantly through fractional crystallization. Early fractional crystallization from the parental magma gave rise to magnetite pyroxenite, gabbro, diorite, syenite and quartz syenite for the silica-saturated to oversaturated series. Resorption of amphiboles into the parent melt then resulted in peralkaline undersaturated magma which underwent successive fractionation and immiscibility processes (see *7.3* in this chapter), giving rise to foyaite, melteigite, ijolite, urtite, phonolite and carbonatite. The course of fractionation within the undersaturated rock series is not clear because of a lack of complete field observations and other information. Urtite could result from liquid immiscibility taking place in an ijolite at plutonic mid-crustal levels (Le Bas, 1987).

The U, REE, Nb and Ta-bearing minerals represent late stage fractionation products and support the hypothesis that nepheline syenite and ijolite rocks originate from a fractionated residual magma.

Mass balance calculations define several magma evolutionary stages that are consistent with the fractional crystallization model.

The relationship between the satellite intrusion and the main intrusions is enigmatic. The large difference of mineral chemistry between the satellite rocks and the main intrusive rocks suggests, perhaps an indirect fractional crystallization relationship between them or no relationship at all.

7.2 The amphibole dissolution process

Primary amphibole is confined to the silica-saturated to oversaturated series and is absent in the silica-undersaturated rocks. Crystallization of aegirine augite rather than amphibole in the undersaturated rocks indicates an environment of higher fO_2 (see chapter 5.) and lower aH_2O and suggests that amphibole was probably dissolved into the evolving magma.

In the gabbro and magnetite pyroxenite, kaersutite displays evidence of resorption which is illustrated by skeletal kaersutite grains (plate 4) enclosed by titanian augite which is the attendant precipitation phase. In alkaline volcanic rocks, the breakdown of kaersutite is commonly observed (Tomita, 1934).

Available experimental data on amphibole-magma relations demonstrate that amphiboles could break down because of modification of factors such as pressure, temperature, water, volatile content. According to Bonin and Bardintzeffe (1989), the amphibole breakdown could be expected at pressures of less than 1.5-2 kbar at magmatic temperatures (950-1000°C). Thus, in a wide range of compositions of magmas and volatiles, amphibole dissolution would be expected at depths of about 5-8 km. Varne (1968) invoked partial melting of pargasite to generate the olivine melanephelinites and nephelinites. According to Luth (1974), if amphibole is transported to a P-T region nearer the surface, the amphibole could be resorbed by an alkaline olivine basalt to produce the same result. Resorption of primary amphiboles have been regarded as a crucial means to create residual silica-undersaturated magma (Bowen, 1928; Wones, 1979; Yoder & Tilley, 1962; Foland *et al.*, 1993).

The stability limits of amphibole at crustal depths are essentially controlled by temperature, oxygen fugacity and vapour composition (Helz, 1982; Holloway, 1973; Bonin & Bardintzeff, 1989). According to Holloway (1973), the stability of pargasite decreases continuously with decreasing X_{H_2O} at P<4 kbar. The upper stability limits are reached at higher temperatures (1035°C at 2 kbar) in a water-saturated system than in a mixed water-carbon dioxide system (970°C at 2kbar for $X_{H_2O}=0.3$) (Holloway, 1973). Helz (1973) showed that the upper stability field of hornblende decreases as oxygen fugacity increases, its upper stability limit rises substantially from 960°C to >1000°C as f_{O_2} decreases from that of the hematite-magnetite to that of the quartz-fosterite-magnetite buffer. Thus, the amphibole breakdown reactions could occur under one or a combination of the following conditions:

(1) Modification in vapor composition, by lowering X_{H_2O}, resulting in a lowering of the upper stability limit and a subsequent breakdown reaction.

(2) Increasing of f_{O_2} resulting in the lowering of the upper stability limit of temperature.

(3) A sudden increase of temperature caused by replenishment from the differentiating reservoir (Bonin and Bardintzeffe, 1989).

In the Big Spruce Lake complex, silica-saturated to oversaturated rocks are formed in the presence of sufficient water so that amphibole remains stable in a relatively reducing environment. Silica-undersaturated rocks are formed under a more oxidizing condition with higher X_{CO_2} (indicated by associated carbonatites and interstitial carbonates) and thus lower X_{H_2O} fraction. It is possible that the temperature may have been raised locally during the ascent of magma. Therefore, it is conceivable that a combination of increasing f_{O_2} and temperature and decreasing a_{H_2O} could have resulted in the breakdown of early-formed amphibole crystals in the Big Spruce Lake alkaline complex.

Amphibole could have been extracted primarily through post cumulus reaction when magma circulated through crystal networks (Bedard *et al.*, 1987). According to Giret (1979) and Foden and Green (1992), the amphibole breakdown reaction is as follows:

Liquid 2 + Amphibole = Clinopyroxene + Liquid 1.

The liquid 1 and 2 are successive batches of magma. The magma formed was aegirinic pyroxene-rich, more Si-poor and peralkaline (Giret, 1979).

7.3 The liquid immiscibility process

Immiscibility appears to have occurred in CO_2-enriched foyaite magmas, which, in addition to exsolving carbonates, also underwent continued fractionation giving rise to ijolite in the foyaite intrusive body.

Evidence that supports the formation of carbonatite by immiscibility from CO_2-rich nepheline syenitic magmas includes:

1. The field relationship shows a circular carbonatite core surrounded by the main foyaite intrusion (Martineau, 1970). Ijolite is

also surrounded by the foyaite. This suggests that carbonatite and ijolite were emplaced and produced after foyaite. Since carbonatite magma has very low viscosity (5×10^{-2}) and density compared to silicate magma (Treiman and Schedl, 1983), it tends to be concentrated at the centre. Therefore a carbonatite core could have been formed by silicate-carbonate immiscibility and gravity separation.

2. Petrographic studies show that the amount of carbonate in ocelli or interstitial vesicles increases drastically in nepheline-bearing rocks. The carbonatite ocelli, which are interpreted as being the residual carbonate in the silicate melt after the immiscible separation of the carbonate melt (Le Bas, 1987), suggests a large increase of CO_2 activity in foyaite melts and indicates the presence of an immiscible carbonatitic liquid in equilibrium with silicate minerals during crystallization of nepheline syenite magma.

3. The nepheline syenites and carbonatite have essentially identical major mineral assemblages. The accompanying minerals other than carbonate in carbonatites include aegirine augite, alkali feldspar, biotite, titanite and apatite, and indicate the coexistence of carbonate and silicate in the carbonatite melt. Also, it was observed that alkali feldspar formed fine-grained aggregate within the carbonates. The presence of silicate minerals in carbonatite suggest that the carbonatite magmas were not just calcitic or dolomitic in compositions.

4. The nepheline syenite and carbonatite have similar accessory mineral assemblages. REE, RE and U-bearing minerals such as perovskite, allanite, pyrochlore, fluorite, carbocernaite are found only in these rocks in the complex and suggests that the nepheline syenites and carbonatites were formed from common and highly differentiated melts.

5. The range of initial Sr^{87}/Sr^{86} ratios in the carbonatites (0.70072-0.70323) largely coincide with the range in the silicate rocks (0.68800-0.70228) (Cavell, 1986). The individually higher values in carbonatites were caused by Sr contamination of wall rock (Cavell, 1986). However, all these values are mantle-type isotopic

ratios (Powell & Bell, 1974; Rock, 1976) and suggest the same parental magma.

Experimental studies (Koster Van Groos & Wyllie, 1973; Wyllie, 1978, Wyllie *et al.*, 1990; Kjarsgaard & Hamilton, 1989) have confirmed carbonate-silicate liquid immiscibility which occurs when the carbonate concentration in the host silicate magma reaches some critical level (a function of pressure, temperature and volatile content). Fluid inclusions in apatite within ijolite have bulk compositions close to natrocarbonatite (Le Bas & Aspden, 1981; Rankin & Le Bas, 1974). Abundance of P_2O_5 strongly affects the degree of liquid polymerization (Mysen, 1988), enlarging the miscibility gap in the system (Ryerson & Hess, 1980). These studies provided another line of evidence that liquid immiscibility can separate carbonate and silicate magmas.

7.4 Chemical evolution of alkaline magmas as a result of differentiation of rock-forming minerals

Clinopyroxene and amphibole versus the whole rock Fe/(Fe+Mg) ratio and SiO_2 content are plotted in Figs. 23 and 24 to quantify the rôle played by mafic minerals in influencing the chemical variation in magmas. The diagonal is the line on which $K_{D(min/wr)}=1$.

Calcic clinopyroxenes from silica-saturated rocks show an Fe/(Fe+Mg) ratio which is much lower than that in the corresponding whole rocks (Fig. 23). Thus, fractionation of calcic clinopyroxene would cause Fe enrichment in a differentiated alkaline rock series. Sodic-calcic and sodic clinopyroxenes from silica-undersaturated rocks plot around the 1:1 line indicating equal Fe/(Mg+Fe) ratio with the residual liquids. Therefore crystallization of late alkali clinopyroxenes does not exert an influence on the magma's Fe/(Mg+Fe) ratio but only reflects the residual magma chemistry.

The calcic amphiboles in the Big Spruce Lake complex are characterized by a much lower silica content compared to their host rocks (Fig. 24). Therefore, fractionation of amphibole would lead to more and more silica-enriched residual liquids. On the other hand, resorption of amphibole would lead to silica-undersaturated and peralkaline liquids as described by Giret (1979) and Giret *et al.*

(1980). The contrasting behavior of amphibole, fractionation and resorption, results in the coexistence of the silica-saturated and undersaturated alkaline plutonic rock series.

Calcic plagioclases play an essential rôle in the enrichment of sodium and silica by the "plagioclase effect" (Bowen, 1945). This effect is evident in the silica-saturated to oversaturated trend, and is not apparent in the silica-undersaturated series as plagioclase disappears.

Crystallization of alkali feldspars leads to strongly peralkaline and sodic residual liquids by the "orthoclase effect" (Bailey and Schairer, 1964). However, the alkali feldspar only plays a significant rôle in highly differentiated rocks (alkali syenite and nepheline syenite).

Late minerals such as aegirine augite, riebeckite, albite, annite-rich mica, microcline, feldspathoids and quartz crystallize after the calcic minerals and plagioclase, and therefore they do not play an active rôle in differentiation of liquids. In this scheme, they mainly reflect the late stage of differentiation (Martin and Bowden, 1981).

7.5 Inferred parental magma

In alkaline volcanic and plutonic complexes, all rock types encountered are formed from more or less evolved melts derived by differentiation of primary magmas in deep magma chambers (Bonin and Bardintzeff, 1989)

Most rocks exposed in the Big Spruce lake alkaline complex are cumulates, and therefore, there is no direct evidence of the compositions of parental magma. The gabbros and olivine magnetite pyroxenite indicate accumulation from melts that were saturated in olivine, clinopyroxene and plagioclase. The gabbro represents the intrusive equivalent of a basalt and suggests crystallization from a basaltic magma. The olivine magnetite pyroxenite may represent early fractional crystallization from an alkali olivine basalt melt.

Therefore, the primitive magma is inferred to be a critically undersaturated alkali olivine basalt. Nephelinite and basanite are precluded from being the parent magma because no equivalent extrusive and intrusive rocks are found. In this scheme, the nepheline syenite in the Big Spruce Lake complex is more probably formed from an evolved magma.

Rock (1991) proposed that lamprophyres may represent the parental melts from which other rocks such as shonkinite and alkali basalt have been evolved. Philpotts (1974) inferred that camptonite, monchiquite and alnoite were parental magma to the plutonic cumulate suites of gabbro-syenite, essexite-foyaite and ijolite-carbonatite in the Monteregian province.

The lamprophyre dykes are available candidates for parental magmas in the Big Spruce Lake complex. The presence of diopside and An_{70}-plagioclase which are the most primitive in the complex suggests that the lamprophyre and highly potassic rocks were derived from relatively unevolved magma. However, the enrichment of K, Rb, Zr, Nb, and REE observed in these rocks relative to basalts (Yoder and Tilley, 1962) poses severe problems if the lamprophyres are to be considered parental.

7.6. Physical process of the magma evolution of the Big Spruce Lake alkaline complex

It is proposed that the magma evolution follows the schematic flow chart in Fig. 25.

A primary alkaline olivine basalt was formed by partial melting of mantle. The olivine fractionated in the basalt, yielding an olivine magnetite pyroxenite cumulate, some of the cumulate was squeezed up into the crust as olivine magnetite pyroxenite dykes. At the same time, an olivine-poor gabbroic magma was left over.

In situ fractionation of the gabbroic melt yielded gabbro cumulate, and diorite melt from which a diorite intrusive body was formed. Some gabbro cumulate was later squeezed into the diorite.

Fractionation from the diorite melt produced the alkali syenite melt which fractionated to quartz-free syenite and then quartz syenite. Migration of source magma with time caused the later intrusions (alkali syenites) to the southwest along the Snare fault weakness.

Dissolution of amphiboles in the alkali syenitic magma created a foyaitic melt from which a foyaite cumulate was formed. Part of the cumulate was squeezed into upper level to form an intrusive foyaite body. Carbonatitic melt was separated from the foyaitic melt by liquid immiscibility and intruded as dykes and pipes at higher levels. Continuing fractionation from the foyaitic magma produced the series melteigite, ijolite and phonolite. The intrusion of centres 3 and 4 migrated further to the southwest along the Snare fault.

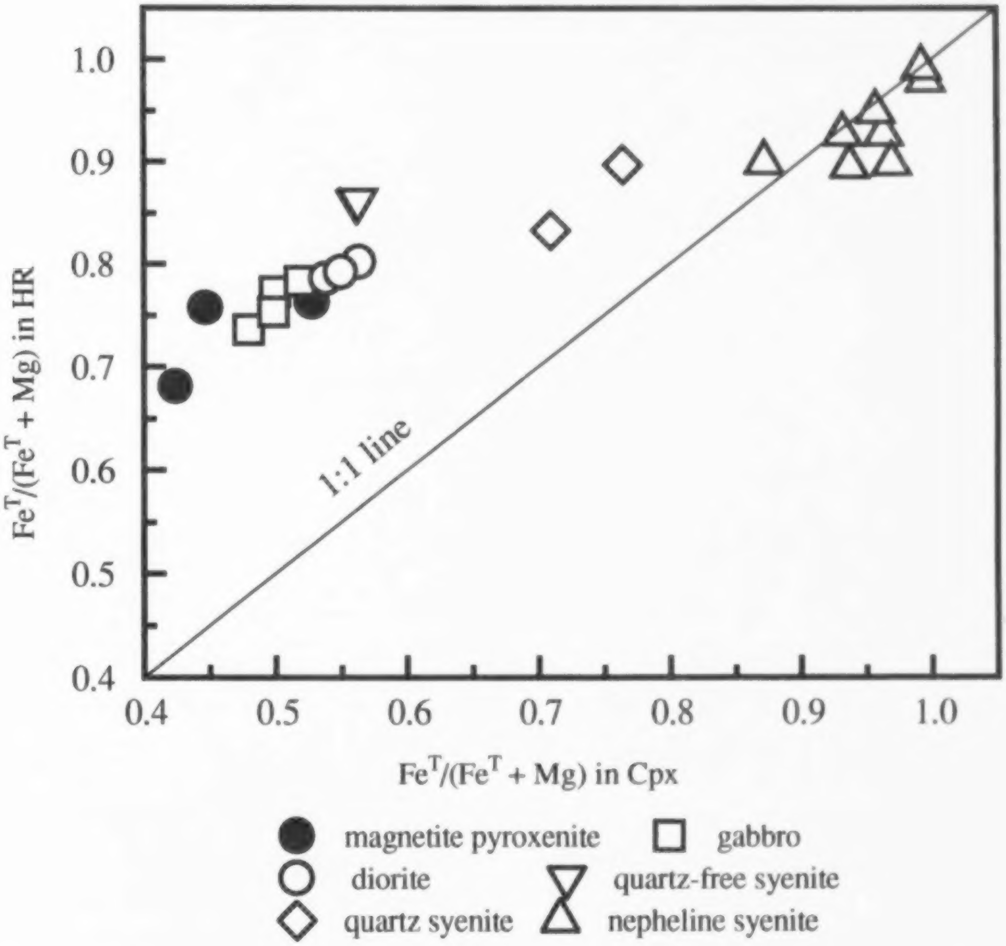

Fig. 23: Relations between $Fe^T/(Fe^T+Mg)$ (wt.) ratios in clinopyroxenes (Cpx) and in host rocks (HR). The diagram emphasizes the role played by calcic pyroxenes in Fe enrichment of the liquid. It also shows the equilibrium of the late pyroxenes with residual liquids. Rock data is from Cavell (1986) and Martineau (1970).

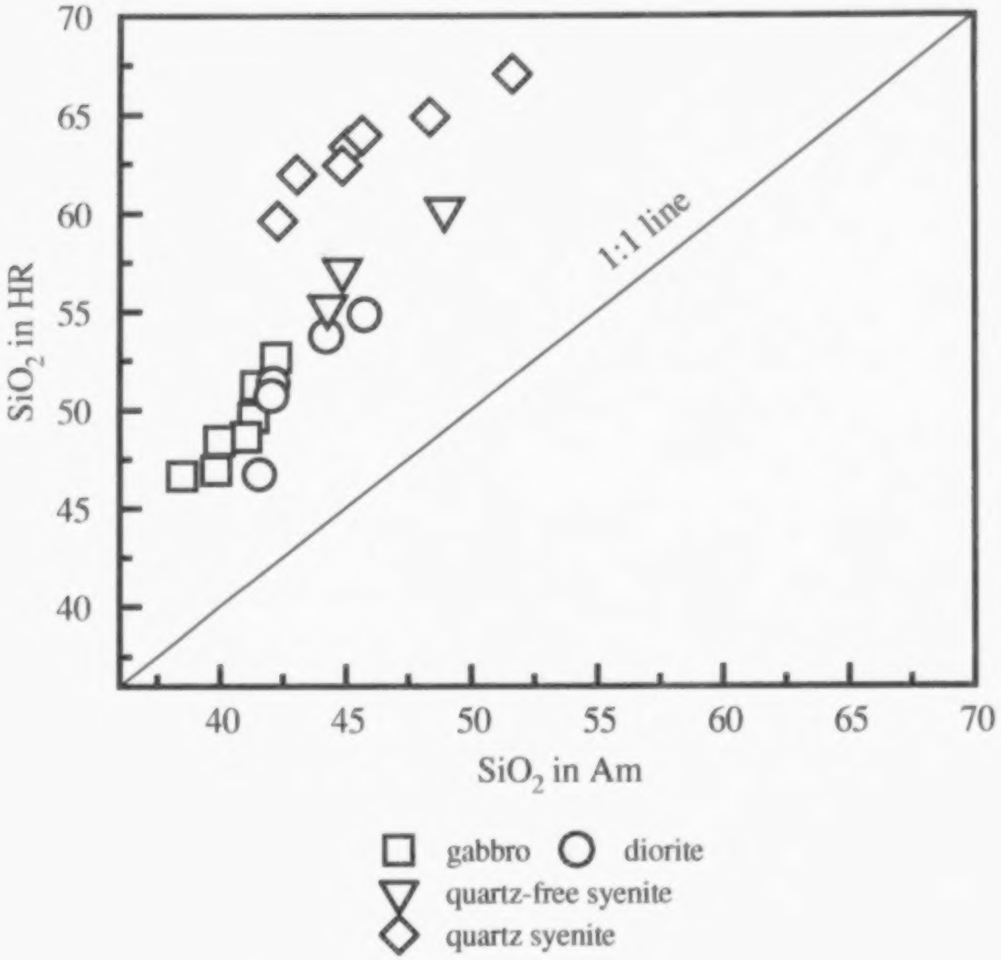

Fig. 24: Relations between SiO$_2$ (wt.%) in amphiboles (Am) and in host rocks (HR). The diagram emphasizes the role played by calcic amphiboles in Si enrichment in the liquid.

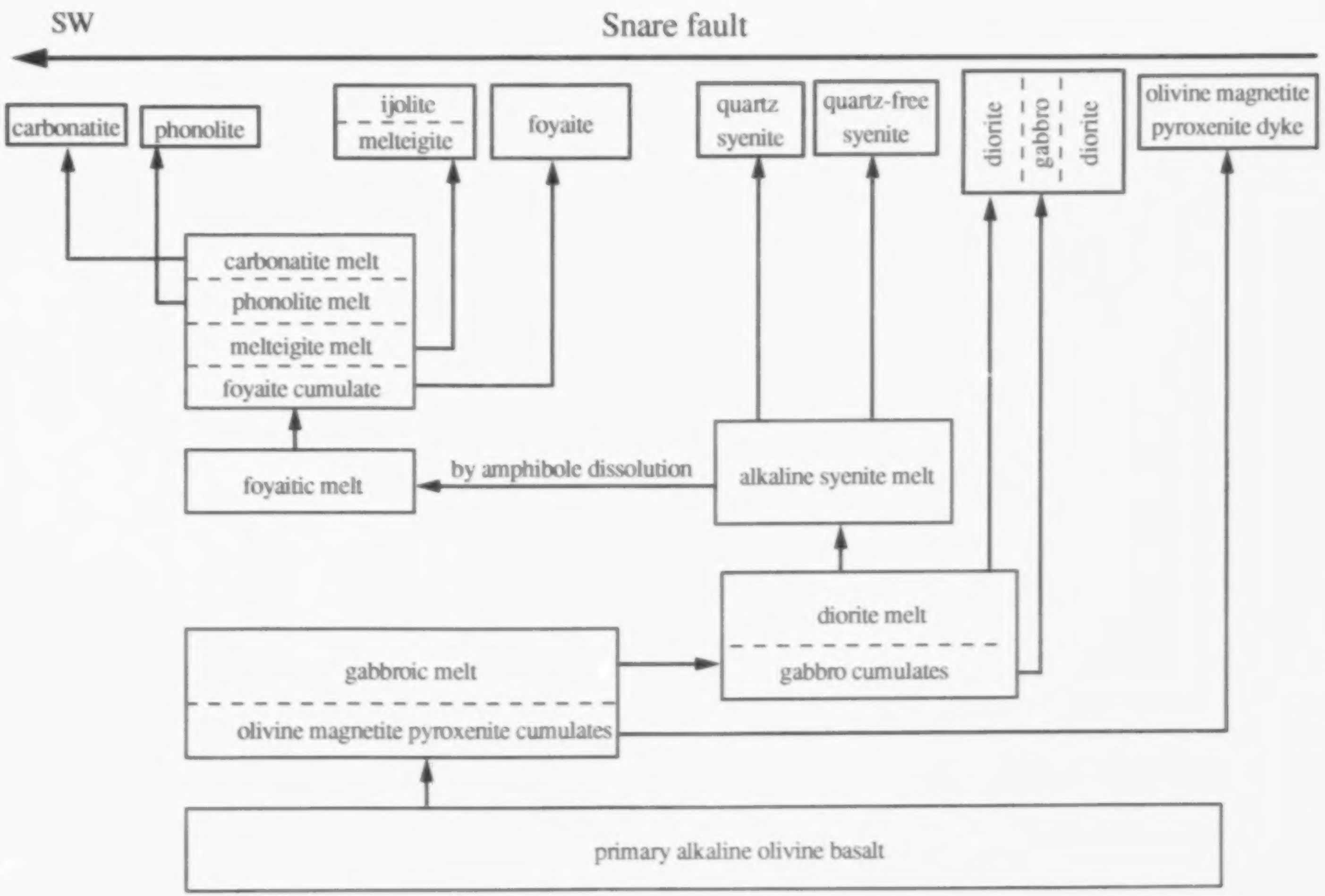
SW
Snare fault
carbonatite
phonolite
ijolite
melteigite
foyaite
quartz syenite
quartz-free syenite
diorite
gabbro
diorite
olivine magnetite pyroxenite dyke
carbonatite melt
phonolite melt
melteigite melt
foyaite cumulate
foyaitic melt
by amphibole dissolution
alkaline syenite melt
diorite melt
gabbro cumulates
gabbroic melt
olivine magnetite pyroxenite cumulates
primary alkaline olivine basalt

Fig.25: Flow chart of the magma types and intrusive processes of the Big Spruce Lake alkaline complex. The horizontal dimension roughly represents the locations of various intrusive bodies.

Chapter 8.
Conclusion.

Mineral fractionation played an essential rôle in the evolution of the alkaline magmas in the Big Spruce Lake complex. Fractionation of calcic clinopyroxenes had the effect of Fe enrichment, while plagioclase and alkali feldspar had effect on Na enrichment in the magma. The rôle of calcic amphiboles was fundamental to the silica content of the magma. Fractionation of calcic amphiboles had the effect of Si enrichment. Resorption of calcic amphiboles (especially hastingsite and kaersutite) had a significant effect on silica depletion and changed the course of magma evolution from silica-oversaturation towards silica-undersaturation. The coexistence of silica-saturated to oversaturated and silica-undersaturated rock series could be controlled by differentiation of these minerals.

Crystallization conditions in the Big Spruce Lake alkali complex varied from relatively high T (temperature), X_{H_2O} and low fO_2 towards relatively low T, X_{H_2O} (high X_{CO_2}) and high fO_2. The stability of amphibole is essentially influenced by T, X_{H_2O} and fO_2 changes.

The parent magma is inferred to be a critically-undersaturated, alkali olivine basalt. Fractional crystallization from this basalt controlled the silica-saturated to oversaturated rock series. Amphibole dissolution controlled the formation of a nepheline syenitic melt. Liquid immiscibility from the modified nepheline syenitic magma produced the carbonatite and probably ijolite and urtite.

Bibliography.

Andersen, T., 1988, Evolution of peralkaline calcite carbonatite magma in the Fen complex, southeast Norway. *Lithos,* 22, 99-112.

Azambre, B., Rossy, M. and Albarede, F., 1992, Petrology of the alkaline magmatism from the Cretaceous North-Pyrenean Rift Zone (France and Spain), *European Journal of Mineralogy,* 4, 813-834.

Bailey, D.K. and Schairer, J.F., 1966, The system Na_2O-Al_2O_3-Fe_2O_3-SiO_2 at 1 atmosphere. *Journal of Petrology,* 7, 114-170.

Bailey, D.K. and Schairer, J.F., 1964, Feldspar-liquid equilibria in peralkaline liquids: the orthoclase effect. *American Journal of Science,* 262, 1198-1206.

Bayliss, 1975, Nomenclature of the trioctahedral chlorites. *Canadian Mineralogist*, 13, 178-180.

Bedard, J.H.J., Francis, D.M., and Ludden, J., 1988, Petrology and pyroxene chemistry of Monteregian dykes: the origin of concentric zoning and green cores in clinopyroxenes from alkali basalts and lamprophyres. *Canadian Journal of Earth Sciences,* 25, 2041-2058.

Bedard, J.H.J., Ludden, J.N. and Francis, D.M., 1987, The Megantic Intrusive Complex, Quebec: a Study of the derivation of silica-oversaturated Anorogenic magmas of alkaline affinity. *Journal of Petrology,* 28, 355-388.

Bonin, B. and Bardintzeff, J.M., 1989, Plutonic rocks from Tahiti-Nui caldera (French Polynesia) II -- Evolution of thermodynamic parameters during magma differentiation and emplacement. Applications to other alkaline magmatic provinces. *Bulletin Societé Géologique de France,* 8, 1091-1099.

Bonin, B. and Giret, A., 1985, Contrasting rôles of rock-forming minerals in alkaline ring complexes, *Journal of African Earth Sciences,* 3, 41-49.

Bowen, N.L. 1945, Phase equilibria bearing on the origin and differentiation of the alkaline rocks. *American Journal of Science,* 243A, 75-89.

Bowen, N.L., 1928, The evolution of igneous rocks. Princeton university Press, Princeton, NJ, 384pp.

Bowen, N.L., 1922, The reaction principle in petrogenesis. *Journal of Geology*, 30, 77-198.

Bryan, W. B., Finger, L.W. and Chayes, F., 1969, Estimating proportions in petrographic mixing equations by least-squares approximation. *Science*, 163, 926-927.

Buerger, M.J., Klein, G.E. and Hamburger, G., 1947, The structure of nepheline. *American Mineralogist*, 32, p.197.

Carmichael, I.S.E., Turner, F.J. and Verhoogen, J., 1974, Igneous Petrology. McGraw-Hill, New York, 282-285.

Carr, M.J., 1991, IGPET 3.0, In: Smith, D.G.W. (ed.): IMA Catalogue of software for Mineralogists, IMA (WGDCA), 1st edition (1992), Edmonton, 197pp.

Cavell, P.A., 1986, The geochronology and petrogenesis of the Big Spruce Lake alkaline complex. Unpublished Ph.D. thesis, University of Alberta, Edmonton, Canada, 448pp.

Coombs D.S. and Wilkinson, J.F.G., 1969, Lineages and Fractionation trends in undersaturated volcanic rocks from the East Otago Volcanic Province (New Zealand) and related rocks. *Journal of Petrology*, 10, 440-501.

Dorais, M.J. and Floss, C., 1992, An ion and electron microprobe study of the mineralogy of enclaves and host syenites of the Red Hill complex, New Hampshire, USA. *Journal of Petrology*, 33, 1193-1218.

Dowty, E., 1976, Crystal structure and crystal growth, II, Sector zoning in minerals. *American Mineralogist*, 61, 460-469.

Ernst, W.G., 1968, Amphiboles. Springer, New York, 125pp.

Ferguson, A. K., 1978, The crystallization of pyroxene and amphibole in some alkaline rocks and the presence of a pyroxene compositional gap. *Contributions to Mineralogy and Petrology*, 67, 11-15.

Foden, J.D. and Green, D.H., 1992, Possible rôle of amphibole in the origin of andesite: some experimental and natural evidence. *Contributions to Mineralogy and Petrology*, 109, 479-493.

Foland, K.A., Landoll, J.D., Henderson, C.M.B. and Chen, J., 1993, Formation of cogenetic quartz and nepheline syenites. *Geochimica. et Cosmochimica Acta*, 57, 697-704.

Forbes, W.C. and Starmer, R.J., 1974, Kaersutite is a possible source of alkali olivine basalts. *Nature,* 250, 209-210.

Freestone, I.C. and Hamilton, D.L., 1980, The rôle of liquid immiscibility in the genesis of carbonatites - an experimental study. *Contributions to Mineralogy and Petrology,* 73, 105-117.

Fudali, R.F., 1965, Oxygen fugacities of basaltic and andesitic magmas. *Geochimica et Cosmochimica Acta,* 29, 1063-1075.

Gay, P. and La Maitre, R.W., 1961, Some observation on "iddingsite". *American Mineralogist,* 46, 92-111.

Gilbert, M.C., Helz, R.T., Popp, R.K. and Spear, F.S., 1982, Experimental studies of amphibole stability. In: Veblen, D.R. and Ribbe, P.H. (ed.) Amphibole II: Petrology and Experimental phase relations. *Reviews in Mineralogy 9B,* Mineralogical Society of America, 229-278.

Giret, A., 1979, Genèse de roches feldspathoïdiques par la destabilisation des amphiboles: massif des Montagnes Vertes, Kerguelen (T.A.A.F.) C.R. Academie Science, Paris, 289, 379-382.

Giret, A., Bonin, B., and Leger, J.M., 1980, Amphibole compositional trends in oversaturated and undersaturated alkaline plutonic ring complexes, *Canadian Mineralogist,* 18, 481-495.

Giret, A. and Lameyre, J., 1980, Mise en place et évolution magmatique des complexes plutonique de la Caldera de Courbet, Iles Kerguelen (T.A.A.F.). *Bulletin Societé Géologique de France,* 22, 437-446.

Gittins, J., 1989, The origin and evolution of carbonatite magmas, In: Bell, K. (ed.) Carbonatites -- Genesis and evolution, London, Unwin Hyman, 580-600.

Gomez, J.M.C., 1990, PX: A Program for pyroxene classification and calculation of end-members, *American Mineralogist,* 75, 1426-1427.

Hamilton, D.L., 1961, Nepheline as crystallization temperature indicators. *Journal of Geology,* 69, 321-329.

Helz, R.T., 1973, Phase relations of basalts in their melting range at P H_2O=5 kbar as a function of oxygen fugacity. *Journal of Petrology,* 14, 249-302.

Helz, R.T., 1982, Phase relations and compositions of amphiboles produced in studies of the melting behaviour of rocks. In: Veblen, D.R. & Ribbe, P.H. (Eds), Amphiboles II: Petrology and experimental phase relations. *Reviews in mineralogy 9B,* Mineralogical Society of America, 279-353.

Henderson, C.M.B., Pendlebury, K. and Foland, K.A., 1989, Mineralogy and petrology of the Red Hill alkaline igneous complex, New Hampshire, U.S.A., *Journal of Petrology,* 30, 627-666.

Hervig, R.L., Smith, J.V. and Dawson, J.B., 1986, Lherzolite xenoliths in kimberlites and basalts; petrogenetic and crystallochemical significance of some minor and trace elements in olivine, pyroxenes, garnet and spinel. *Transactions of the Royal Society of Edinburgh: Earth Science,* 77, 181-201.

Holloway, J.R., 1973, The system pargasite-H_2O-CO_2: a model for melting of a hydrous mineral with a mixed-volatile fluid. I. Experimental result to 8 kbar. *Geochimica et Cosmochimica Acta,* 37, 651-666.

IUGS, 1989, A classification of igneous rocks and glossary of terms: recommendations of the International Union of Geological Sciences Subcommission on the Systematics of Igneous Rocks, edited by R.W. Le Maitre, Blackwell, Oxford, 193pp.

Kjarsgaard, B.A. and Hamilton, D.L., 1989, The genesis of carbonatites by immiscibility. In: Bell, K. (ed.), Carbonatites -- Genesis and evolution, London, Unwin Hyman, 388-404.

Koster van Groos, A.F. and Wyllie, P.J., 1973, Liquid immiscibility in the join $NaAlSi_3O_8$-$CaAl_2Si_2O_8$-Na_2CO_3-H_2O. *American Journal of Science,* 273, 465-487.

Lambert, R.St.J., 1964, The Big Spruce Lake nepheline syenite complex, Snare River, Northwest Territory. Unpublished preliminary report to the Boreal Institute, 8pp.

Leake, B.E., 1978, Nomenclature of amphiboles. *Canadian Mineralogist,* 16, 501-520.

Le Bas, M.J., 1989, Diversification of carbonatite, In: Bell, K. (ed.) Carbonatites -- Genesis and evolution, London, Unwin Hyman, 428-447.

Le Bas, M.J., 1987, Nephelinites and carbonatites. In: Fitton, J.G. and Upton, B.G.J. (ed.), Alkaline Rocks, Geological Society Special Publication No. 30, 53-83.

Le Bas, M.J., 1977, Carbonatite-Nephelinite Volcanism, New York, John Wiley, 347pp.

Le Bas, M.J. and Aspden, J.A., 1981, The comparability of carbonatitic fluid inclusions in ijolites with natrocarbonatite lava. *Bulletin Volcanologique,* 44, 429-438.

Luth, W.C., 1974, Resorption of silicate minerals. In: Sørensen, H. (ed.), The Alkaline Rocks, John Wiley and Sons, New York, 500-515.

Martin, R.F. and Bowden, P. 1981, Peraluminous granites produced by rock-fluid interaction in the Ririiwai nonorogenic ring complex, Nigeria: mineralogical evidence. *Canadian Mineralogist,* 19, 65-82.

Martineau, M.P., 1970, The petrology of the Big Spruce Lake complex. Ph.D. Thesis, Oxford University, Oxford, England, 93pp.

Maury, R.C., 1976, Contamination (par l'encaissant et les enclaves) et cristallisation fractionnée de séries volcaniques alcalines, continentales (Massif Central Fransais) et océaniques (Pacifique Central): l'origine des laves acides, Thèse doctorat d'Etat, Université Paris-Sud, Orsay, 455pp.

Mitchell, R.H., 1990, A review of the compositional variation of amphiboles in alkaline plutonic complexes. *Lithos,* 26, 135-156.

Mitchell, R.H., 1985, A review of the mineralogy of lamproites. *Transactions Geological Society of South Africa,* 88, 411-437.

Mitchell, R.H., 1981, Titaniferous phlogopites from the Leucite lamproites of the West Kimberley area, Western Australia. *Contributions to Mineralogy and Petrology,* 76, 243-251.

Mitchell, R.H., Platt, R.G., Lukosius-Sanders, J., Artist-Downey, M. and Moogk-Pickard, S., 1993, Petrology of syenites from centre III of the Coldwell alkaline complex, northwestern Ontario, Canada. *Canadian Journal of Earth Sciences,* 30, 145-158.

Mitchell, R.H., Platt, R.G., Downey, M. and Laderoute, D.G., 1991, Petrology of alkaline lamprophyres from the Coldwell alkaline complex, northwestern Ontario. *Canadian Journal of Earth Sciences,* 28, 1653-1663.

Mogessie, A., Tessadri, R. and Veltman, C.B., 1988, EMP-AMPH: Amphibole classification scheme. Department of Mineralogy and Petrography, University of Innsbruck, Austria.

Morimoto, N., 1989, Nomenclature of pyroxenes. *Canadian Mineralogist,* 27, 143-156.

Morimoto, N. and Kitamura, M., 1983, Q-J diagram for classification of pyroxenes. *Journal of Japanese Association of Mineralogists, Petrologists and Economical Geologists,* 78, 141.

Morozewicz, J., 1928, Über die chemische Zusammensetzung des gesteinsbildenden Nephelines. *Fennia,* 22, 1-16.

Mysen, B.O., 1988, Structure and properties of silicate melts. Elsevier, Amsterdam, 354pp.

Philpotts, A.R., 1974, The Monteregian Hills, in: Sørenson, H. (ed.): The Alkaline Rocks, John Wiley and Sons, New York, 293-310.

Platt, R. G. and Woolley, A.R., 1986, The mafic mineralogy of the peralkaline syenites and granites of the Mulanje complex, Malawi. *Mineralogical Magazine,* 50, 85-99.

Powell, J. L. and Bell, K., 1974, Isotopic composition of strontium in alkalic rocks, In: Sørenson, H. (ed.): The Alkaline Rocks, John Wiley & Sons, London, 412-421.

Rankin, A.H. and Le Bas, M.J., 1974, Liquid immiscibility between silicate and carbonate melts in naturally occurring ijolite magma, *Nature,* 259, 206-209.

Rock, N.M.S., 1991, Lamprophyres, Blackie and Van Nostrand Reinhold,. 43-46 & 147-149.

Rock, N.M.S., 1978, Petrology and petrogenesis of the Monchique alkaline complex, Southern Portugal. *Journal of Petrology,* 19, 171-214.

Rock, N.M.S., 1976, The comparative strontium isotopic composition of alkaline rocks: New data from southern Portugal and East Africa. *Contributions to Mineralogy and Petrology,* 56, 205-228.

Roedder, E., 1979, Silicate liquid immiscibility in magmas, In, Yoder, H.S. (ed.), The evolution of the Igneous Rocks, Princeton University Press, Princeton, NJ., 15-57.

Ryerson, F.J. and Hess, P.C., 1980, The rôle of P_2O_5 in silicate melts. *Geochimica et Cosmochimica Acta,* 44, 611-624.

Smith, Dorian G.W., 1989, Identification of rare earth and yttrium minerals using the MinIdent database, in: Russel, P.E. (ed.): Microbeam Analysis -- 1989, San Francisco Press, 559-562

Smith, D.G.W. and Leibovitz, D.P., 1986, MinIdent: A data base for minerals and a computer program for their identification. Canadian Mineralogist, 24, 695-708.

Stephenson, D. and Upton, B.G.J., 1982, Ferromagnesian silicates in a differentiated alkaline complex: Kungnat Field, South Greenland. *Mineralogical Magazine,* 46, 282-300.

Strong, D.F. and Taylor, R.P., 1984, Magmatic-subsolidus and Oxidation trends in composition of amphiboles from silica-saturated peralkaline igneous rocks, *Tschermaks Mineralogische und Petrographische Mitteilungen,* 32, 211-222.

Tilley, C.E., 1956, Nepheline associations. *Verhandelingen Koninklijke Nederlands Geologisch Mijnbouwkundig Genootschap,*16, 403-413.

Tilley, C.E., 1954, Nepheline-Alkali feldspar parageneses. *American Journal of Science,* 252, 65-75.

Tomita, T., 1934, On kaersutite from Dogo, Oki Islands, Japan, and its magmatic alteration and absorption. *Journal of Shanghai Science Institute,* 1, 99-136.

Treiman, A.H. and Schedl, A., 1983, Properties of carbonatite magma and processes in carbonatite magma chambers. *Journal of Geology,* 91, 437-47.

Varne, R., 1968, The petrology of Moroto mountain, eastern Uganda, and the origin of nephelinites. *Journal of Petrology,* 9, 169-190.

Veksler, I.V. and Teptelev, M.P., 1990, Conditions for crystallization and concentration of perovskite-type minerals in alkaline magmas. *Lithos,* 26, 177-189.

Wall, F., Le Bas, M.J. and Srivastava, R.K., 1993, Calcite and carbocernaite exsolution and cotectic textures in a Sr, RE-rich carbonatite dyke from Rajasthan, India, *Mineralogical Magazine,* 57, 495-513.

Wass, S.Y., 1979, Multiple origins of clinopyroxenes in alkali basaltic rocks. *Lithos,* 12, 115-132.

Wones, D.R., 1979, The fractional resorption of complex minerals and the formation of strongly femic alkaline rocks. In: Yoder, H.S. (ed.), The Evolution of Igneous Rocks, Princeton University Press, Princeton, NJ, 413-422.

Wones, D.R. and Eugster, H.P., 1965, Stability of biotite: experiment, theory, and application. *American Mineralogist,* 50, 1228-1272.

Wones, D.R. and Gilbert, M.C., 1969, The fayalite-magnetite-quartz assemblage between 600^{0}C and 800^{0}C. In: The Schairer Volume, *American Journal of Science,* 267-A, 480-488.

Woolley, A. R. and Jones, G.C., 1992, The alkaline/peralkaline syenite-granite complex of Zomba-Malosa, Malawi: mafic mineralogy and genesis. *Journal of African Earth Sciences,* 14, 1-12.

Woolley, A.R. and Platt, R. G., 1988, The peralkaline nepheline syenites of the Junguni intrusion, Chilwa province, Malawi. *Mineralogical Magazine,* 52, 425-33.

Woolley, A.R., and Platt, R.G., 1986, The mineralogy of nepheline syenite complexes from the northern part of the Chilwa Province, Malawi, *Mineralogical Magazine,* 50, 597-610.

Wyllie, P.J., 1987, Discussion of recent papers on carbonated peridotite, bearing on mantle metasomatism and magmatism. *Earth and Planetary Science Letter,* 82, 391-397.

Wyllie, P.J., 1978, Peridotite-CO_2-H_2O and the low-velocity zone. *Bulletin Volcanologique,* 41, 670-683.

Wyllie, P.J., Baker, M.B. and White, B.S., 1990, Experimental boundaries for the origin and evolution of carbonatites. *Lithos,* 26, 3-19.

Yoder, H.S.JR. and Tilley, C.E., 1962, Origin of Basalt magmas: An experimental study of natural and synthetic rock systems, *Journal of Petrology,* 3, 342-532.

Appendix 1.
Photomicrographs.

Plate 1. Gabbro. Titanian augite (aug) is replaced by greenish amphibole (am). Feldspar (fsp) is partly altered. Opaque minerals include titanian magnetite and ilmenite. Magnification 51x. Plane polarized light.

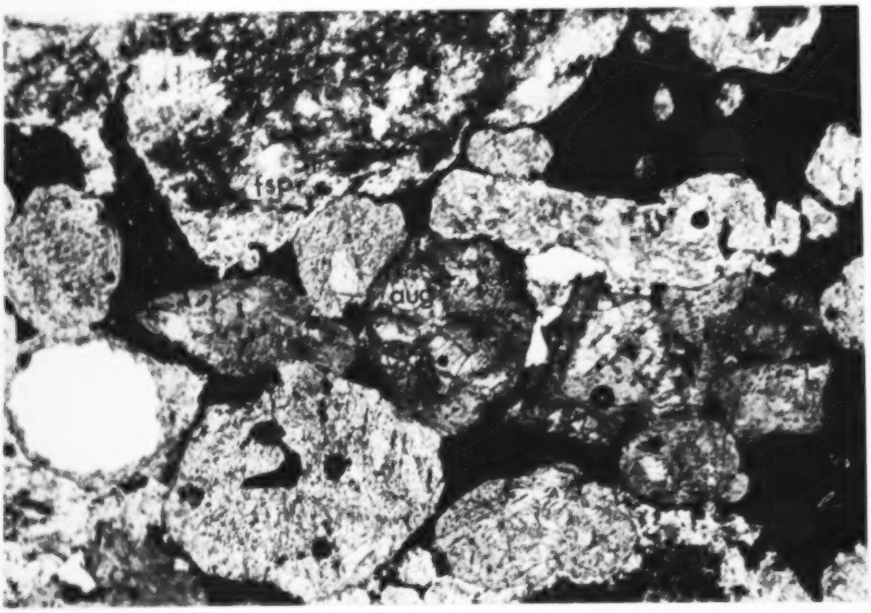

Plate 2. Gabbro, containing titanian augite (aug), and subhedral kaersutite (brown) which also occurs as inclusions in augite. Greenish ferro-hornblende rims augite and kaersutite. Biotite (bi) and magnetite (opaque) are present. Magnification 51x. Plane polarized light.

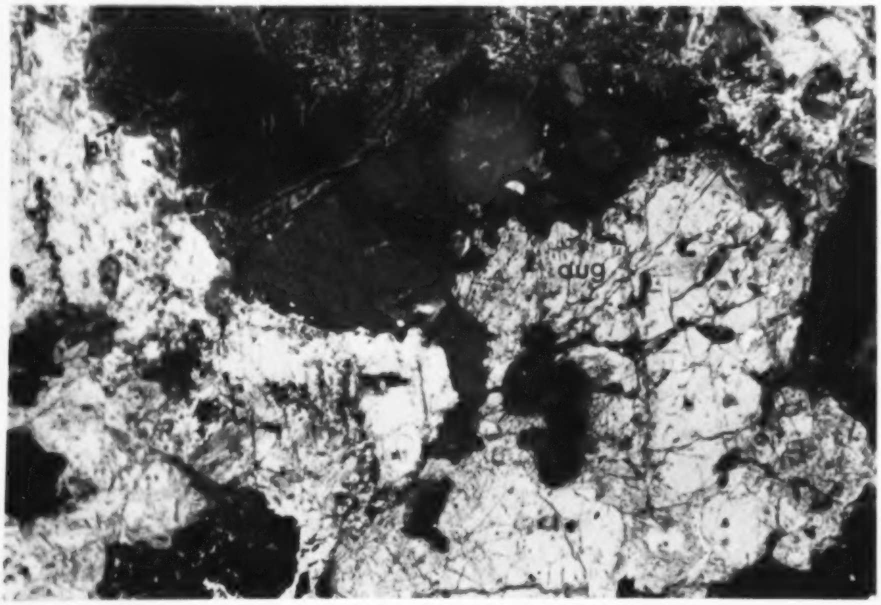

Plate 3. Olivine magnetite pyroxenite. Olivine (ol) is traversed by serpentine veinlets (blue grey). Titanian augite (aug) and opaque oxides (titanian magnetite & ilmenite) are other major phases. Magnification 41x. Crossed Nicols.

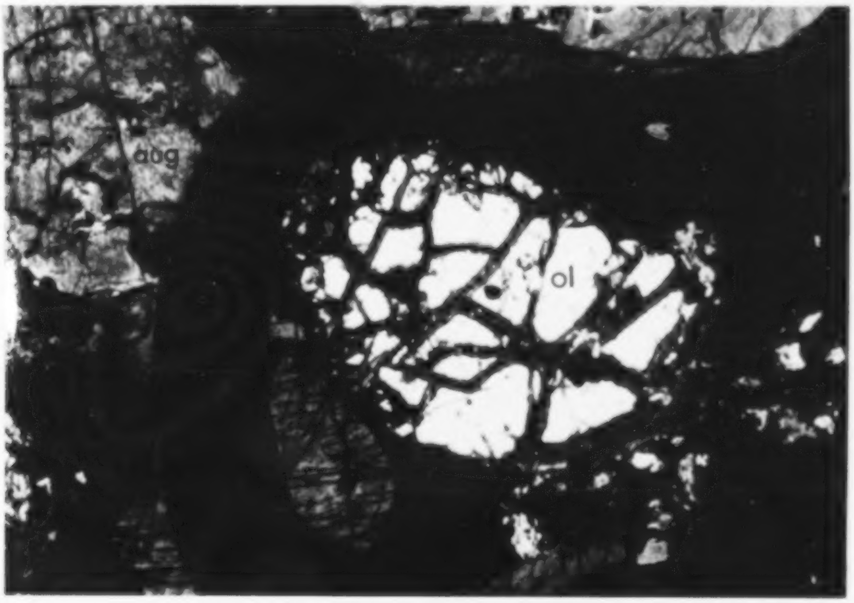

Plate 4. Magnetite pyroxenite. Kaersutite (brown) is resorbed in an augite groundmass, new augite is formed around the kaersutite. The original augite contains exsolution blebs which consist of Ti, Fe-bearing oxide. The fracture is filled by Fe, Ti oxide in augite. Magnification 128x. Plane polarized light.

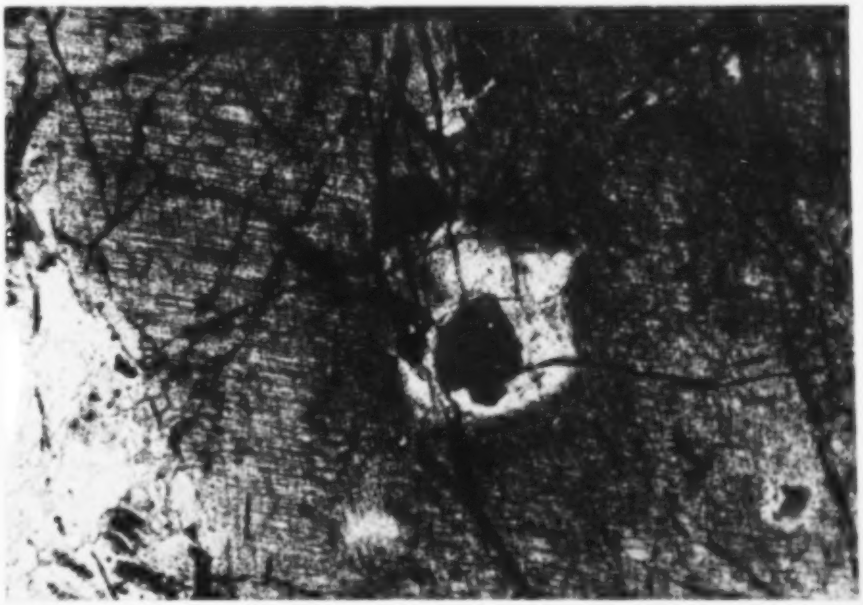

Plate 5. Kaersutite (brown) occurring as a vein in magnetite pyroxenite. Magnification 51x. Plane polarized light.

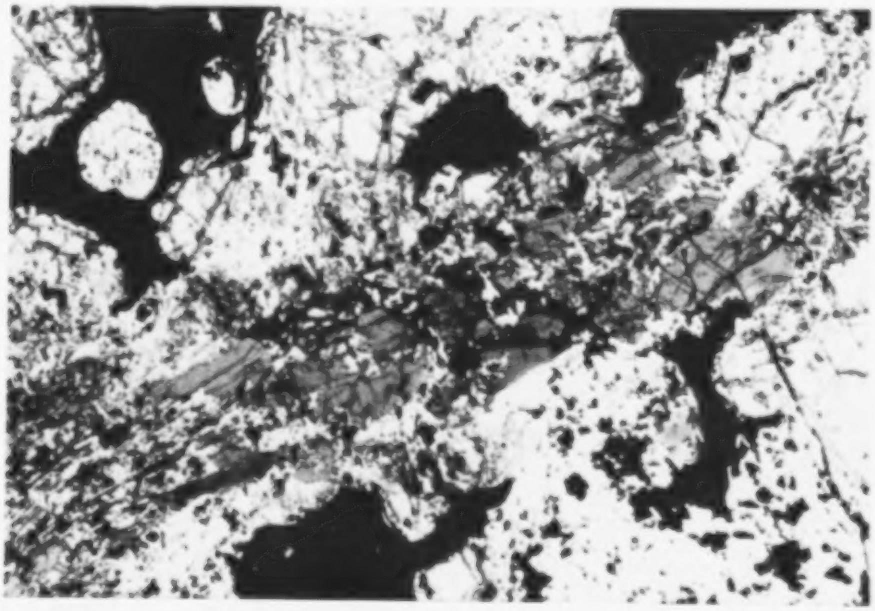

Plate 6. An amphibole vein intruding magnetite pyroxenite which consists of augite (aug) and titanian magnetite and ilmenite. The vein consists of hastingsite (has) and apatite (ap) which contains subhedral hastingsitic hornblende inclusions. Magnification 51x. Plane polarized light.

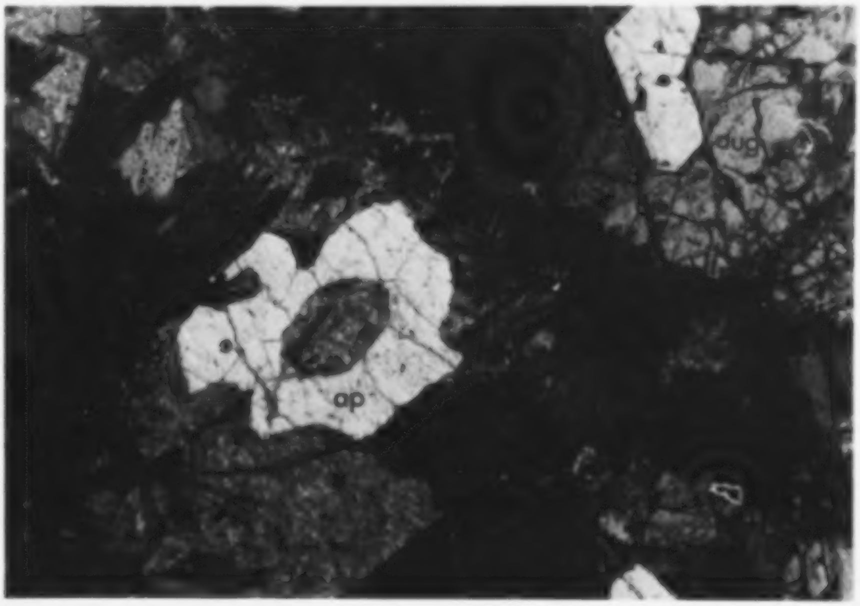

Plate 7. The augite (aug) and opaque minerals (titanian magnetite and ilmenite) are replaced and rounded alongside a hastingsite (blue green)-apatite (ap) vein. Magnification 51x. Plane polarized light.

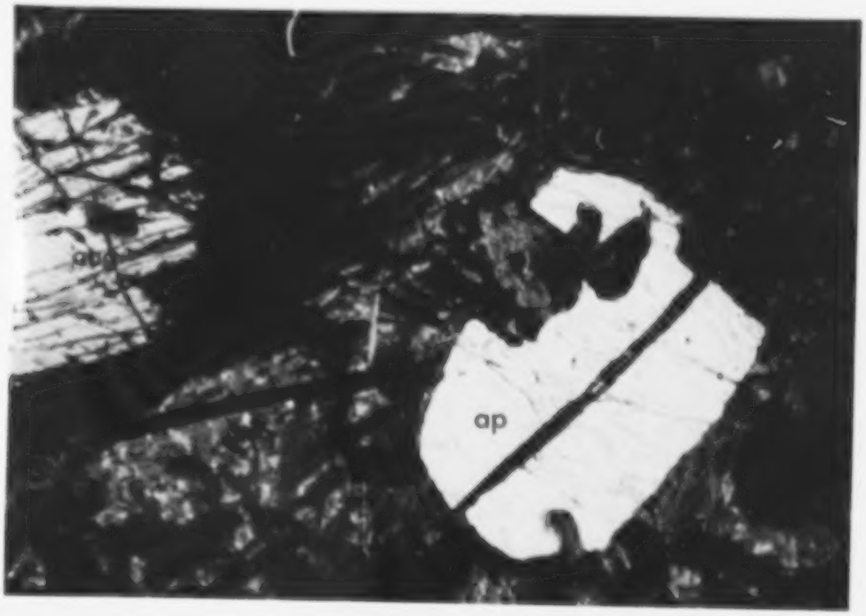

Plate 8. Diorite. Augite is rimmed by edenitic hornblende (hn) which is surrounded by biotite (brown). Apatite (ap) and opaque phases (ilmenite & titanian magnetite) are commonly associated with the mafic minerals. Magnification 51x. Plane polarized light.

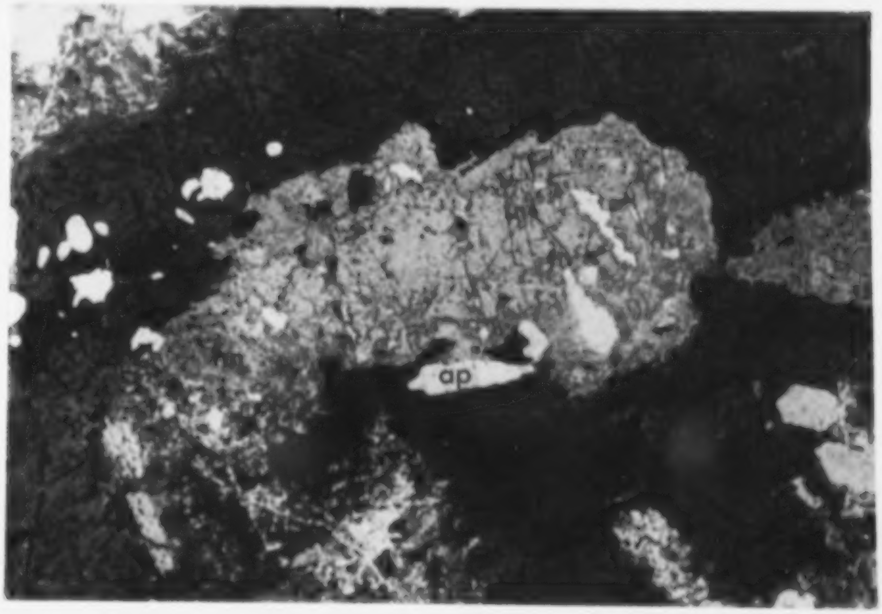

Plate 9. Quartz-free syenite, containing alkali feldspar (fsp), augite (aug), primary ferro-hornblende (hn), biotite (bi) and opaque magnetite. Secondary actinolite (act) has replaced augite. Magnification 51x. Plane polarized light.

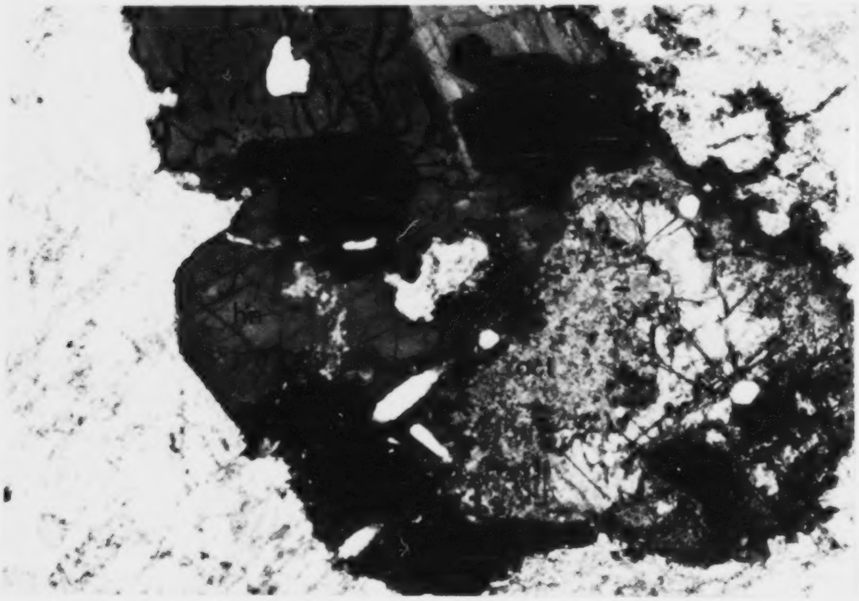

Plate 10. Quartz syenite, containing edenite (am), alkali feldspar (fsp) and quartz (qz). Magnification 51x. Crossed Nicols.

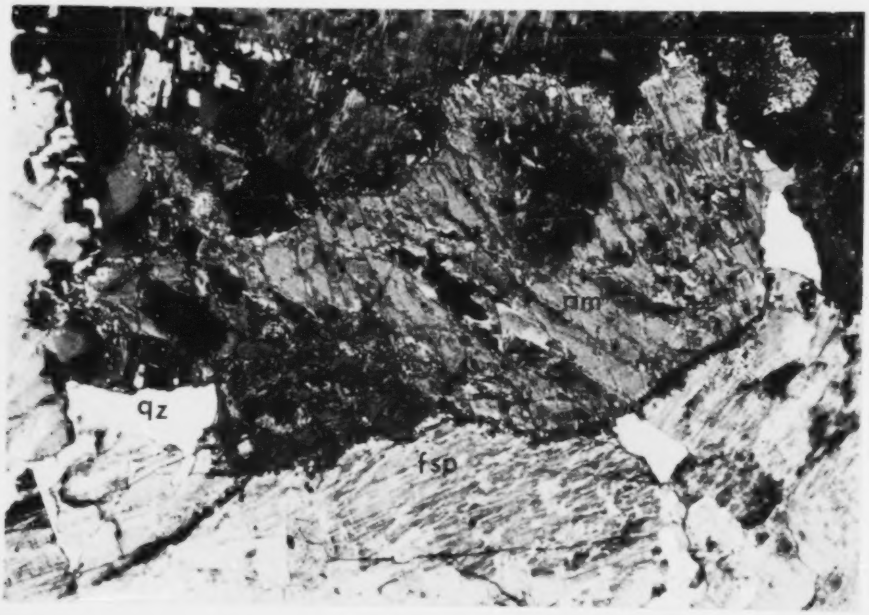

Plate 11. Foyaite, containing aegirine augite (green), nepheline which is altered to cancrinite (cac), and alkali feldspar (fsp). Biotite (bi) is present in minor amount. Magnification 51x. Crossed Nicols.

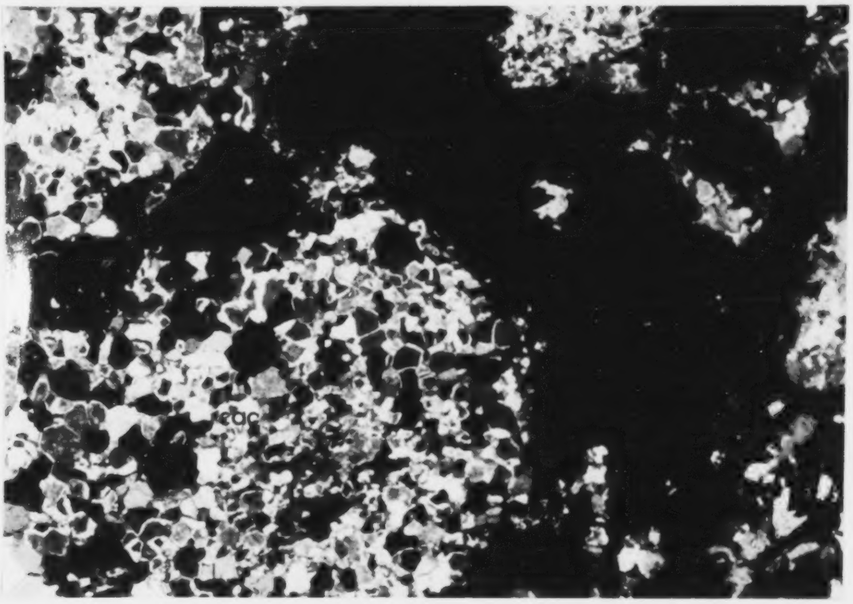

Plate 12. Carbocernaite (brown) included in aegirine augite (green) of foyaite. Magnification 128x. Plane polarized light.

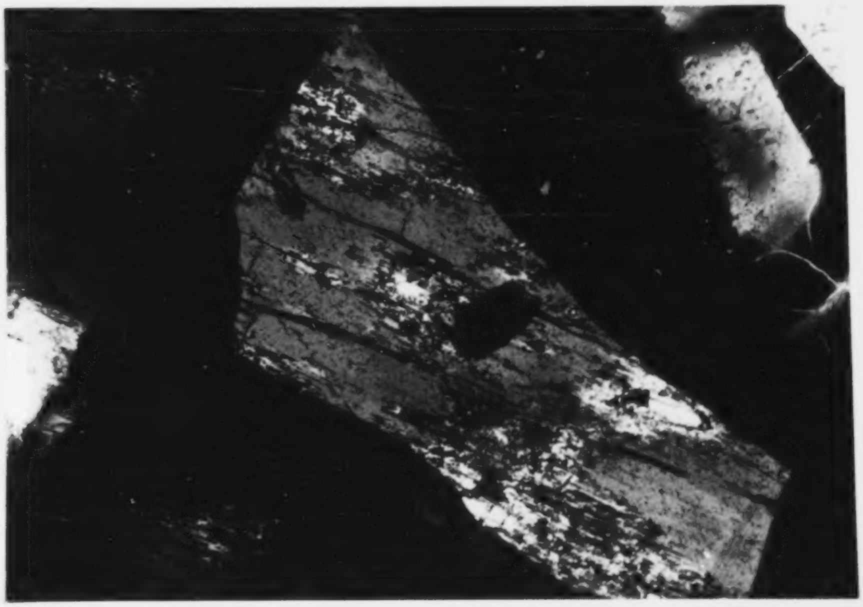

Plate 13. Foyaite, containing carbonate ocelli (cat) which are interstitial to aegirine augite (green). Magnification 128x. Crossed Nicols.

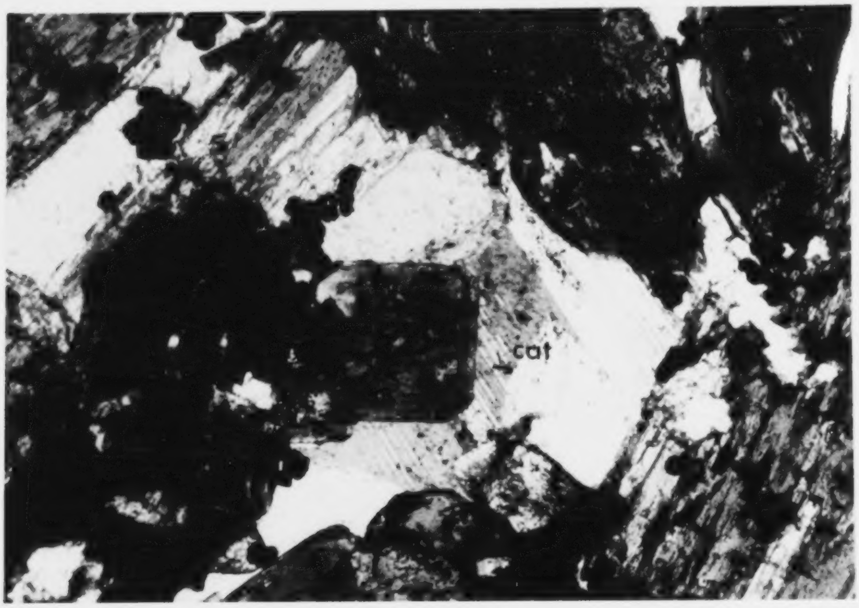

Plate 14. Riebeckite-metasomatized rock. Radiating riebeckite (blue) grows on aegirine augite (green). Magnification 41x. Plane polarized light.

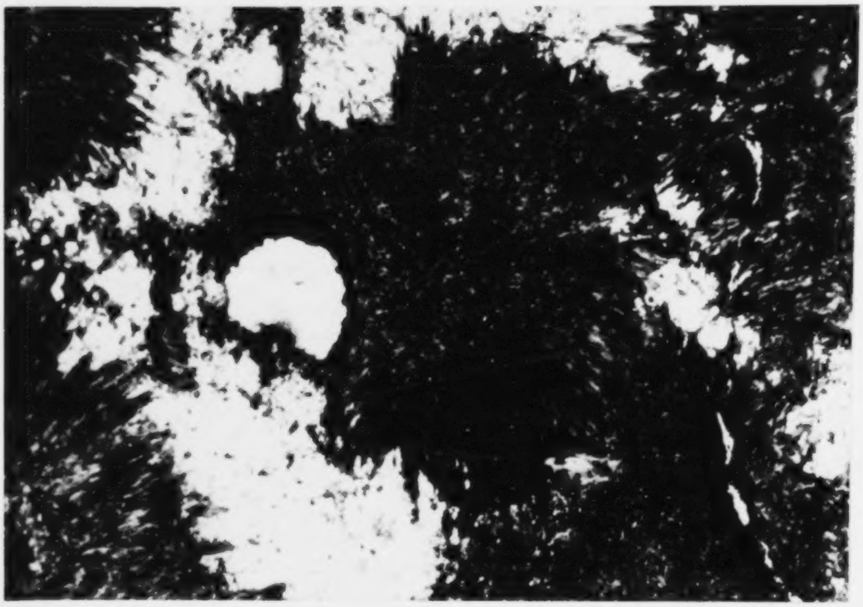

Plate 15. Titanite melteigite, containing titanite (tan) and aegirine augite (green). Magnification 41x. Plane polarized light.

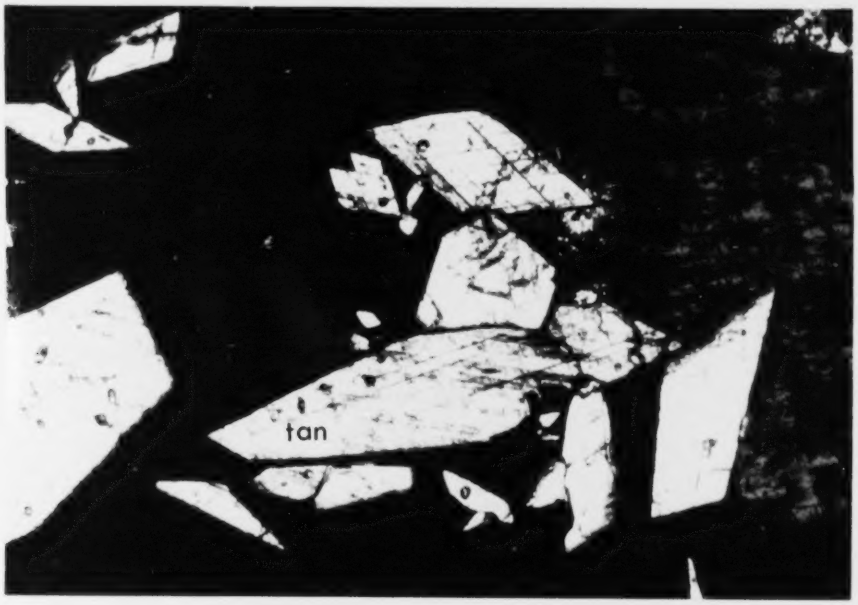

Plate 16. Pyrochlore (brown) included in aegirine augite (green) of melteigite. Magnification 128x. Plane polarized light.

Plate 17. Ijolite, containing nepheline (nep), aegirine augite (greyish green) and sodalite (dark). Magnification 128x. Crossed Nicols.

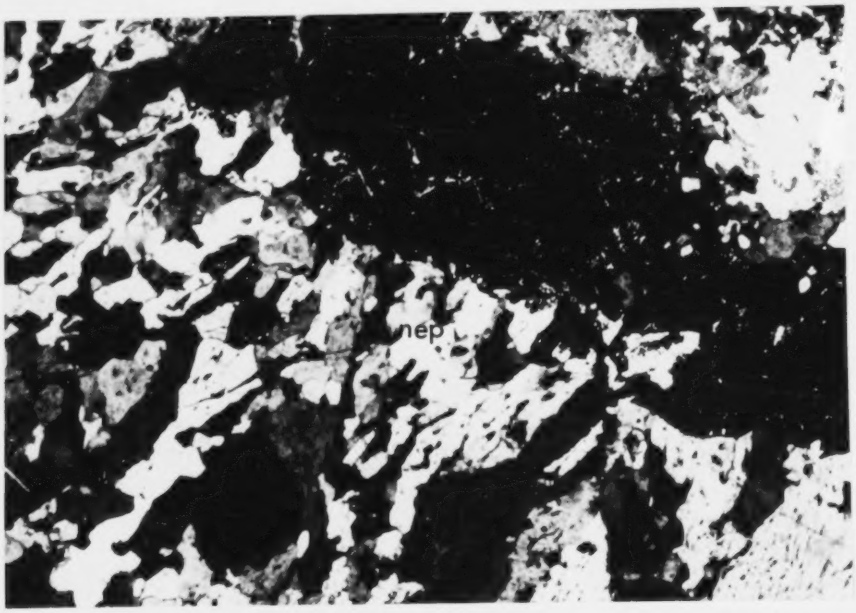

Plate 18. Urtite, consisting dominantly of nepheline (nep) which is partly altered to cancrinite (cac). Minor aegirine augite (green) is present. Magnification 41x. Crossed Nicols.

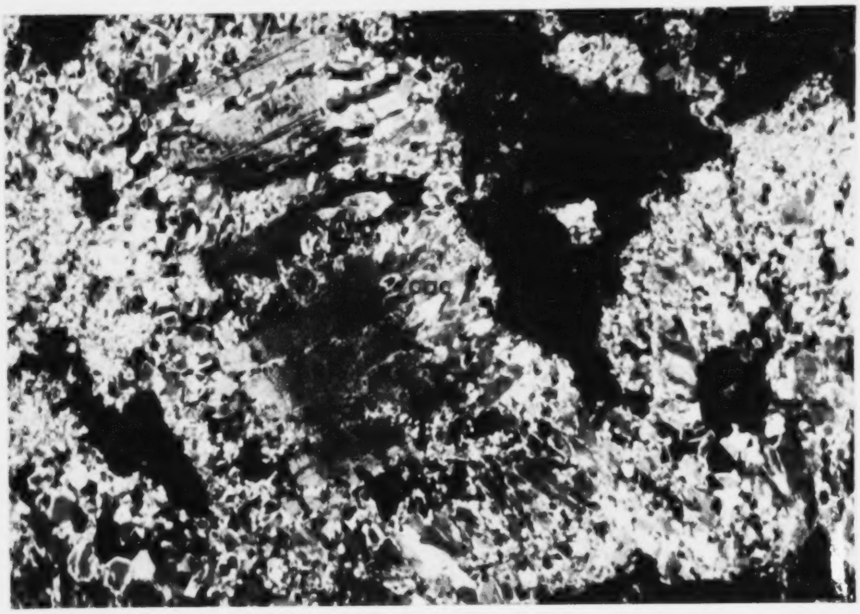

Plate 19. Phonolite. The phenocryst is orthoclase, and the groundmass contains aegirine augite, alkali feldspar and nepheline. Magnification 41x. Crossed Nicols.

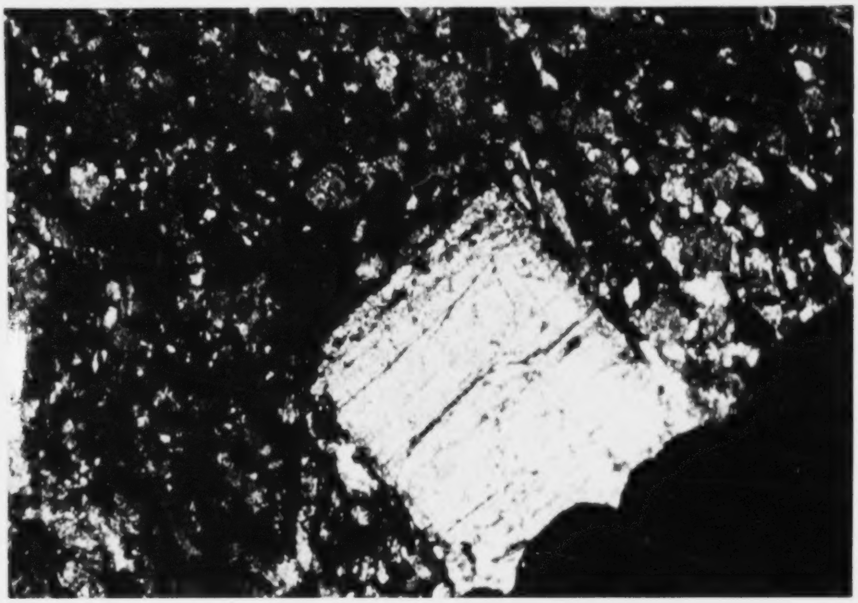

Plate 20. Apatite carbonatite. Apatite forms grey, hexagonal grains. Magnification 128x. Crossed Nicols.

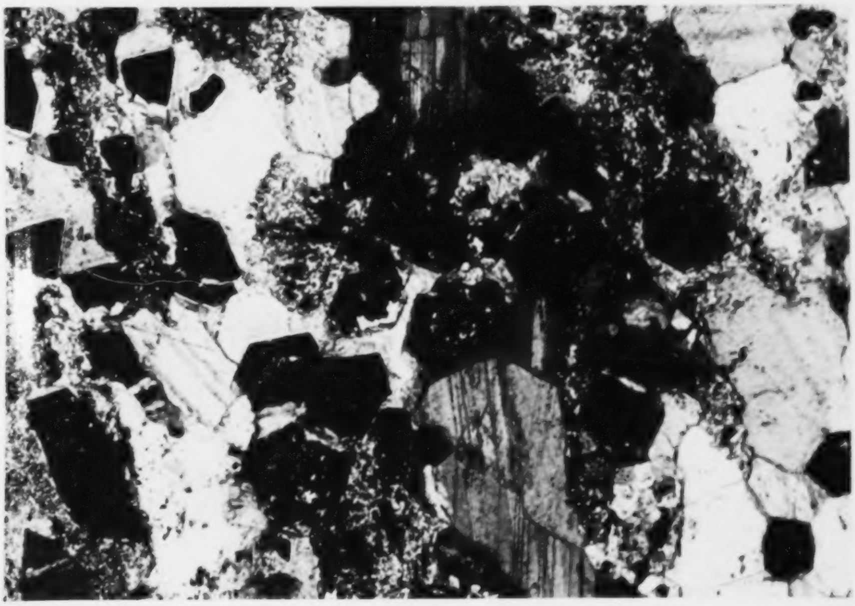

Plate 21. Silicate carbonatite, containing alkali feldspar aggregates (fsp) and epidote (ep). Magnification 128x. Crossed Nicols.

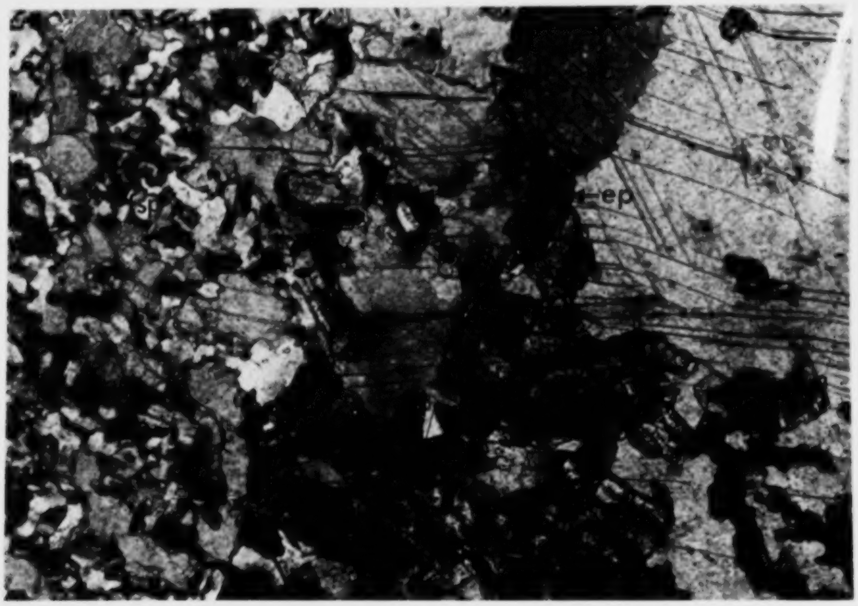

Plate 22. Fluorite carbonatite, consisting of purple fluorite and calcite. Magnification 41x. Plane polarized light.

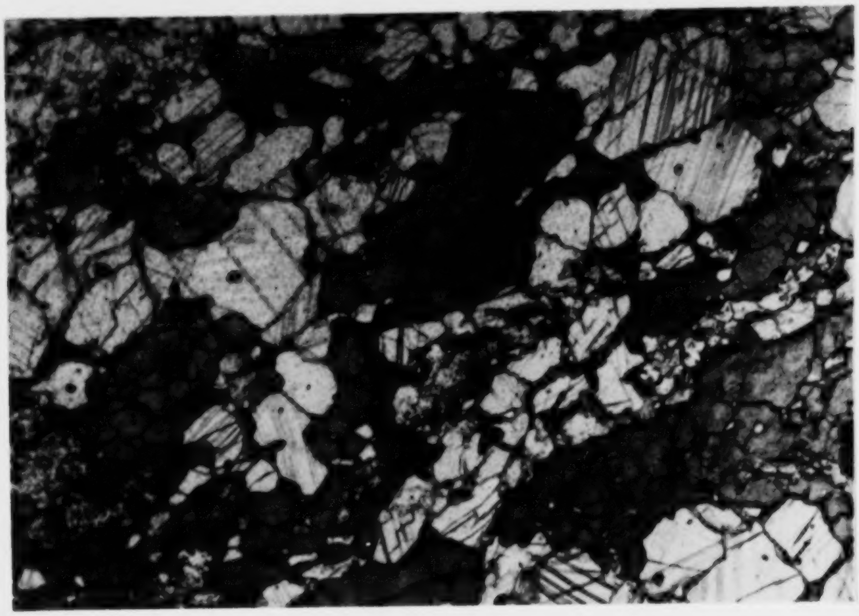

Plate 23. Carbonatite, containing biotite (brown) and aegirine augite (green) in calcite groundmass. Magnification 128x. Plane polarized light.

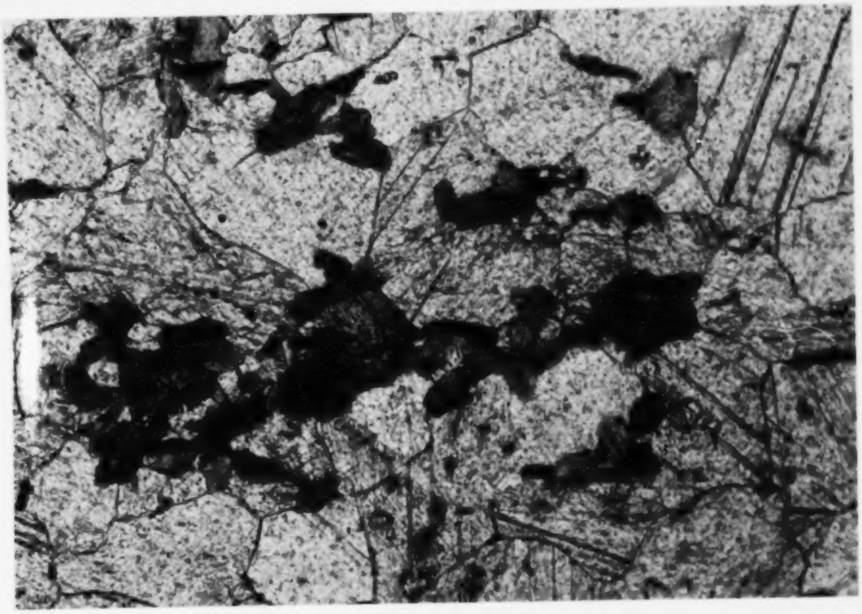

Plate 24. Allanite (dark brown) forms discrete bands in carbonatite. Magnification 128x. Plane polarized light.

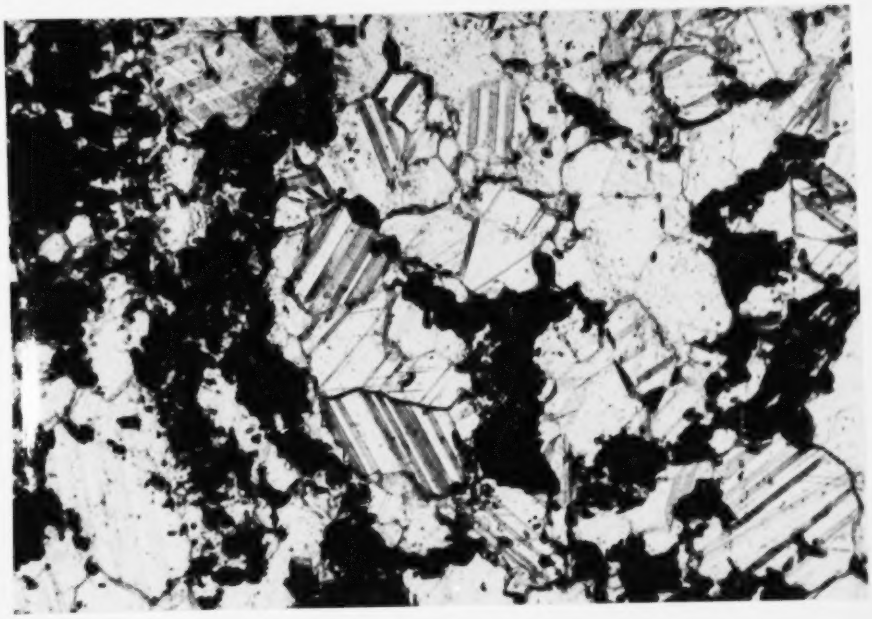

Plate 25. Melanocratic syenite, containing olivine (ol), diopside (dio), biotite (brown) and alkali feldspar (fsp). Magnification 51x. Plane polarized light.

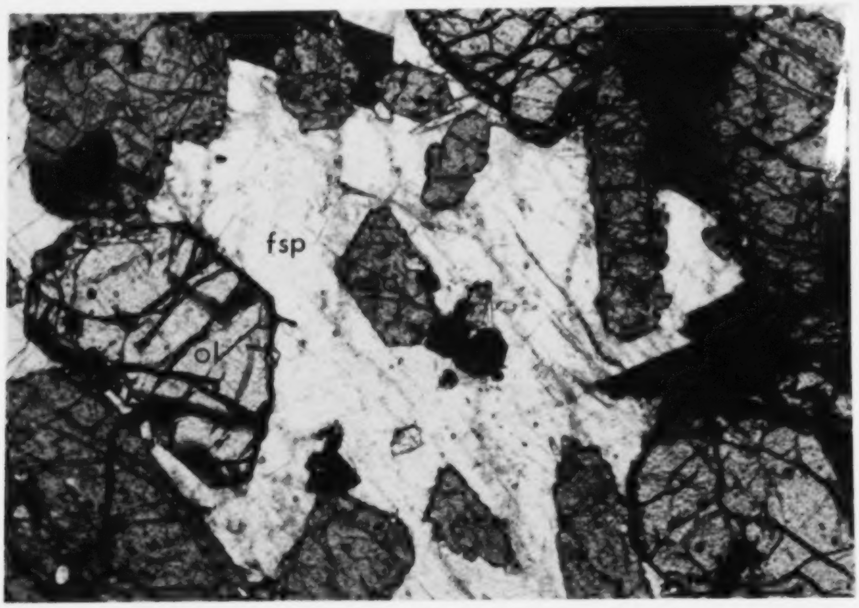

Plate 26. Biotite pyroxenite, consisting of augite (aug) and biotite (brown). Augite is stained by greenish chlorite phase. Magnification 128x. Plane polarized light.

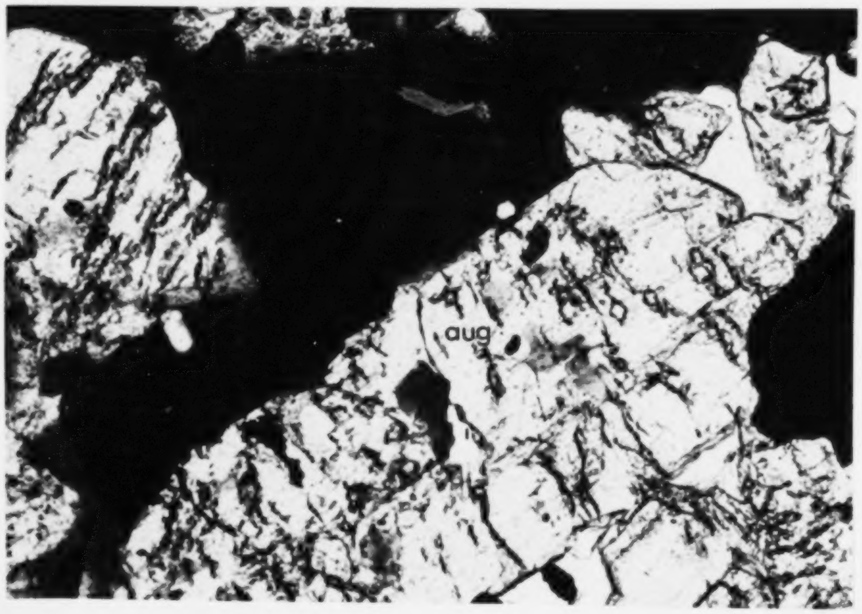

Plate 27. Biotite peridotite, containing biotite (brown), olivine (ol), carbonate (cat) and opaque phases (titanian magnetite). Magnification 128x. Plane polarized light.

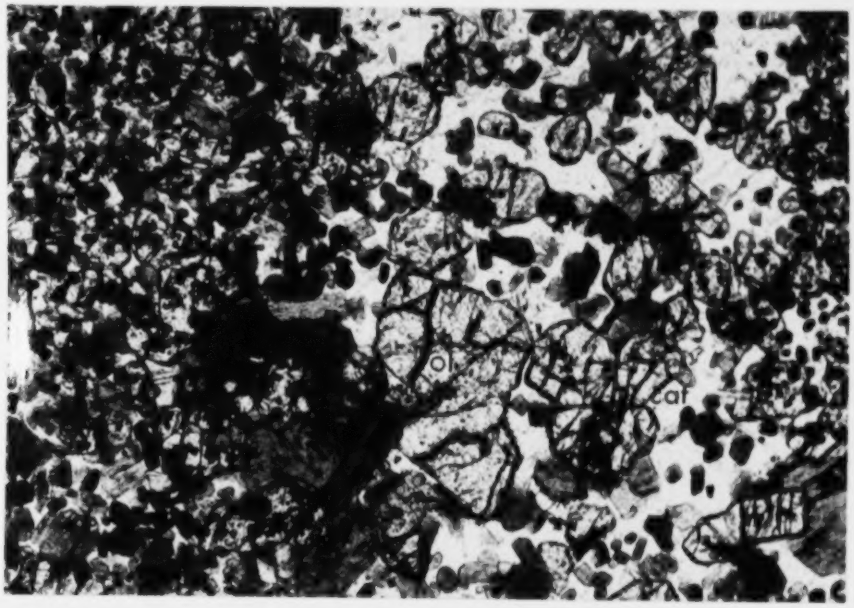

Plate 28. Minette. Zoned phlogopite phenocrysts (brown) occur in fine-grained groundmass. Magnification 41x. Plane polarized light.

Plate 29. Lamprophyre, containing a carbonate-epidote globule. The matrix contains the opaque mineral ilmenite & magnetite, chlorite, sericite and uralite. Magnification 51x. Crossed Nicols.

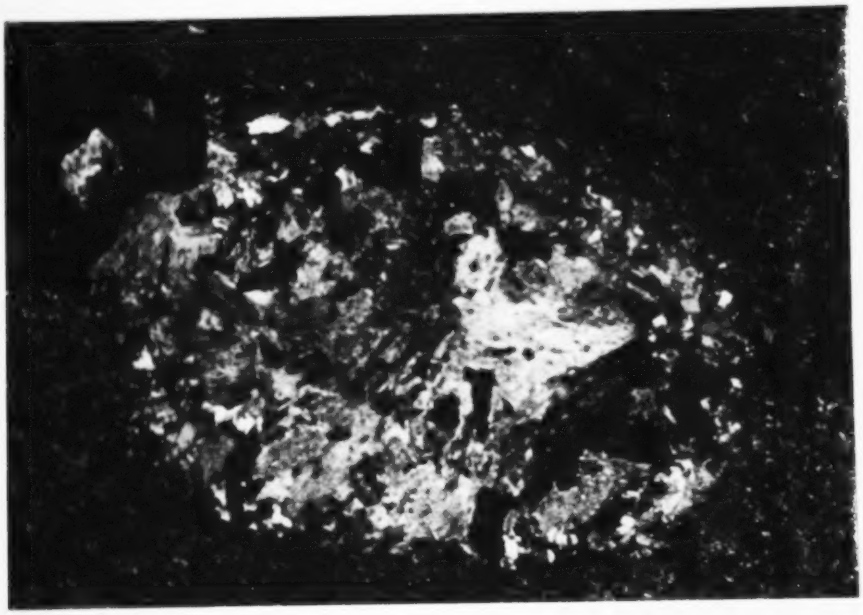

Appendix 2. Estimation of modal mineral proportions (volume %).

Rock #	1	2	3	4	5	6	7	8	9	10	11	12
Olivine	10	2									15	
calcic pyroxene	70	60	10	5	5	2					22	50
alkali pyroxene								25	40			
calcic amphibole		5	15	20	15	15	15				2	
biotite			5		10	T	5	3	1		30	35
plagioclase	M		55	50	T		30					
alkali feldspar			5	20	60	75	40	20			30	M
quartz						5	5					
nepheline								28	20			
sodalite								2	4			
cancrinite								15	35			
Fe-Ti oxide	20	30	8	3	5	2		3		2	M	5
apatite			5		5	1				15	1	10
zircon					T	T						
fluorite								t		t		
carbocernaite								t		t		
calcite & dolomite							3	2		80		
sphene			M	M	M	T	T	M	M	M		
pyrochlore										M		
allanite										M		

Note: 1 & 2: pc-81004 & pc-81001 (olivine) magnetite pyroxenite;

3: pc-82198 gabbro; 4: pc-81272 diorite;

5: pc-81006 quartz-free syenite; 6: pc-81083 quartz syenite;

7: pc-82119 comendite; 8: pc-81223 foyaite;

9: pc-81165 ijolite; 10: pc-81408 calcite carbonatite;

11: c-82468 melanocratic syenite; 12: pc-82462 biotite pyroxenite.

M: minor; T: trace.

Appendix 3.
Experimental method.

Mineral compositional analyses were performed on a ARL SEMQ electron microprobe at the Department of Geology, University of Alberta, employing four wavelength dispersive spectrometer (WDS) for quantitative analyses and one energy dispersive spectrometer (EDS) for qualitative analyses. The data collected by the WDS were processed by a PHI-RHO-Z matrix correction program. For operating conditions, accelerating potential was set at 15 *kV* and probe current at 10 *nA*. Samples of interest were observed firstly under a polarized optical microscope and points for analyses were then chosen and brought to the microprobe.

The standards used for analyzing all the minerals and related elements are listed below:

Mineral for analysis	Standards used	Elements for analysis
Clinopyroxene	kaersutite	Na, K, Ti, Fe
	augite	Mg, Al, Si, Ca
	Cr-augite	Cr
	willemite	Mn
	fosterite 90	Ni
	diopside	Ca
	hyperthene	Fe
Amphibole	kaersutite	Na, Mg, Al, Si, Ti, Ca, K
	willemite	Mn
	Cr-augite	Cr
	grunerite	Fe
	tugtupite	Cl
Mica	kaersutite	Na, Ti, Mg
	willemite	Mn
	biotite	Al, K, Si, Fe

	tugtupite	Cl
Feldspar	albite	Si, Na
	willemite	Mn
	obsidian	Fe
	sanidine	Ba
	osumilite	Mg
	anorthite	Al, Ca
Nepheline	willemite	Mn
	orthoclase	K
	plagioclase	Si, Ca
	anorthite	Al
	osumilite	Mg
	albite	Na
	obsidian	Fe
Olivine	augite	Mg, Ca, Al
	forsterite 90	Si, Mg, Fe, Ni
	kaersutite	Ti
	Cr-augite	Cr
	willemite	Mn
Ilmenite & titanian magnetite	ilmenite	Ti, Mn, Fe
	fayalite	Si
	chromite	Mg, Al
	Cr-augite	Cr
	kaersutite	Na

Appendix 4
Method of calculation of structural formulae for pyroxenes.

The structural formula for pyroxenes may be defined as $M2M1T_2O_6$, where M2 refers to cations in a distorted octahedral site, and M1 refers to cations in a regular octahedral site, and T to tetrahedrally coordinated cations.

In electron microprobe analysis, only total Fe can be determined, and hence the Fe^{3+}/Fe^T ratio is not available. The PX program (Gomez, 1990) calculates the structural formulae of pyroxene on the basis of four cations and six oxygen atoms. Fe^{3+} is estimated by adjusting Fe^{2+}/Fe^{3+} ratios to fit these constraints. The following procedure is used:

(1) Sum T to 2.000 using Si^{4+}, then Al^{3+}, and then Fe^{3+}, if necessary.

(2) Sum M1 to 1.000 using all Al^{3+} and Fe^{3+} in excess of that used for T sites. If there is insufficient Al^{3+} and Fe^{3+}, then add Ti^{4+}, Cr^{3+}, Zr^{4+}, Mg^{2+}, Fe^{2+} and finally Mn^{2+} in that order, until the sum is 1.000.

(3) Sum M2 using all Mg^{2+}, Fe^{2+} and Mn^{2+} in excess of that used for M_1 sites. Then add Ca^{2+}, Na^+ and K^+ in that order so that the sum becomes 1.000 or close to it.

The program assigns pyroxene compositions to one of the four chemical groups defined in the Q-J diagram of Morimoto and Kitamura (1983): Ca-Mg-Fe pyroxene (Quad), Na-Ca pyroxene (Na-Ca), Na pyroxene (Na) and other pyroxenes (other), where, $Q=Ca+Mg+Fe^{2+}$, and J=2Na (Fig. 2). Further division of the major groups is done by the following procedures:

(1) The Quad pyroxenes are classified in the Enstatite-Ferrosillite-Diopside-Hedenbergite quadrilateral, with normalized Ca, Mg, and Fe ($=Fe^{2+} + Fe^{3+} + Mn$) atomic proportions (Fig. 3).

(2) The Ca-Na and Na pyroxenes are classified in the Quad-Jd-Ae diagram with normalized Q (=Wo + En + Fs), Jd and Ae components (Fig. 4).

Appendix 5

Method of calculation of structural formulae for amphiboles and abbreviations for amphibole nomenclature.

The standard amphibole formula may be taken to have the general form $A_{0-1}X_2Y^{VI}{}_5T^{IV}{}_8O_{22}(OH,F,Cl)_2$, where T (tetrahedral site): Si + Al^{IV} + Fe^{3+IV} = 8.00, Y (octahedral M1 to M3): Al^{VI} + Ti + Fe^{3+} + Fe^{2+} + Mn + Mg = 5.00, X (Octahedral M4): Ca + Na + Fe^{2+} + Mn = 2.000, A: Na + K + Ca = 0-1.000.

In the calculation of the standard amphibole formula, the following procedure is used:

(1) since the hydroxyl and halogen content were not determined by electron microprobe analysis, the formulae are calculated on a volatile-free basis to 23 oxygen.

(2) Sum T to 8.000 using Si, then Al, then Cr, then, Fe^{3+}, then Ti^{4+}.

(3) Sum Y to 5.00 using excess Al, Cr, Ti, Fe^{3+} from (2), then Mg, then Fe^{2+}, and then Mn.

(4) Sum X to 2.00 using excess Fe^{2+}, Mn, Mg, from (3), then Ca, then Na.

(5) Excess Na from (4) is assigned to A, then all K. Total A should be between 0 and 1.00.

The standard amphibole formula is classified into one of the four principal amphibole groups on the basis of the numbers of atoms of $(Ca + Na)_X$ and Na_X. Three principal amphibole groups are present in the complex. They are: (a) the calcic amphibole group with $(Ca + Na)_X \geq 1.34$ and $Na_X < 0.67$; (b) the sodic-calcic amphibole group with $(Ca + Na)_X \geq 1.34$ and $0.67 \leq Na_X < 1.34$; (c) the alkali amphibole group with $(Na)_X \geq 1.34$.

Within each of the principal groups, the various species are named by reference to the amphibole classification diagrams (Leake, 1978).

The Fe^{3+}/Fe^{2+} ratio is adjusted by normalizing the total cations, (excluding Ca, Na, K) to 13.

The abbreviation for amphibole nomenclature used in the thesis are listed as follows:

Ac -- actinolite
Ac Hn -- actinolitic hornblende
Fan Ac Hn -- ferrian actinolitic hornblende
Fan Fo Hn -- ferrian-ferro hornblende
Fan Pts Tsch Hn -- ferrian-potassian-tschermakitic hornblende
Fi Fo Hn -- ferri-ferro hornblende
Fi Pts Kat -- ferri-potassium katophorite
Fo Ac -- ferro-actinolite
Fo Ac Hn -- ferro actinolitic hornblende
Fo Ed -- ferro-edenite
Fo Ed Hn -- ferro-edenitic hornblende
Fo Hn -- ferro-hornblende
Fo Ric -- ferro-richterite
Fo Tsch Hn -- ferro-tschermakitic hornblende
Fo Win -- ferro-winchite
Fon Pg -- ferroan pargasite
Fon Pg Hn -- ferroan pargasitic hornblende
Has -- hastingsite
Has Hn -- hastingsitic hornblende
Kae -- kaersutite
Kat -- katophorite
Mgn Has -- magnesian hastingsite
Mgn Has Hn -- magnesian hastingsitic hornblende
Mgo Hn -- magnesio-hornblende
Pts Fo Tsch Hn -- potassian-ferro tschermakitic hornblende
Pts Kae -- potassian kaersutite
Pts Ti Has Hn -- potassian titanian-hastingsitic hornblende
Pts Ti Mgn Has Hn -- potassian titanian-magnesian hastingsitic hornblende
Rie -- riebeckite
Ti Fo Pg -- titanian-ferroan pargasite
Ti Fon Pg Hn - titanian ferroan pargasitic hornblende
Ti Mgn Has Hn -- titanian-magnesian hastingsitic hornblende
Trem -- tremolite
Tsch Hn -- tschermakitic hornblende

Appendix 6

The Principles of the Calculations by Least-squares Approximation

The principle of the calculation is taken after Bryan *et al.* (1968). In this work, x_{ij} is assumed to be the observed amount of the i th oxide in the j th component, where $i = 1, n$, and $j = 1, k$; b_j is the estimated amount of component j required; y_j is the observed amount of oxide j in the composition to be approximated.

Therefore, a linear equation may be written as:

$$XB = Y \qquad (1)$$

where $X =$

$$\begin{pmatrix} x_{11} & x_{12} & x_{13} & \cdots\cdots & x_{1k} \\ x_{21} & x_{22} & x_{23} & \cdots\cdots & x_{2k} \\ x_{31} & x_{32} & x_{33} & \cdots\cdots & x_{3k} \\ \vdots & \vdots & \vdots & & \vdots \\ x_{n1} & x_{n2} & x_{n3} & \cdots\cdots & x_{nk} \end{pmatrix}$$

$$B = \begin{pmatrix} b_1 \\ b_2 \\ b_3 \\ \vdots \\ b_k \end{pmatrix} \qquad Y = \begin{pmatrix} y_1 \\ y_2 \\ y_3 \\ \vdots \\ y_k \end{pmatrix}$$

In this mass-balance calculation, the matrix X represents the chemical compositions of various mineral phases and melt which makes up the assumed parental magma. For example, x_{11} and x_{21} may be assumed to be the SiO_2 and TiO_2 contents in olivine, x_{12} and x_{22} to be the SiO_2 and TiO_2 contents in clinopyroxene. The vector Y represents the observed chemical composition of the parental magma (*e.g.*, gabbro); and the vector B is the amount of minerals and daughter melt to be estimated.

Premultiplication of equation (1) by the transpose of X gives the following equation:

$$X'XB = X'Y \qquad (2)$$

where X' is the transpose of X.

Premultiplication of equation (2) by the inverse of [X'X] gives the solution:

$\hat{B} = [X'X]^{-1}X'Y$ (3)

Substitute $\hat{B}$ in equation (3) in the left side of equation (1) and perform the indicated multiplication, a vector $\hat{Y}$ is obtained and this represents the least-squares approximation of Y. In other word, the elements of $\hat{Y}$ are those which minimize the sum of squares of the residuals: $r^2 = \sum (Y_i - \hat{Y}_i)^2$.